Ternary Coding and Triangular Modulation

by

Mahmoud Karem Mahmoud Abdelaziz
B.Sc., Military Technical College, 2002
M.Sc., Military Technical College, 2011

A Dissertation Submitted in Partial Fulfillment of the
Requirements for the Degree of

DOCTOR OF PHILOSOPHY

in the Department of Electrical and Computer Engineering

Ternary Coding and Triangular Modulation

by

Mahmoud Karem Mahmoud Abdelaziz
B.Sc., Military Technical College, 2002
M.Sc., Military Technical College, 2011

Supervisory Committee

Dr. T. Aaron Gulliver, Supervisor
(Department of Electrical and Computer Engineering)

Dr. Xiaodai Dong, Departmental Member
(Department of Electrical and Computer Engineering)

Dr. Alex Thomo, Outside Member
(Department of Computer Science)

Supervisory Committee

Dr. T. Aaron Gulliver, Supervisor
(Department of Electrical and Computer Engineering)

Dr. Xiaodai Dong, Departmental Member
(Department of Electrical and Computer Engineering)

Dr. Alex Thomo, Outside Member
(Department of Computer Science)

ABSTRACT

Adaptive modulation is widely employed to improve spectral efficiency. To date, square signal constellations have been used for adaptive modulation. In this dissertation, triangular constellations are considered for this purpose. Triangle quadrature amplitude modulation (TQAM) for both power-of-two and non-power-of-two modulation orders is examined. A technique for TQAM mapping is presented which is better than existing approaches. A new type of TQAM called semi-regular TQAM (S-TQAM) is introduced. Bit error rate expressions for TQAM are derived, and the detection complexity of S-TQAM is compared with that of regular TQAM (R-TQAM) and irregular TQAM (I-TQAM). The performance of S-TQAM over additive white Gaussian noise and Rayleigh fading channels is compared with that of R-TQAM and I-TQAM.

The construction of ternary convolutional codes (TCCs) for ternary phase shift keying (TPSK) modulation is considered. Tables of non-recursive non-systematic TCCs with maximum free distance are given for rates 1/2, 1/3 and 1/4. The conversion from binary data to ternary symbols is investigated. The performance of TCCs with binary to ternary conversion using TPSK is compared with the best BCCs using binary phase shift keying (BPSK).

Ternary trellis coded modulation (TTCM) is introduced. This combines triangular signal constellations with ternary convolutional codes. The performance of TTCM is presented and compared with binary trellis coded modulation (BTCM) which employs square quadrature amplitude modulation (SQAM) and binary convolutional coding. Ternary set partitioning (TSP) for TTCM is introduced and binary to ternary conversion is introduced that is suitable for TTCM. Triangular QAM (TQAM) constellations that are compatible with TSP are presented. The performance of BTCM is compared with that of TTCM, which TTCM is better performance.

Contents

List of Tables

List of Figures

ACKNOWLEDGEMENTS

I am grateful to Allah, for good health, loving parents, and my beautiful family who were supportive and instrumental in me completing this dissertation. I am thankful to many sources that have contributed to this work, from advice on research to financial support. First, I wish to express my sincere thanks to Dr. T. Aaron Gulliver whose expertise, understanding, and patience added considerably to my graduate experience. Second, I am indebted to the other members of my supervisory committee, Dr. Xiaodai Dong and Dr. Alex Thomo, for their insightful comments and encouragement. Finally, I would like to thank the government of Egypt for scholarship funding.

DEDICATION

To my parents
for their continuous guidance and dedication
To my lovely wife
for her love and support

Chapter 1

Introduction

The use of wireless communications has rapidly increased in recent years, and there has been world wide development of new systems to meet the needs of this growing market. Characteristics such as low power operation, high data rate and low bit error rate (BER) are the dominant design criteria by which these systems are judged. These criteria are conflicting, so there are tradeoffs between them. Sending m bits per symbol rather than one bit per symbol increases the data rate. However, this requires a higher transmit power for the same BER. Forward error correction (FEC) techniques are used to correct errors due to a noisy channel. For a given transmit power, FEC can reduce the error rate. However using FEC in a communication system increases the complexity. The motivation of this dissertation is to achieve a high data rate, low transmit power, low system complexity, and low BER.

1.1 Modulation Constellations

A constellation diagram is a representation of modulation signal in two dimensions. Maximum likelihood (ML) detection is optimal for equiprobable symbols [2]. The complexity of ML detection is a function of the number of nearest nighbor symbols [3]. The minimum distance between constellation symbols is called the minimum Euclidean distance (d_{min}). A large d_{min} increases the probability of obtaining the correct symbol using ML detection. Therefore, it is important to have a signal constellation with a large d_{min}. With phase shift keying (PSK) modulation, the signals have a constant amplitude [4]. However, increasing the number of phase shifts increases the error rate in the presence of noise [4]. Therefore, quadrature amplitude modulation

(QAM) is used in modern communication systems as it has a larger distance between constellation points than PSK for the same constellation size.

The performance with a signal constellation is often measured in terms of its power efficiency and bandwidth efficiency. The power efficiency of a signal constellation is defined as the squared minimum Euclidean distance (d^2_{min}) divided by the average symbol power [4]. A good signal constellation has a low average symbol power and a high d_{min}. Square QAM (SQAM) has a higher power efficiency than PSK, so it is commonly used in wireless communication systems [4]. However, SQAM does not have the highest power efficiency. Therefore other constellations have been developed such as hexagonal [6], triangular [7] and circular QAM [8]. SQAM has a simpler detection complexity than circular, hexagonal and triangular QAM constellations. Triangular QAM has a higher power efficiency than SQAM, however it also has a higher detection complexity [7]. In this dissertation, the tradeoff between detection complexity and power efficiency is examined, and a new type of TQAM is introduced which provides a good tradeoff.

1.2 Adaptive Modulation

In a wireless communication environment, fading causes the amplitude of the received signal to vary. Fading is caused by multipath propagation or shadowing due to obstacles in the propagation path. The bit rate can be adapted according to the channel condition to maximize the throughput [1]. This is achieved by choosing the modulation order, which is the size of the signal constellation M. For the same transmit power, a higher modulation order has a smaller d_{min}, so the BER is larger. Therefore, a high modulation order is used with good channels, and a low modulation order with poor channels. Adapting the modulation order according to the channel condition is called adaptive modulation.

Adaptive modulation requires accurate channel state information (CSI) to select the appropriate modulation. The number of modulation orders is finite and increasing the number of orders for a given maximum M can improve performance. One means of increasing this number is to use non-power-of-two modulation orders. In this dissertation, non-power-of-two modulation orders are a combination of bits and trits (ternary digits). Recently, non-power-of-two SQAM was introduced in [9]. The BER performance of non-power-of-two SQAM is between the BER performance of power-of-two SQAM. Therefore, having more modulation orders allows for a better match

to the channel conditions. Adaptive modulation with non-power-of-two SQAM was presented in [10]. In this dissertation, adaptive modulation with non-power-of-two TQAM is introduced, and the performance and power efficiency are examined.

1.3 Ternary Systems

In this dissertation, ternary arithmetic is employed with non-power-of-two modulation orders. Ternary systems employ ternary arithmetic operations, ternary logic circuits and ternary memory. Ternary arithmetic operations and logic circuits are faster and require less energy than binary arithmetic operations and logic circuits [11, 12, 13]. Ternary memory cells have a higher storage density than binary memory cells [14, 15]. Further, the error rate performance of ternary PSK (TPSK) is better than binary PSK (BPSK) and quadrature PSK [16]. Therefore, ternary communication systems have been introduced, for example ternary optical communication systems [17]. Ternary system have been proposed for future digital systems [18], so ternary wireless communications are an important research topic.

Although ternary systems outperform binary systems, wireless communication systems operate with binary data. To overcome this issue, ternary subsystems can be embedded in binary systems. This can be done by converting binary data to ternary data via binary to ternary (BT) conversion. Converting m bits to n trits requires that $2^m < 3^n$, and the binary string is mapped to a ternary string using a look-up table (LUT). Since $2^m < 3^n$, there is a conversion loss. Different BT conversions have been studied in the literature such as three bits to two trits conversion (3B2T), six bits to four trits conversion (6B4T) and eleven bits to seven trits conversion (11B7T) [19, 20]. Of these, 11B7T has the best conversion efficiency, while 3B2T has the worst efficiency. The bit errors due to BT conversion errors have a significant effect on the performance. Therefore, in this dissertation, the average number bit errors due to one trit error with BT conversion is examined.

1.4 Convolutional Codes

Convolutional codes were introduced in 1955 as an alternative to block codes [21]. A block code encodes fixed length data, whereas a convolutional code encodes a continuous stream of data. Convolutional codes are widely used in practical communication systems due to their lower decoding complexity [22]. With binary convolutional codes,

a bit sequence is passed through shift registers. The encoded bits are obtained by modulo-2 addition of the input bits and the contents of the shift registers. A convolutional encoder is defined by three parameters (n, k, m), where n is the number of encoded bits, k is the number of input bits, and m is the memory length. The code rate is $R = \frac{k}{n}$, and is a measure of the efficiency of the code. A convolutional encoder can be defined as a finite state machine, where the contents of the shift registers define the states of the encoder [22]. The trellis diagram of a convolutional code is obtained from the state diagram. The error correction capability of a convolutional code is determined by the minimum free distance d_{free}, which is the minimum weight of a path that diverges from the all-zero path in the trellis and then merges with this path.

The Viterbi algorithm (VA) was proposed in 1967 for decoding convolutional codes [23]. It finds the minimum weight path through a weighted, directed graph. The VA provides the maximum likelihood codeword of a convolutional code [24]. For hard decision decoding, the branch metric is the Hamming distance between the received word and the codeword associated with that branch. The path entering a state with the lowest metric is chosen as the survivor path. The soft decision VA is similar to the hard decision algorithm except that the Euclidean distance (d_E) is used in the branch metrics instead of the Hamming distance.

Ternary convolutional codes (TCCs) were studied in [19, 25]. A TCC has a structure similar to that of a binary convolutional code (BCC) but the arithmetic operations are ternary. TCCs up to $m = 9$ for different code rates are pressented in this dissertation. It is shown that TCCs provide a better coding gain than BCCs as d_{free} is larger for the same memory length.

1.5 Trellis Coded Modulation

In a bandwidth-limited environment, the use of higher order modulation can increase the bandwidth efficiency. In this case, a large transmit power is required to obtain the same BER. In order to achieve improved reliability without increasing the transmit power or bandwidth, coding and modulation are combined together in trellis coded modulation (TCM). TCM was introduced by Ungerboeck [26] to increase the Euclidean distance between possible symbol sequences. The free Euclidean distance (d_{Efree}) is the distance between two coded symbol sequences. This allows the loss from the expansion of the signal set to provide the redundancy for coding to be over-

come. For the same transmit power, TCM has a lower BER than with separate coding and modulation for the same code rate and M [26].

Ungerboeck introduced a mapping technique called set partitioning which divides a symbol set into smaller subsets with increasing distance between the subset symbols. Using set partitioning, an M-ary constellation is partitioned into 2, 4, ..., $2^{\log_2 M-1}$ subsets, with sizes $M/2$, $M/4$, $M/8$, ..., 2 and progressively larger minimum distances. Each set partitioning step is called a partitioning level. A convolutional code is used in TCM, so a VA decoder is employed at the receiver. When there are uncoded bits, the trellis diagram has parallel paths between states. Therefore a transition metric unit is used to find the best paths among the groups of parallel paths for the branch metrics [27]. In this dissertation, TCM using TQAM is examined. Further, ternary set partitioning is introduced which is compatible with TQAM. Ternary set partitioning requires ternary data, therefore ternary convolutional coding and TQAM are combined to obtain ternary trellis coded modulation (TTCM).

1.6 Contributions

TPSK and BPSK are compared and the advantages of a triangular constellation lattice over a square lattice are illustrated. TQAM is compared with SQAM, which shows that TQAM provides a better BER performance at high signal to noise ratios (SNRs). Non-power-of-two M-ary TQAM is used in adaptive modulation to reduce the transmit power and increase the data rate for the same BER. TCCs with TPSK are compared with BCCs with BPSK. BTCM with TQAM is studied and compared with BTCM with SQAM. Ternary set partitioning for TQAM is introduced, and TTCM with TQAM is compared with BTCM with SQAM. BT conversion for TCC and TTCM are illustrated and the best BT conversions are presented. The contributions of this dissertation are as follows.

- TQAM for non-power-of-two modulation orders is presented which is a combination of bits and a ternary digit (trit).
- A new type of TQAM called semi-regular TQAM (S-TQAM) is introduced which provides a good tradeoff between detection complexity and BER performance.
- S-TQAM is analyzed for both power-of-two and non-power-of-two modulation

orders with $6 \leq M \leq 256$. Both the power gain and average energy per symbol are derived.

- An improved mapping methodology for TQAM is introduced which can be employed with both binary and non-binary TQAM. The mapping for non-binary TQAM has not previously been investigated. The Gray penalty is obtained for $6 \leq M \leq 256$.

- The detection complexity of TQAM is derived. This shows that the complexity with S-TQAM is similar to that with R-TQAM, and less than with I-TQAM.

- The probability of symbol error and bit error for S-TQAM over additive white Gaussian noise (AWGN) and Rayleigh fading channels are derived and verified by simulation. These results are used to illustrate that S-TQAM has performance close to I-TQAM.

- Optimal TCCs are obtained for memory length up to $m = 9$ for $R = 1/2$, up to $m = 7$ for $R = 1/3$, and up to $m = 6$ for $R = 1/4$.

- The mapping from binary data to ternary symbols is considered based on the average number of bit errors due to a single trit error, e_{av}. The best mapping is presented for converting three bits to two trits.

- TCM is proposed which employs TQAM rather than SQAM or PSK.

- A new set partitioning called ternary set partitioning is introduced and applied to TQAM.

- The performance of TCM with TQAM and ternary convolutional codes (TTCM) is evaluated and compared with that of TCM with SQAM and binary convolutional codes (BTCM).

- A detailed comparison of BTCM with 16 SQAM (16 S-BTCM) and TTCM with 18 TQAM (18 TTCM) is presented to illustrate the advantages of TTCM. Several 18 TQAM signal constellations are considered for TTCM.

- A method is presented to construct a TQAM constellation which is suitable for TTCM.

- A new BT conversion for TTCM is proposed.

- The performance of TTCM is evaluated and compared to that of BTCM over additive white Gaussian noise (AWGN) and Rayleigh fading channels.

1.7 Dissertation Organization

Chapter One: Signal constellations and adaptive modulation were introduced. The use of non-power-of-two modulation orders in adaptive modulation was discussed. The advantages of a ternary system over a binary system were given. Further, the use of ternary convolutional codes in ternary trellis coded modulation was discused. Finally, the dissertation contributions and organization were given.

Chapter Two: Signal constellations are examined, and the advantages of triangular constellations over square constellation are discussed. Adaptive triangular modulation is presented. TQAM is investigated and S-TQAM is introduced. The performance of S-TQAM is analyzed, and the proposed symbol mapping methodology is explained. Numerical and simulation results are presented to evaluate and compare the performance of the signal constellations.

Chapter Three: BT conversion is considered, and the construction of TCCs is presented. TCCs with the highest free distance are presented. The advantage of TPSK over BPSK are discussed. The performance of TCCs is investigated and compared with the best binary convolutional codes.

Chapter Four: BTCM with SQAM is introduced and BTCM with TQAM is considered. TSP is presented, which is employed for TTCM. A method of constructing a compatible TQAM constellation with TSP is given. Further, BT conversion is studied. Performance and simulation results are given to illustrate the advantages of TTCM over BTCM.

Chapter Five: Some conclusions are provided and suggestions for future work are given.

Chapter 2

Triangular Constellations

Next generation wireless communication systems are currently being developed to provide higher data rates and improved power efficiency, i.e. lower average transmit power for a given error rate. There are conflicting requirements as typically transmitting more data over a given bandwidth requires more power to maintain the same performance. Adaptive modulation is a technique used in wireless communication systems such as fourth generation (4G) cellular systems to provide good bandwidth efficiency according to the channel conditions [28]. A high data rate is employed with good channels and a low data rate with poor channels. Adaptive modulation has been shown to provide better spectral efficiency than using fixed modulation [29]. Square quadrature amplitude modulation (SQAM) is typically employed with adaptive modulation. SQAM here indicates points on a square lattice, and includes both cross and the square signal constellations [10]. SQAM has a higher power efficiency than phase shift keying (PSK) for the same number of constellation points M (called the modulation order), because the minimum Euclidean distance d_E between constellation points with SQAM is larger than that with PSK for the same value of M. Thus, SQAM requires less symbol energy on average to achieve the same bit error rate (BER).

The number of modulation orders employed has an effect on the spectral efficiency of adaptive modulation. SQAM has modulation orders which are a power-of-two. A larger number of modulation orders for a given maximum M allows better adaptation to channel conditions, which can improve spectral efficiency [10]. Thus in this dissertation, both power-of-two and non-power-of-two modulation orders are considered. For example, using 4, 6, and 8 QAM can provide better spectral efficiency than using just 4 and 8 QAM.

At the receiver, maximum likelihood (ML) detection is achieved by choosing the constellation point closest to the received signal. Thus, the performance depends on the Euclidean distances between these points. However, it can be complex to calculate the distances from the received signal to the constellation points, particularly when the modulation order M is high [7]. A practical solution to this problem is to divide the constellation into vertical regions. Then the received signal is first located in a region, and the closest constellation point is found within this region. This reduces the number of distance calculations required compared to other approaches [7]. Thus, this two step method is considered here.

There is a tradeoff between the detection complexity and power efficiency in constructing a signal constellation [30]. The regular structure of SQAM results in a low detection complexity, which is one of the reasons it is widely used in communication systems. However, it is not optimum in terms of BER or power efficiency [32]. The optimum signal constellations in terms of BER performance were obtained by Foschini et al. [33], but the detection complexity for these can be high [30]. They determined that the optimum constellation envelope for large M is circular. Further, it was shown that for large M, choosing constellation points from a triangular lattice is close to optimum [33], e.g. triangular lattice point constellations are close to optimum for $M = 7$ and 8, and optimum for $M = 19$. Considering two-dimensional lattices, a triangular lattice provides the most compact QAM constellations, i.e. constellation points closest to the origin [7]. For a given minimum Euclidean distance between signal points d_E, the more compact the constellation the better the power efficiency, so a triangular lattice provides the best power efficiency.

A signal constellation formed of points from a triangular lattice is called triangular QAM (TQAM) [7, 34]. Regular TQAM (R-TQAM) was introduced which has a lower detection complexity than the optimum constellations in [33]. Irregular TQAM (I-TQAM) was introduced in [30], and shown to have an envelope which is close to optimum for large M. The ML detection of R-TQAM is more complex than SQAM [7], but simpler than I-TQAM. In this dissertation, a new type of TQAM called semi-regular TQAM (S-TQAM) is introduced which has detection complexity similar to that of R-TQAM, but provides better power efficiency.

The symbol mapping is a key factor in the error rate with QAM. The best possible mapping is a Gray code [35] which is used with SQAM. However, this mapping is not possible with TQAM, so a quasi-Gray mapping was employed for R-TQAM in [34]. The performance degradation with a given mapping compared to a Gray

code mapping is defined using the Gray penalty, which is the average number of bit differences between adjacent constellation symbols. In this dissertation, a new mapping methodology for R-TQAM is presented which provides a better Gray penalty than the mapping in [34]. Further, it can be employed with non-power-of-two R-TQAM. This methodology is also considered for S-TQAM and I-TQAM, and the corresponding Gray penalty is determined.

The remainder of this chapter is organized as follows. Adaptive triangular modulation is discussed in Section 2.1. In Section 2.2, TQAM is investigated and S-TQAM is introduced. The performance of S-TQAM is analyzed, and the proposed mapping methodology is explained. Numerical and simulation results are presented in Section 2.3 to evaluate and compare the performance of the signal constellations. Finally, some conclusions are given in Section 2.4.

2.1 Adaptive Modulation

Adaptive modulation is a powerful technique for improving the spectral efficiency of wireless communication systems which requires accurate estimation of the channel conditions to determine the appropriate modulation order. Adaptive modulation was first proposed more than 50 years ago [36], but because of implementation issues and poor channel estimation algorithms interest declined. Subsequent improvements in technology provided solutions to these problems and led to the use of adaptive modulation in third generation (3G) cellular systems [29]. The accuracy of the channel estimation and the number of modulation orders has a significant effect on the spectral efficiency [10].

The modulation order in adaptive modulation is selected according to the channel conditions and the desired performance. Increasing the number of modulation orders for a given maximum value of M can improve the spectral efficiency [10], [37]. A simple means of increasing the number of modulation orders is to use non-power-of-two orders. This can be achieved by combining binary and ternary symbols. For example, 8 QAM, 12 QAM and 16 QAM provide smaller differences in modulation orders than just 8 QAM and 16 QAM. In this chapter, non-power-of-two QAM is considered where $M = 3 \times 2^l$, so that a symbol has one trit and l bits. For example, 12 QAM symbol corresponds to one trit and two bits. Thus, bits must be converted to ternary symbols. The conversion employed here is three bits to two trits (3B2T). In this case, the binary data stream is divided into two groups with the first group

Table 2.1: Modulation Orders and Indexes for $6 \leq M \leq 256$

Modulation order M (constellation size)	modulation index J (bits/symbol)
6	2.5
8	3
12	3.5
16	4
24	4.5
32	5
48	5.5
64	6
96	6.5
128	7
192	7.5
256	8

converted to trits. For example, consider 12 QAM so that $l = 2$. Each pair of constellation points requires 7 bits. The first 3 bits are converted to 2 trits using 3B2T conversion. Each trit is combined with two bits to create a 12 QAM symbol, so that each symbol represents $J = 3.5$ bits, where J is the modulation index.

For M a power-of-two, the relationship between the modulation order and index is

$$J = \log_2 M \text{ bits/symbol.} \tag{2.1}$$

When M not a power-of-two, the relationship between the modulation order and index with $n\text{B}m\text{T}$ conversion is

$$J = \frac{n}{m} + \log_2 \frac{M}{3} \text{ bits/symbol,} \tag{2.2}$$

so for the proposed system using 3B2T conversion

$$J = \frac{3}{2} + \log_2 \frac{M}{3} \text{ bits/symbol.} \tag{2.3}$$

Values of J for power-of-two and non-power-of-two modulation orders are given in Table 2.1 for $6 \leq M \leq 256$. This shows that using non-power-of-two modulation orders provides a difference of only half a bit between modulation indexes.

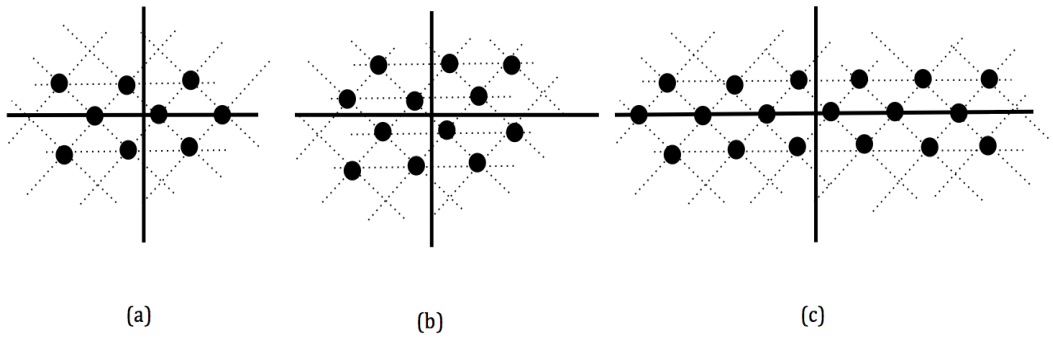

Figure 2.1: R-TQAM constellations for (a) $M = 16$, (b) $M = 24$, and (c) $M = 32$.

2.2 M-ary Triangular QAM

In this chapter, TQAM is considered where the number of constellation points is $M = 2^l$ or $M = 3 \times 2^l$. Including non-power-of-two values of M doubles the number of modulation orders available for adaptive modulation. For example, there are twelve values in Table 2.1, but only six are a power-of-two. R-TQAM and I-TQAM were proposed in [7, 34, 30], but non-power-of-two values of M were not considered.

With TQAM, the distance between all adjacent symbols is equal. Thus, the ML decision regions in the center of the constellation are hexagonal while the regions on the boundary vary according to the constellation geometry. An R-TQAM constellation is symmetric about the origin [7, 34]. For even-bit modulation orders (l even), such as 16, 64 and 256, the R-TQAM constellation has a square shape [7], while for odd-bit modulation orders (l odd), such as 32 and 128, the R-TQAM constellation has a cross shape [34]. For non-power-of-two modulation orders, $M = 3 \times 2^l$, such as 12, 24 and 48, R-TQAM has rectangular constellation. Fig. 2.1 shows the R-TQAM constellations for $M = 16, 24$ and 32. I-TQAM constellations have circular shapes, so they are more compact than R-TQAM constellations [30].

For a given value of M, the average energy per I-TQAM symbol E_{TI} is less than the average energy per SQAM symbol E_S [30]. Further, E_{TI} is equal to the average energy per R-TQAM symbol E_{TR} for $M = 6$ and 12, and less than E_{TR} for other values of M. However, the detection complexity of I-TQAM is much higher than that of R-TQAM, as will be shown later. Therefore in this chapter, new signal constellations called semi-regular TQAM (S-TQAM) are presented which provide a good tradeoff between detection complexity and power efficiency. S-TQAM has a lower average energy per symbol E_{TS} than E_S for all M. The S-TQAM constellation

is the same as that for R-TQAM for even-bit modulation orders, but S-TQAM has a more square envelope for other values of M. For $M = 32$ and 128, E_{TS} is higher than E_{TR}, but S-TQAM has a lower detection complexity than R-TQAM, and the BER performance is similar, as will be shown later. E_{TS} is lower than E_{TR} for other values of M. The values of E_{TI}, E_{TR}, E_{TS} and E_S are given in Table 4.1 for a minimum distance between adjacent constellation points of $d_E = 2d$, where d is a constant.

Non-power-of-two R-TQAM has an equal number of symbols in each row so the constellation has a rectangular envelope. For example, the R-TQAM constellation for $M = 24$ has 4 rows with 6 symbols each, as shown in Fig 2.2(a). The corresponding S-TQAM constellation has a more square envelope, and not all rows have the same number of symbols. As shown in Fig. 2.2(b), 24 S-TQAM has 5 rows, four with 5 symbols and one (the farthest from the origin) with 4 symbols. The constellation for 24 I-TQAM is given in Fig. 2.2(c) for comparison.

In general, the number of rows and constellation points per row for non-power-of-two R-TQAM and S-TQAM are chosen as follows. For R-TQAM, the two closest integer factors of M are chosen. The smallest is the number of rows, and the largest is the number of constellation points per row. The reason for choosing the smaller value for the number of rows is that a new row in the constellation increases the average power more than adding a new constellation point per row. For example, 96 R-TQAM has 8 rows and 12 constellation points per row. This provides a lower value of E_{TR} than using 12 rows and 8 constellation points per row. For S-TQAM, the two integers greater than or equal to $\sqrt{M}$ are chosen. Row points are then eliminated to obtain a constellation of size M such that the rows closest to the origin have more points, and the number of points per row varies by only 1. The eliminated points are those furthest from the origin. Using 96 S-TQAM as an example, $\sqrt{96} = 9.8$ so there are initially 10 rows and 10 constellation points per row. Then, the four points furthest from the origin are eliminated so the 6 rows closest to the origin have 10 points and the remaining four rows have 9 points. Fig. 2.3 illustrates the 48, 96 and 192 S-TQAM constellations. Table 2.2 gives the number of rows and constellation points per row for R-TQAM and S-TQAM which achieve the lowest values of E_{Ti}, $i = R, S$.

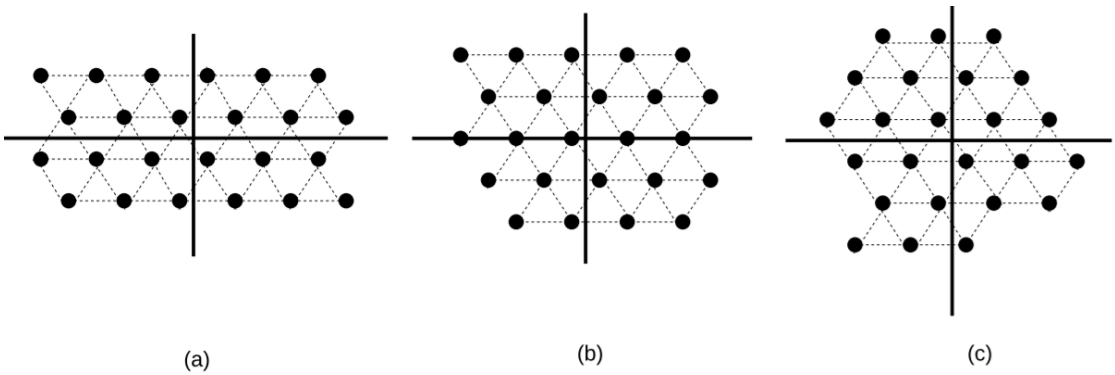

Figure 2.2: Signal constellations for (a) 24 R-TQAM, (b) 24 S-TQAM, and (c) 24 I-TQAM.

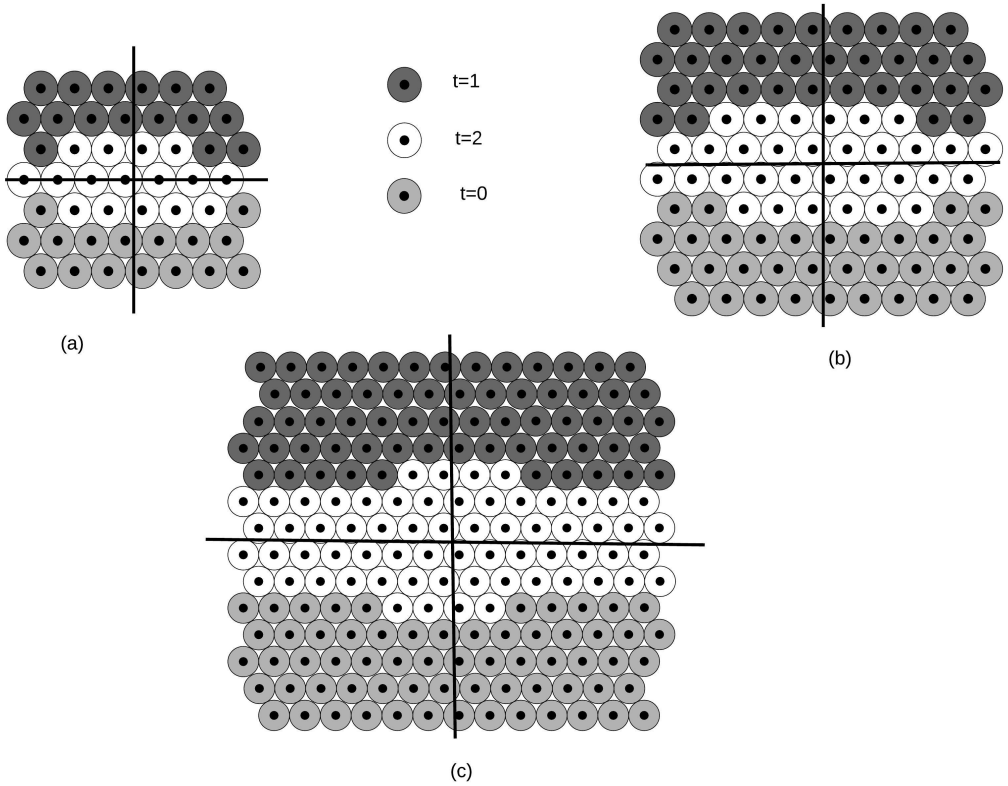

Figure 2.3: Signal constellations and trit mappings for (a) 48 S-TQAM, (b) 96 S-TQAM, and (c) 192 S-TQAM.

Table 2.2: Constellation Parameters for R-TQAM and S-TQAM

M	rows	symbols per row	rows	symbols per row
	R-TQAM		S-TQAM	
6	2	3	2	3
8	2	4	3	2 or 3
12	3	4	3	4
16	4	4	4	4
24	4	6	5	4 or 5
32	-	-	6	5 or 6
48	6	8	7	6 or 7
64	8	8	8	8
96	8	12	10	9 or 10
128	-	-	10	12 or 13
192	12	16	14	13 or 14
256	16	16	16	16

Table 2.3: Average Energy per Symbol, Power Gain, and Gray Penalty for STQAM, R-TQAM, S-TQAM, and I-TQAM

M	E_S	E_{TR}	PG_R (dB)	G_{PR}	G_{PR}	E_{TS}	PG_S (dB)	G_{PS}	E_{TI}	PG_I (dB)	G_{PI}	G_{PI}
6	$3.5d^2$ [10]	$3.118d^2$	0.523	1.525	-	$3.118d^2$	0.523	1.525	$3.118d^2$	0.523	1.525	-
8	$6d^2$	$5d^2$	0.791	1.275	1.275 [34]	$4.5d^2$ [10]	1.25	1.287	$4.5d^2$ [10]	1.25	1.287	-
12	$7.5d^2$ [10]	$7d^2$	0.3	1.533	-	$6.906d^2$	0.36	1.535	$6.906d^2$	0.36	1.532	-
16	$10d^2$	$9d^2$ [42]	0.457	1.181	-	$9d^2$ [42]	0.457	1.181	$8.75d^2$ [30]	0.579	1.27	1.27[30]
24	$17.406d^2$	$15.67d^2$	0.456	1.527	-	$13.84d^2$	0.995	1.543	$12.843d^2$	1.32	1.633	-
32	$20d^2$	$17.75d^2$	−0.969	1.351	1.3885 [34]	$17.875d^2$	0.338	1.4	$16.625d^2$	0.802	1.52	-
48	$31.33d^2$	$27.3125d^2$	0.596	1.418	-	$26.164d^2$	0.783	1.472	$25.835d^2$	0.837	1.511	-
64	$42d^2$	$37d^2$ [42]	0.55	1.248	1.28229 [40]	$37d^2$ [42]	0.55	1.248	$35.25d^2$ [30]	0.761	1.348	1.351[30]
96	$62d^2$	$59.87d^2$	0.152	1.418	-	$55.65d^2$	0.469	1.533	$51.335d^2$	0.82	1.633	-
128	$82d^2$	$72d^2$	−0.905	1.351	1.3635 [38]	$74.875d^2$	0.169	1.356	$67.67d^2$	0.83	1.392	1.48[38]
192	$125.67d^2$	$118.8d^2$	0.244	1.388	-	$107d^2$	0.698	1.545	$103.609d^2$	0.838	1.663	-
256	$170d^2$	$149d^2$	0.572	1.304	-	$149d^2$	0.572	1.304	$141.01d^2$ [30]	0.812	1.355	-

2.2.1 Bit Mapping

The labeling of the constellation points has a significant effect on the BER performance. The goal is a small number of bit differences between adjacent points since an incorrect symbol decision is likely to be one of these points. Thus, an optimum mapping has the smallest average number of bit differences between adjacent symbols. The optimum bit mapping for SQAM is a Gray code mapping [35], which has just one bit difference between adjacent symbols. However, such a mapping is not possible for TQAM [34]. The average number of bit differences between adjacent constellation symbols is called the Gray penalty G_{Pi}, $i = R, S, I$, which is given by [38].

For non-power-of-two TQAM, two values are needed to calculate G_{Pi} the number

Table 2.4: Optimal Three Bit to Two Trit Conversion

Binary Block Input	Ternary Block	Binary Block Output
0 0 0	1 2	0 0 0
0 0 1	1 1	0 0 1
0 1 1	0 1	0 1 1
1 1 1	0 0	1 1 1
1 0 1	0 2	1 0 1
1 0 0	2 2	1 0 0
1 1 0	2 1	1 1 0
0 1 0	2 0	0 1 0
x x x	1 0	0 1 0

of trit differences and the number of bit differences. A trit difference is converted to a bit difference based on the binary to ternary (BT) conversion employed, which determines the average number of bit differences due to a trit difference e_{av}. Binary data is converted to ternary symbols using a lookup table (LUT) which maps n bits to m trits. The 11 bit to 7 trit (11B7T) conversion has $e_{av} = 4.37$. The 3B2T conversion presented in [20] has $e_{av} = 1.666$, while the 3B2T conversion in Table 2.4 provides the lowest value $e_{av} = 1.555$ bits. Therefore, the 3B2T conversion shown in Table 2.4 is employed here, so that on average each trit difference corresponds to a difference of 1.555 bits.

From Table 2.4, 8 blocks of 3 bits are mapped to 8 blocks of 2 trits, so there is an unused trit block. Thus after 3B2T conversion, the trit values are not equiprobable. From Table 2.4, the probability of 0 and 1 occurring is 0.3125, while the probability of 2 occurring is 0.375. Therefore, to minimize the transmit power, the higher probability trit should be mapped closer to the origin than the other trits [39].

The bit mapping for power-of-two R-TQAM given in [40] is called quasi-Gary. This mapping employs the Gray code mapping used with SQAM, and then after labeling, the constellation points are relocated to obtain the TQAM constellation. In [38], a bit mapping was proposed for R-TQAM. However, the mapping proposed here provides better values of G_{PR} for TQAM as will be shown. Power-of-two TQAM has equiprobable symbols, but trit 2 has a higher probability than 0 or 1 with non-power-of-two TQAM. Thus, the Gray penalty for non-power-two TQAM cannot be obtained using the approach in [38]. This can be extended by including the symbol

probabilities which gives

$$\begin{aligned} G_{Pi} &= \sum_{j=1}^{M} Pr(s_j) G_{Pi}^{s_j}, \\ &= \sum_{j=1}^{M} Pr(s_j) \frac{\sum_{k=1}^{N(s_j)} B_d(s_j, s_k)}{N(s_k)}, \end{aligned} \tag{2.4}$$

where s_j and s_k denote the jth and kth symbols, respectively, $N(s_j)$ is the number of nearest neighbours of s_j, $Pr(s_j)$ is the probability of s_j, and $B_d(s_j, s_k)$ is the corresponding number of bit differences.

The proposed mapping for R-TQAM divides the constellations into groups of points which have regular shapes. For example, Fig. 2.4 shows the mapping for 48 R-TQAM, where each constellation point is labeled (b_0, b_1, b_2, t, b_3). For simplicity, the trit label (t) is represented by different colours in Fig. 2.4. The constellation points are first divided into four groups, and each is labeled by two bits, b_0 and b_1 (underlined in the figure). These groups are labeled using a Gray code mapping so there is only one bit difference between any two groups. Next, the constellation points in each group are divided into two groups labeled by bit b_3 (shown as bold in the figure). Now, the 48 R-TQAM constellation has 8 rectangular groups, and each has 6 points. Each pair of points in these groups are labeled with a different trit value, t. This is done such that the trit values on the borders of the groups are the same. In addition, because of the higher probability of 2 occurring, it is assigned to the region closest to the origin to minimize the transmit power [39]. The last step is to assign bit labels b_4 in the pairs, and is done to keep the number of bit difference between groups as small as possible. This method for mapping non-power-of-two M-ary R-TQAM results in a lower value of G_{PR} compared to the mapping in [34, 40]. The mapping for power-of-two R-TQAM is similar to that for non-power-of-two R-TQAM except that the trit mapping step is ignored. Thus, each constellation point for non-power-of-two R-TQAM is labeled (b_0, b_1, ..., t, ..., $b_{(l-2)}$, $b_{(l-1)}$), and each constellation point for power-of-two R-TQAM is labeled $(b_0, b_1, \ldots, b_{(l-1)})$.

For S-TQAM, the mapping employed for I-TQAM in [30] can be considered. This uses the corresponding R-TQAM mapping in [40, 38], and relocates some of the points to obtain the I-TQAM constellation. However, this results in poor values of G_{PS} and G_{PI}, particularly for large M. The mapping for S-TQAM proposed here is based on dividing the constellation points similar to the approach given above for R-TQAM.

As the geometry is not regular, the first division varies depending on M as shown in Fig. 2.3 for $M = 48$, 96 and 192. Note that the divisions are more regular for larger values of M.

For non-power-of-two S-TQAM, the constellation points are first divided into three groups, and then these groups are divided according to the value of l. For example, in Fig 2.5(a), the 48 S-TQAM constellation is divided into three groups labeled $t = 0, 1$ and 2, with 2 assigned to the middle group [39]. For simplicity, the trit label is represented by different colours. Each group is divided into two equal halves which are labelled $b_0 = 0$ or $b_0 = 1$ (underlined in the figure). Then each half in the top and the bottom groups is further divided into two parts which are labeled $b_1 = 0$ or $b_1 = 1$ (shown as bold in the figure). The borders of these parts are assigned the same b_1 value. The top and bottom thirds now have 4 groups as shown in Fig. 2.5(a), and each group has 4 constellation points. The points in each group are assigned bit values so that the bit differences with the points in neighbouring groups is minimized. For example, the top right group (diamond shape), has two neighbouring points in the group to the left (parallelogram shape). These adjacent points have the same values of b_2 and b_3. The shape of the middle third of the constellations for $6 \leq M \leq 64$ is far from regular, but for $96 \leq M \leq 256$ it is close to regular as shown in Fig. 2.3. Thus for $6 \leq M \leq 64$, the points in the middle third are labeled such that the number of bit differences is kept low, while for $96 \leq M \leq 256$, these points can be mapped similar to the approach for the top and bottom thirds. For power-of-two S-TQAM, the same approach is employed but the first division into thirds is omitted.

The proposed mapping can also be employed for I-TQAM. Table 4.1 shows that this is better than the mapping in [30]. The mapping for 48 I-TQAM is shown in Fig. 2.5(b). It is similar to the mapping for S-TQAM except that the groups have more irregular shapes. This irregularity results in a higher G_{PI} compared to G_{PR} and G_{PS} for the same value of M.

Table 4.1 presents the average energy per symbol, power gain and Gray penalty for SQAM, R-TQAM, S-TQAM, and I-TQAM. I-TQAM has the lowest average energy per symbol, E_{TI}, for all values of M, while the average energy per symbol for SQAM, E_S, is the highest. S-TQAM has a lower average energy per symbol E_{TS} than E_S for all values of M. This is because the S-TQAM constellation is the same as that for R-TQAM when $\sqrt{M}$ is an integer, while for other values of M S-TQAM has a more square envelope. The power gain indicates the transmit power saved using TQAM

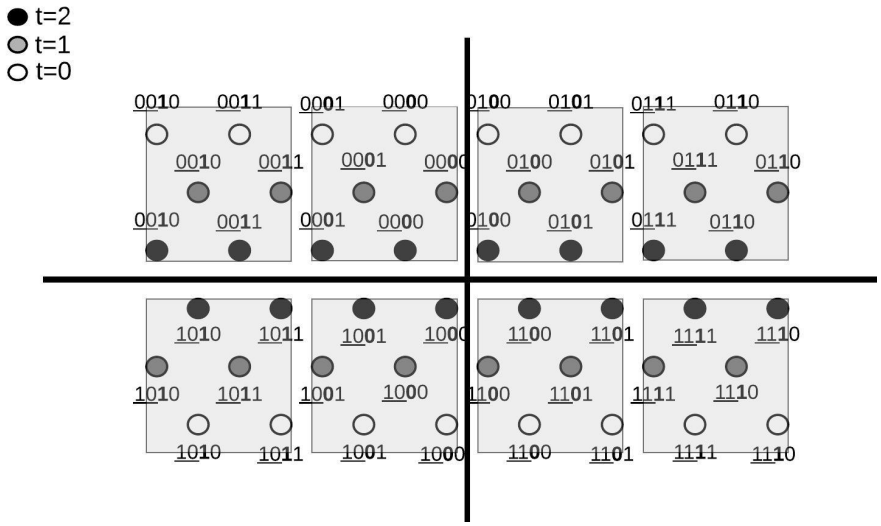

Figure 2.4: The proposed mapping for 48 R-TQAM.

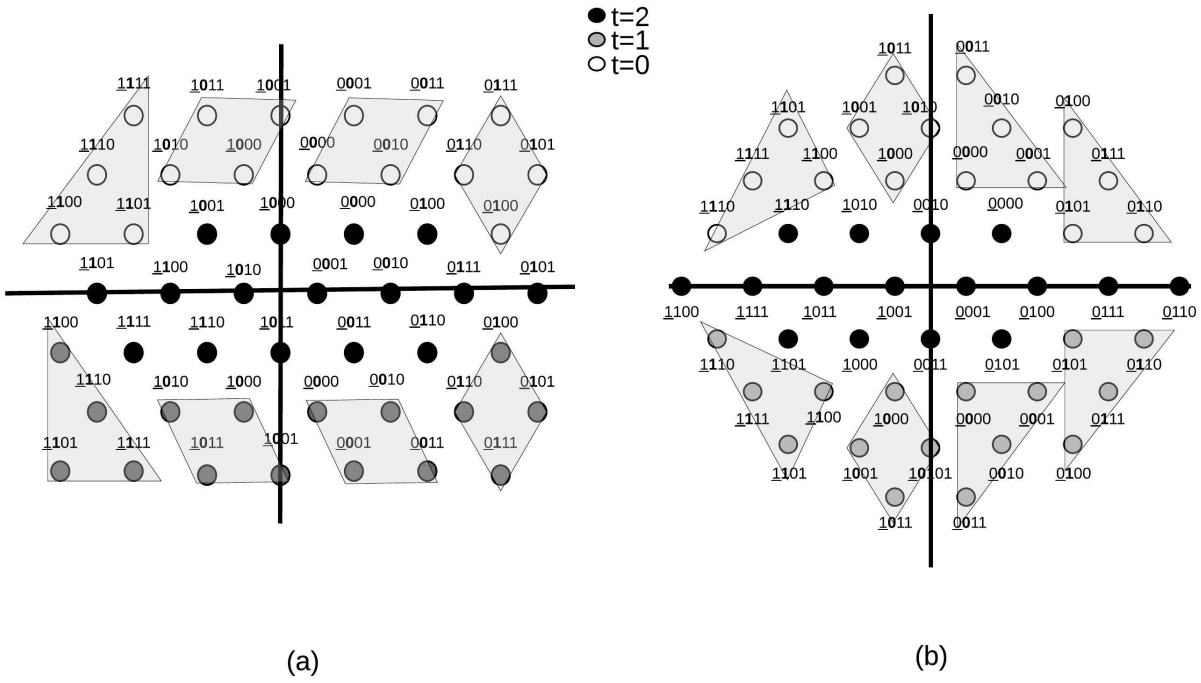

Figure 2.5: The proposed mapping for 48 S-TQAM and 48 I-TQAM.

rather than SQAM and is given by

$$PG_i = 10 \log_{10} \left(\frac{E_S}{E_{Ti}} \right), \tag{2.5}$$

for $i = R, I, S$. A positive value means that TQAM requires less power. Table 4.1 shows that PG_S is greater than or equal to PG_R for all values of M except 32 and 128. The Gray penalty G_{PR} of the proposed mapping for 32, 64 and 128 R-TQAM is lower than that in [40, 38]. For 16 I-TQAM, G_{PI} is the same for the proposed mapping and the mapping in [30], while for 64 I-TQAM, G_{PI} is lower with the proposed mapping. These results indicate that the proposed TQAM mapping is better than the mappings given in [30, 40, 38]. Further, with the proposed mapping G_{PS} is smaller than G_{PI} for $M \geq 16$, and is equal to or higher than G_{PR} for all values of M. For example, from Table 4.1, 48 R-TQAM has $G_{PR} = 1.418$ and 48 S-TQAM has $G_{PS} = 1.472$, while 48 I-TQAM has the worst value $G_{PI} = 1.511$.

2.2.2 TQAM Detection

Maximum a posteriori probability (MAP) detection provides optimal performance and is equivalent to maximum likelihood (ML) detection when the symbols are equiprobable [39]. ML decoding is less complex and so is preferable in communication systems. The goal of MAP and ML detection is to maximize the probability of a correct decision at the receiver in the presence of additive white Gaussian noise (AWGN). A MAP detector computes the a posteriori probabilities for all constellation symbols and selects the maximum as the estimate of the transmitted symbol. For power-of-two M-ary TQAM, the M signals are equiprobable, so that MAP detection and ML detection are equivalent. The ML detection of TQAM was investigated in [7, 30]. This requires calculating the Euclidean distances between the received signal and the constellation points. As ML detection is simpler than MAP detection, it is widely used in practice. A comparison between MAP and ML detection is given in the following section.

With R-TQAM, S-TQAM and I-TQAM, the decision regions are hexagonal in the center of the constellation, as shown in Figs. 2.6 and 2.7, but have different shapes on the boundaries. R-TQAM detection in [7] and I-TQAM detection in [30] were determined using a two step process, and this was analyzed in [31]. The first step divides the constellation into vertical regions R_i as shown in Fig. 2.6. Let the received

signal be $z = x + jy$. The real value x is used to determine the vertical region R_i. Then the imaginary value is used to determine the symbol m_i in this vertical region which is closest to z. The equations of the decision lines in the vertical regions are $l_i = k + C$, where C is a constant and k is a function of x, $k = f(x)$, and are based on the constellation geometry. Thus, the value of k indicates the relationship between x and the decision lines l_i in R_i. For R-TQAM, there is one expression for k in each vertical region, while for I-TQAM, there can be several expressions for k in a vertical region [7, 30]. Once a value for l_i is obtained, y is compared with this value to obtain the estimated constellation point.

ML detection for S-TQAM is similar to that for R-TQAM and I-TQAM. Fig. 2.7 illustrates the detection for 24 S-TQAM with $d = 1$. If $z = 1.5 + j1.73$, then the estimated constellation point is located in region R_7, so it must be one of one of the five points m_1, m_2, m_3, m_4, m_5. Table 2.6 gives the expressions for k in terms of x for the middle vertical regions R_1 to R_9 with 24 S-TQAM. For the boundary regions R_0 and R_{10}, the expressions for k are different [31]. For example, from Fig. 2.7 there are two equations for R_0, $k = 0$ and $k = \frac{2(x+5d)}{\sqrt{3}}$. With S-TQAM, there is one expression for k in these middle regions similar to R-TQAM. Substituting $x = 1.5$ in the equation for region R_7, $k = \frac{2(x-2d)}{\sqrt{3}}$, gives $k = -0.577$. The equations for the decision lines in regions R_2 to R_8 in terms of k are as follows

$$l_1 = k + \frac{3\sqrt{3}}{2}d, \tag{2.6}$$

$$l_2 = -k + \frac{\sqrt{3}}{2}d, \tag{2.7}$$

$$l_3 = k - \frac{\sqrt{3}}{2}d, \tag{2.8}$$

$$l_4 = -k - \frac{3\sqrt{3}}{2}d. \tag{2.9}$$

Substituting $k = -0.577$ in these equations gives $l_1 = 2.02$, $l_2 = 1.44$, $l_3 = -1.44$ and $l_4 = -2.02$, which are used to determine the estimated symbol. If $y > l_1$, the symbol is m_1, if $l_i \geq y > l_{i+1}$, the symbol is m_{i+1}, $i = 1, 2, 3$, and if $y \leq l_4$, the symbol is m_5. For this example, $l_1 = 2.02 > y = 1.73 > l_2 = 1.44$, so the estimated symbol is m_2, which is closest to z as shown in Fig. 2.7.

The detection complexity for TQAM depends on two factors, the number of vertical regions N_R and the maximum number of constellation points in the regions

N_P [41]. Table 2.5 gives N_P and N_R for R-TQAM, S-TQAM and I-TQAM with $6 \leq M \leq 256$. The computational complexity in determining the vertical region R_i is $\mathcal{O}(N_R)$ [18], and the computational complexity in determining the constellation point in a region is $\mathcal{O}({N_P}^2)$ [41]. The overall detection complexity is then

$$\mathcal{O}(Mi) = \mathcal{O}({N_P}^2) + \mathcal{O}(N_R), \tag{2.10}$$

where $i = R, S, I$, so N_P is the dominant factor. For example, Fig. 2.6 shows that $N_R = 15$ for 24 R-TQAM and $N_R = 11$ for 24 I-TQAM. Thus, 24 R-TQAM has lower detection complexity because $N_P = 4$ with 24 R-TQAM and $N_P = 7$ with 24 I-TQAM, and from (2.10), $(\mathcal{O}(24R) = 31) < (\mathcal{O}(24I) = 60)$. Further, N_P with S-TQAM is close to that with R-TQAM for all M, and N_R for S-TQAM is close to that for I-TQAM, and lower than for R-TQAM. Thus, S-TQAM has lower complexity than I-TQAM and similar complexity to R-TQAM. For example, $\mathcal{O}(48i)$ for R-TQAM and S-TQAM are 55 and 66, respectively, but for I-TQAM it is 98. Therefore, the detection complexity of 48 S-TQAM and 48 R-TQAM is approximately the same. For $M = 6$, and 12 the detection complexity of R-TQAM, S-TQAM and I-TQAM is the same as they have the same constellations. From Table 2.5, R-TQAM has lower detection complexity than I-TQAM for $16 \leq M \leq 256$. For $M = 16, 64$ and 256, the complexity of R-TQAM and S-TQAM is equal. However, for $M = 32$ and 128 the complexity of R-TQAM is higher than that of S-TQAM. The reason is that N_P for 32 and 128 R-TQAM is higher than for 32 and 128 S-TQAM, respectively, as shown in Table 2.5. For other values of M, the complexity of R-TQAM is slightly less than that of S-TQAM.

2.2.3 Performance Analysis

In this section, bit and symbol error probabilities are derived for TQAM over AWGN and Rayleigh fading channels. Approximations for these probabilities for power-of-two R-TQAM and I-TQAM were derived in [42, 43] and [30], respectively. With power-of-2 TQAM, the symbols are equiprobable, so the bit and symbol error probabilities can be obtained using the approach in [44]. This method is based on the geometry of the decision regions. With non-power-of-2 TQAM, the symbols are not equiprobable, so this approach cannot be used. In this case, the average number of nearest neighbours

Table 2.5: Maximum Number of Constellation Points N_P in a Region, the Number of Regions N_R, and the Detection Complexity for R-TQAM, S-TQAM and I-TQAM

M	R-TQAM			S-TQAM			I-TQAM		
	N_P	N_R	$\mathcal{O}(R)$	N_P	N_R	$\mathcal{O}(S)$	N_P	N_R	$\mathcal{O}(I)$
6	3	7	16	3	7	16	3	7	16
8	2	11	15	3	8	17	3	8	17
12	3	11	27	3	11	20	3	9	18
16	4	11	27	4	11	27	7	11	60
24	4	15	31	5	11	46	7	11	60
32	7	15	64	6	15	51	8	15	79
48	6	19	55	7	17	66	9	17	98
64	8	19	83	8	19	83	10	18	118
96	8	25	89	10	23	123	13	23	192
128	12	27	171	10	27	127	14	27	223
192	12	35	179	14	31	257	18	29	353
256	16	35	291	16	35	291	19	29	390

Table 2.6: Values of k for Middle Vertical Regions R_1 to R_9 for 24 S-TQAM

	R_1	R_2	R_3	R_4	R_5	R_6	R_7	R_8	R_9
k	$\frac{2(x+5d)}{\sqrt{3}}$	$\frac{2(x+4d)}{\sqrt{3}}$	$\frac{2(x+3d)}{\sqrt{3}}$	$\frac{-2(x+2d)}{\sqrt{3}}$	$\frac{2(x+d)}{\sqrt{3}}$	$\frac{-2(x-d)}{\sqrt{3}}$	$\frac{2(x-2d)}{\sqrt{3}}$	$\frac{-2(x-3d)}{\sqrt{3}}$	$\frac{-2(x-4d)}{\sqrt{3}}$

(NNs) is

$$K = \sum_{j=0}^{M-1} Pr(s_j)K(j), \tag{2.11}$$

where $K(j)$ is the number of NNs for the jth symbol. The corresponding average number of pairs of adjacent NNs is

$$K_C = \sum_{j=0}^{M-1} Pr(s_j)K_C(j), \tag{2.12}$$

where $K_C(j)$ is the number of pairs of adjacent NNs for the jth symbol. For example, Fig. 2.8(a) shows the 4 R-TQAM signal constellation. The symbols are equiprobable so $Pr(s_j) = \frac{1}{4}$, which gives $K(3) = 3$ and $K = \frac{1}{4}(2 + 3 + 3 + 2) = 2.5$. The number of pairs of adjacent NNs for s_3 is $K_C(3) = 2$, and the average number of pairs is $K_C = \frac{1}{4}(1 + 2 + 1 + 2) = 1.5$. This figure also gives the decision regions between s_3 and the corresponding NNs. The overlap of these regions is shown in gray, and the

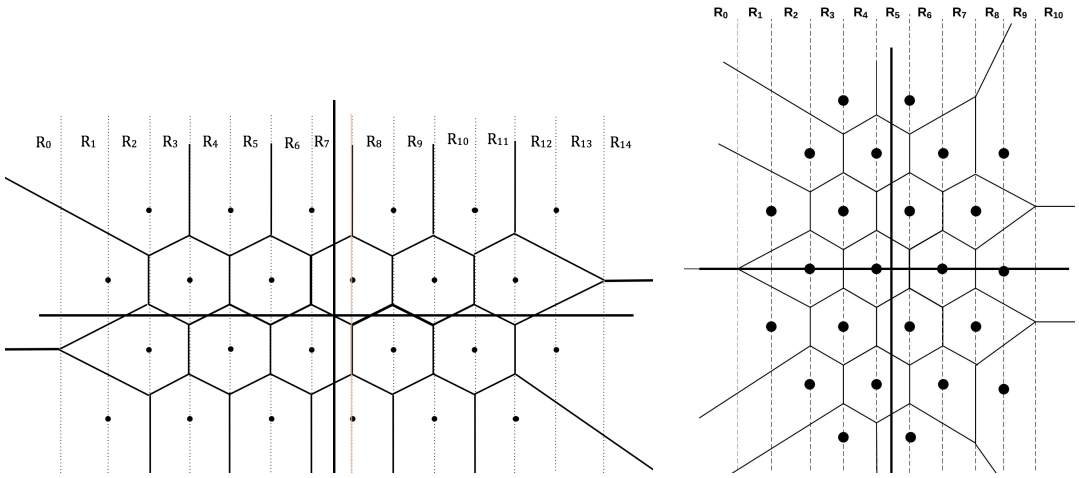

(a) (b)

Figure 2.6: The detection regions for (a) 24 R-TQAM and (b) 24 I-TQAM.

intensity of the colour increases with the number of overlapping regions. Fig. 2.8(b) shows the 3 TQAM signal constellation. In this case, $Pr(s_1) = Pr(s_2) = 0.3125$ while $Pr(s_3) = 0.375$, so that $K = (2 \times 0.3125 + 2 \times 0.3125 + 2 \times 0.375) = 2$ and $K_C = (1 \times 0.3125 + 1 \times 0.3125 + 1 \times 0.375) = 1$.

The general form of the SEP for M-ary TQAM is [44]

$$P_{s,\text{AWGN}} = KQ(\sqrt{\alpha\gamma_s}) + \frac{2}{3}K_C Q^2(\sqrt{2\alpha\gamma_s/3}) - 2K_C Q(\sqrt{\alpha\gamma_s})Q(\sqrt{\alpha\gamma_s/3}), \quad (2.13)$$

where $Q(x) = (2\pi)^{-1/2}\int_x^\infty e^{-u^2/2}du$, $\alpha = [d/2\sigma]^2/\gamma_s$ where d is the minimum distance between NNs, σ^2 is the variance of the AWGN, and the signal to noise ratio (SNR) is $\gamma_s = E_s/N_0$ where E_s is the symbol energy and N_0 is the noise power spectral density. The symbol error probability parameters in (2.13) for M-ary R-TQAM, S-TQAM and I-TQAM are given in Table 2.7 for $6 \leq M \leq 256$. The values for power-of-two R-TQAM and I-TQAM are the same as those in [44] (but $M = 128$ was not considered).

Most wireless communication systems operate in fading environments. Thus, the performance in a frequency-flat Rayleigh fading is now derived. The average symbol energy is $\bar{E}_s = E\{E_s\}$, and the average SNR is $\bar{\gamma}_s = \bar{E}_s/N_0$. Then, the average SEP is given by [44]

$$P_{s,\text{Rayleigh}} = KI_1(\bar{\gamma}_s) + \frac{2}{3}K_C I_2 - 2K_C I_3(\bar{\gamma}_s), \quad (2.14)$$

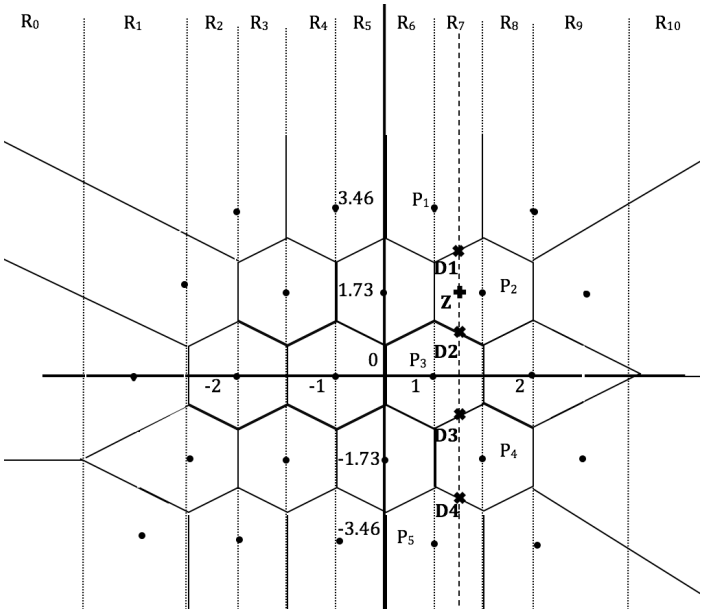

Figure 2.7: The detection regions for 24 S-TQAM.

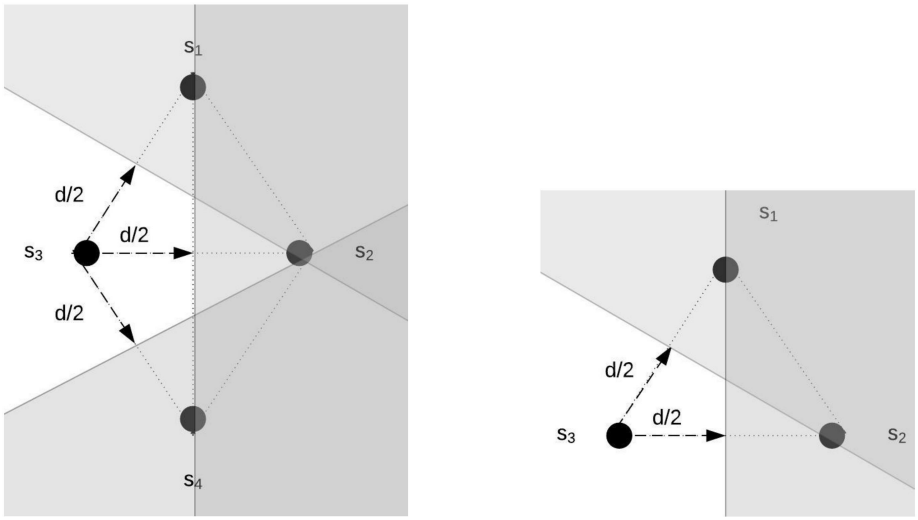

(a) (b)

Figure 2.8: Boundary decision regions for (a) power-of-two TQAM and (b) non-power-of-two TQAM.

Table 2.7: SEP Parameters For M-ary TQAM in AWGN Channels

M	R-TQAM			S-TQAM			I-TQAM		
	α	K	K_C	α	K	K_C	α	K	K_C
6	$\frac{2}{3.11}$	3	2	$\frac{2}{3.118}$	3	2	$\frac{2}{3.118}$	3	2
8	$\frac{2}{5}$	3.25	3	$\frac{2}{4.5}$	3.25	2.25	$\frac{2}{4.5}$	3.25	2.25
12	$\frac{2}{7}$	3.826	2.911	$\frac{2}{6.906}$	$\frac{23}{6}$	3	$\frac{2}{6.906}$	$\frac{23}{6}$	3
16	$\frac{2}{9}$	$\frac{33}{8}$	$\frac{27}{8}$	$\frac{2}{9}$	$\frac{33}{8}$	$\frac{27}{8}$	$\frac{2}{8.75}$	$\frac{33}{8}$	$\frac{27}{8}$
24	$\frac{2}{15.67}$	$\frac{53}{12}$	$\frac{45}{12}$	$\frac{2}{13.84}$	4.5	$\frac{93}{24}$	$\frac{64}{411}$	4.452	3.826
32	$\frac{2}{17.75}$	$\frac{75}{16}$	$\frac{33}{8}$	$\frac{2}{17.875}$	$\frac{145}{32}$	4	$\frac{2}{17.59}$	$\frac{75}{16}$	$\frac{33}{8}$
48	$\frac{2}{27.3125}$	4.746	4.203	$\frac{2}{26.164}$	4.992	4.513	$\frac{256}{3307}$	4.536	3.828
64	$\frac{2}{37}$	$\frac{161}{32}$	$\frac{147}{32}$	$\frac{2}{37}$	$\frac{161}{32}$	$\frac{147}{32}$	$\frac{8}{141}$	$\frac{163}{32}$	$\frac{75}{16}$
96	$\frac{2}{59.87}$	5.179	4.805	$\frac{2}{55.56}$	5.345	4.993	$\frac{256}{6571}$	5.346	5.014
128	$\frac{2}{72}$	$\frac{339}{64}$	$\frac{159}{32}$	$\frac{2}{74.875}$	$\frac{341}{64}$	$\frac{321}{64}$	$\frac{2}{70.54}$	$\frac{349}{64}$	$\frac{165}{32}$
192	$\frac{2}{118.8}$	5.418	5.150	$\frac{2}{107}$	5.503	5.243	$\frac{128}{6631}$	5.493	5.877
256	$\frac{2}{149}$	$\frac{705}{128}$	$\frac{675}{128}$	$\frac{2}{149}$	$\frac{705}{128}$	$\frac{675}{128}$	$\frac{2}{141}$	$\frac{711}{128}$	$\frac{171}{32}$

where

$$I_1(\bar{\gamma_s}) = \frac{1}{2}\left(1 - \sqrt{\frac{\alpha\bar{\gamma_s}}{2+\alpha\bar{\gamma_s}}}\right), \tag{2.15}$$

$$I_2(\bar{\gamma_s}) = \frac{1}{4} - \frac{1}{\pi}\sqrt{\frac{\alpha\bar{\gamma_s}}{3+\alpha\bar{\gamma_s}}}\ \arctan\left(\sqrt{\frac{3+\alpha\bar{\gamma_s}}{\alpha\bar{\gamma_s}}}\right), \tag{2.16}$$

$$I_3(\bar{\gamma_s}) = \frac{1}{4} - \frac{1}{2\pi}\sqrt{\frac{\alpha\bar{\gamma_s}}{2+\alpha\bar{\gamma_s}}}\ \arctan\left(\sqrt{\frac{6+3\alpha\bar{\gamma_s}}{\alpha\bar{\gamma_s}}}\right) - \frac{1}{2\pi}\sqrt{\frac{\alpha\bar{\gamma_s}}{6+\alpha\bar{\gamma_s}}}\ \arctan\left(\sqrt{\frac{6+\alpha\bar{\gamma_s}}{3\alpha\bar{\gamma_s}}}\right). \tag{2.17}$$

The approximate probability of bit error for TQAM is then obtained as

$$P_b = \frac{G_{P_i}}{J} P_s, \tag{2.18}$$

where G_{P_i} is the Gray penalty with $i = R, I$, and S for R-TQAM, I-TQAM and S-TQAM respectively, and J is the modulation index.

2.3 Performance Results

In this section, the TQAM performance for $6 \leq M \leq 256$ is evaluated over additive white Gaussian noise (AWGN) and Rayleigh fading channels. Simulation results are

Table 2.8: Values of E_b/N_0 for R-TQAM and S-TQAM at BER $= 10^{-4}$

	AWGN		Rayleigh Fading	
M	S-TQAM E_b/N_0 (dB)	R-TQAM E_b/N_0 (dB)	S-TQAM E_b/N_0 (dB)	R-TQAM E_b/N_0 (dB)
6	9.7	9.7	34.1	34.1
8	10.5	10.8	35.2	35.3
12	11.7	11.7	36.5	36.5
16	12.3	12.3	37.2	37.2
24	13.4	13.7	37.5	37.8
32	14.1	14.1	38.7	38.7
48	14.9	15.1	40.1	40.3
64	15.7	15.7	41.7	41.7
96	16.7	17.0	42.1	42.4
128	17.4	17.4	43.8	44.1
192	18.4	18.7	44.7	44.8
256	19.5	19.5	46.4	46.4

presented to verify the analysis given in the previous section. The energy per bit is given by $E_b = E_{Ti}\log_2(M)$, and E_{Ti} is a function of d as given in Table 4.1. Thus for a fair comparison, as M increases, d is decreased by a factor $\frac{1}{\sqrt{E_{Ti}}}$ to have the same value of E_b. For example, the distance between two adjacent symbols with 6 S-TQAM is multiplied by $\frac{2d}{\sqrt{3.11d}}$, while for 192 R-TQAM it is multiplied by $\frac{2d}{\sqrt{107d}}$. For a Rayleigh fading channel, the results are given for $\bar{E}_b$. The bit error probability for TQAM over AWGN and Rayleigh fading channels was obtained using (2.13), (2.14), and (2.18). Table 2.8 gives the values of E_b/N_0 for $P_b = 10^{-4}$ with S-TQAM and R-TQAM, where $N_0 = \alpha\frac{E_{Ti}}{(d/2\sigma)^2}$ [44].

The simulation results for MAP and ML detection of S-TQAM over AWGN channels with $M = 12, 24$ and 48 are shown in Fig. 2.9. Since M is not a power-of-two, the symbols are not equiprobable. The corresponding theoretical results assuming equiprobable symbols are also given. These results show that ML and MAP detection for non-power-of-two S-TQAM provide similar results with a difference of less than 0.01 dB at $P_b = 10^{-4}$. Further, the difference between ML detection and the theoretical results is less than 0.01 dB at $P_b = 10^{-4}$. These results indicate that the the effect of non-equiprobable symbols on the BER is minimal, and confirm the analysis given in the previous section.

The bit error probability for S-TQAM and R-TQAM for $6 \leq M \leq 32$ is shown

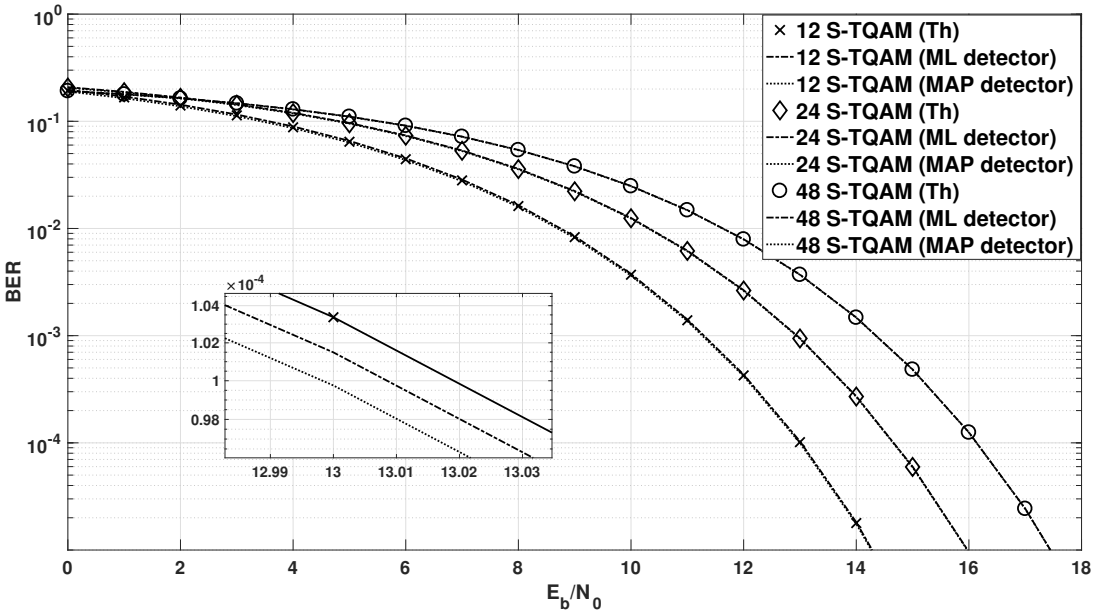

Figure 2.9: Bit error rates for S-TQAM with $M = 12$, 24 and 48 over AWGN channels.

in Fig. 2.10, while Fig. 2.11 gives the corresponding results for $48 \leq M \leq 256$. The simulation results verify the accuracy of (2.13) for AWGN channels. The bit error probability for non-power-of-two S-TQAM lies between the results for power-of-two M-ary S-TQAM, as expected. For example, in Table 2.8, the values of E_b/N_0 to obtain $P_b = 10^{-4}$ with 32, 48 and 64 S-TQAM are 14.1 dB, 14.9 dB and 15.7 dB, respectively. Thus, if $E_b/N_0 = 14.5$ dB and non-power-of-two modulation orders are not used, an adaptive modulation system will choose 32 S-TQAM ($J = 5$) if the bit error probability target is $P_b = 10^{-4}$. However, with non-power-of-two orders, 48 S-TQAM ($J = 5.5$) can be employed, which increases the data rate by 0.5 bit, which shows the advantage of using non-power-of-two modulation orders. In addition, S-TQAM provides better BER performance than R-TQAM, except for $M = 32$ and 128, which is just 0.02 dB worse at $P_b = 10^{-4}$. However, 32 and 128 R-TQAM have a higher detection complexity, as $\mathcal{O}(32R) = 62$ and $\mathcal{O}(128R) = 169$ are higher than $\mathcal{O}(32S) = 49$ and $\mathcal{O}(128S) = 125$.

Fig. 2.12 presents the BER for non-power-of-two S-TQAM and I-TQAM with $24 \leq M \leq 256$. For $M = 6$ and 12, the performance of S-TQAM and I-TQAM is equal because the constellations are the same, while I-TQAM provides better performance for other values of M. The improved performance with I-TQAM is due to the fact that in these cases $E_{TI} < E_{TS}$, so d is larger and hence P_b is lower. This is because

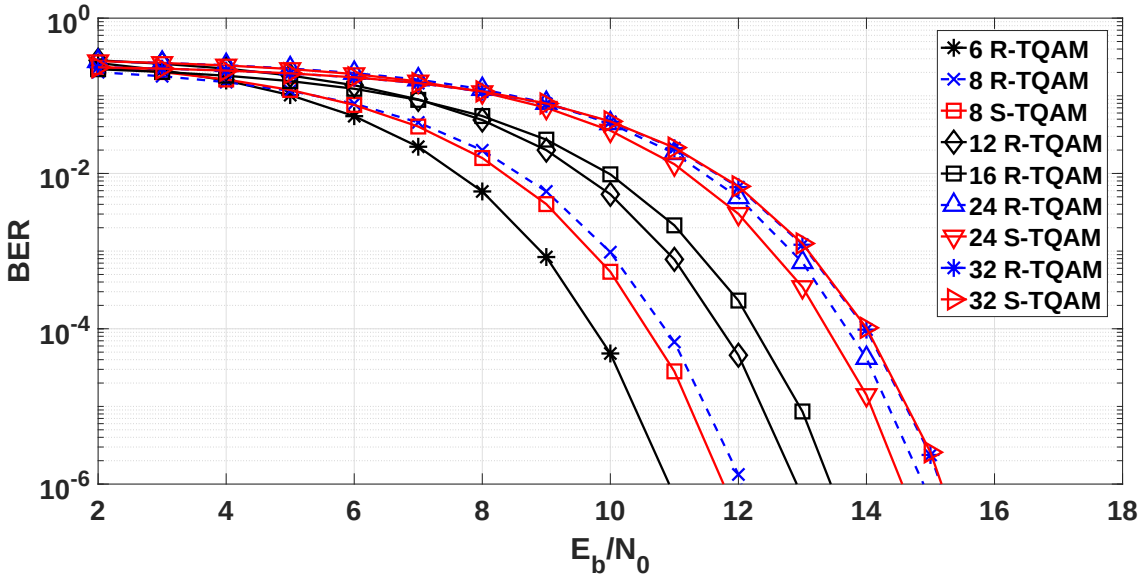

Figure 2.10: Bit error rates for S-TQAM and R-TQAM with $M \leq 32$ over AWGN channels.

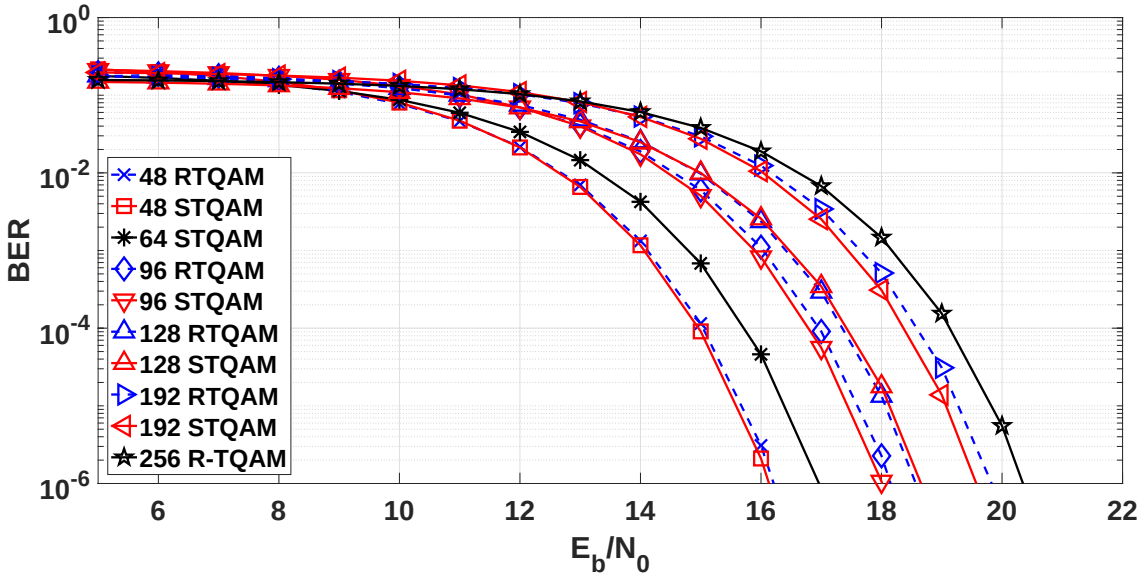

Figure 2.11: Bit error rates for S-TQAM and R-TQAM with $48 \leq M \leq 256$ over AWGN channels.

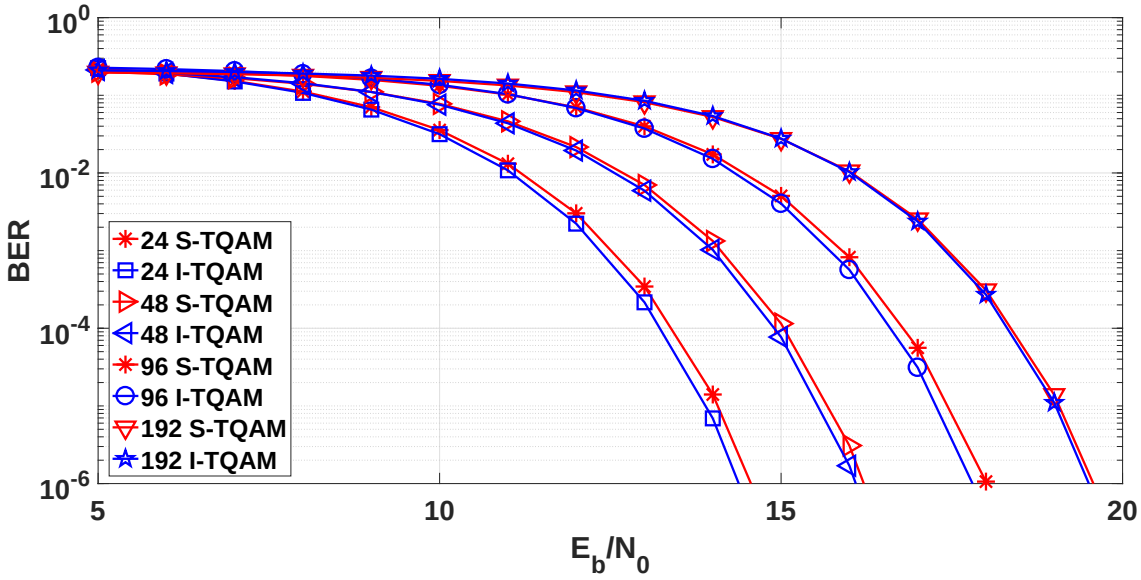

Figure 2.12: Bit error rates for S-TQAM and I-TQAM with non-power-of-two values of M, $24 \leq M \leq 256$ over AWGN channels.

of the more circular shape of the I-TQAM constellation. For example with $M = 48$, I-TQAM is 0.2 dB better than S-TQAM at $P_b = 10^{-4}$. However, from Table 2.5 48 S-TQAM has a lower detection complexity than 48 I-TQAM, i.e. $\mathcal{O}(48S) = 64$ and $\mathcal{O}(48I) = 96$.

There are two factors which should be considered when selecting a TQAM constellation, P_b and $\mathcal{O}(Mi)$. P_b depends on the constellation and the Gray penalty. Fig. 2.13 presents the BER performance of 32, 64 and 192 TQAM. This shows that 32 R-TQAM, S-TQAM and I-TQAM have similar performance. At $P_b = 10^{-4}$, 32 S-TQAM requires an SNR which is 0.01 dB higher than with 32 R-TQAM, and 0.02 dB higher than with 32 I-TQAM. However, from Table 2.5, 32 S-TQAM has a lower detection complexity than 32 R-TQAM and 32 I-TQAM. Therefore, 32 S-TQAM provides the best tradeoff as it has the lowest detection complexity and similar BER performance. For $P_b = 10^{-4}$, the SNR difference between 192 R-TQAM and 192 I-TQAM is 0.35 dB, but the difference between 192 S-TQAM and 192 I-TQAM is only 0.1 dB. The reason is that G_{PI} is higher which negatively affects I-TQAM performance. From Table 2.5, the detection complexity of 192 S-TQAM is close to that of 192 R-TQAM, and is lower than 192 I-TQAM. Thus, the small BER performance difference between 192 S-TQAM and 192 I-TQAM and the similar detection complexity between 192 S-TQAM and 192 R-TQAM means 192 S-TQAM provides a good tradeoff between BER and complexity. Further, 64 R-TQAM and S-TQAM have the

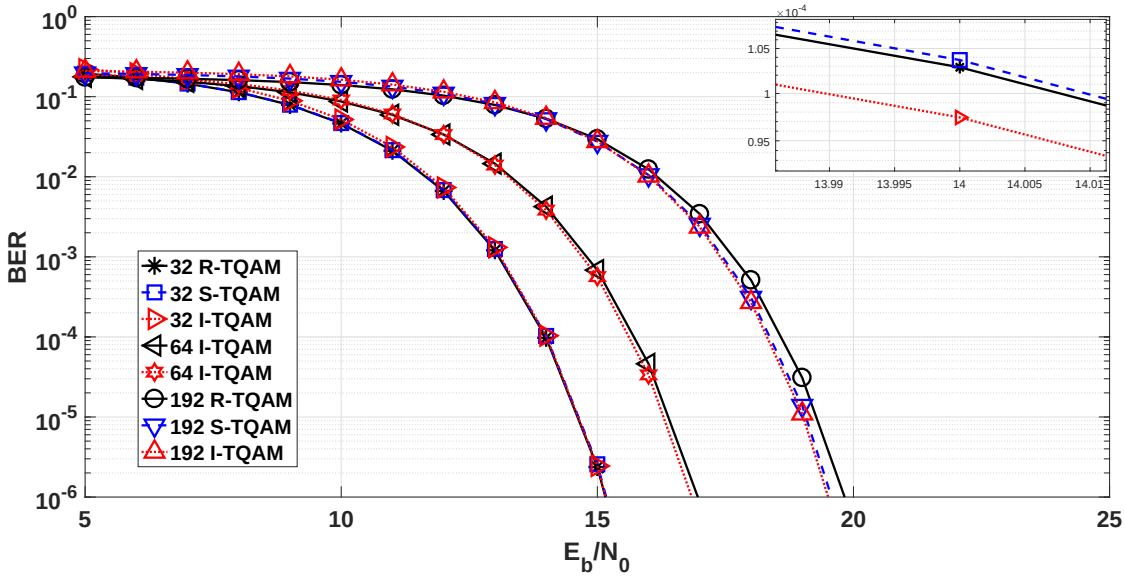

Figure 2.13: BER performance of 32, 64 and 192 TQAM over AWGN channels.

same performance because they have the same constellations and bit mappings, while 64 I-TQAM is 0.15 dB better at $P_b = 10^{-4}$. From Table 2.5, the detection complexity of 64 S-TQAM and R-TQAM is lower than that of 64 I-TQAM, so S-TQAM again provides a favourable tradeoff between performance and complexity.

Fig. 2.14 presents the average BER performance for M-ary S-TQAM and R-TQAM for $6 \leq M \leq 32$ over Rayleigh fading channels, while Fig.2.15 gives the corresponding results for $48 \leq M \leq 256$. The simulation results verify the analysis given in the previous section. Further, they show that S-TQAM provides better average BER performance than R-TQAM except for $M = 32$ and 128 R-TQAM. In addition, similar to the AWGN channel results, the BER with non-power-of-two modulation orders lies between the BER with power-of-two modulation orders. However, the performance differences between R-TQAM, S-TQAM and I-TQAM are smaller compared to those for the AWGN channel.

Fig. 2.16 presents the average BER for 32, 64 and 192 R-TQAM, S-TQAM and I-TQAM over Rayleigh fading channels. These results show that 32 R-TQAM, S-TQAM and I-TQAM have similar performance. At $P_b = 10^{-4}$, 32 S-TQAM requires an SNR 0.02 dB higher than with I-TQAM and 0.01 dB higher than with 32 R-TQAM. However, 32 S-TQAM has a lower detection complexity compared to 32 R-TQAM and 32 I-TQAM. Similar to the results for the AWGN channel, 32 S-TQAM is the best choice. For 64 and 192 TQAM, Fig. 2.16 indicates that S-TQAM provides a good

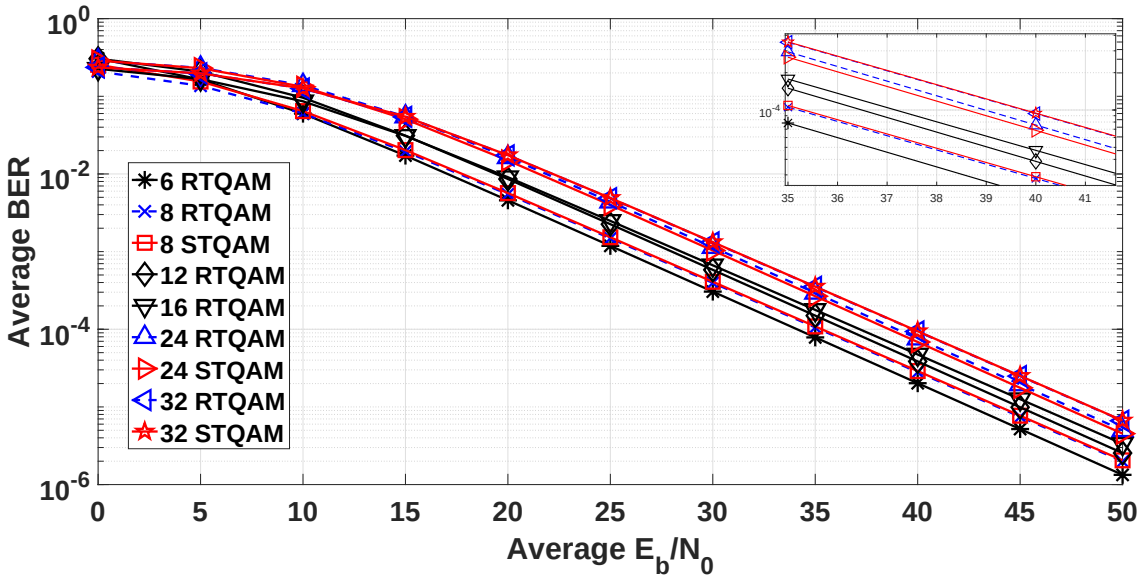

Figure 2.14: BER of R-TQAM and S-TQAM with $M \leq 32$ over Rayleigh fading channels.

tradeoff between complexity and BER performance over Rayleigh fading channels.

2.4 Conclusion

A new type of ternary quadrature amplitude modulation (T-QAM) was introduced called semi-regular TQAM (S-TQAM). In addition, a new mapping methodology for TQAM was presented. This methodology is suitable for both power-of-two and non-power-of-two TQAM, and provides a lower Gray penalty than previous mappings presented in the literature. For most modulation orders M, S-TQAM was shown to have a higher power gain and lower average energy per symbol than R-TQAM with a similar detection complexity. The probability of symbol error and bit error were derived for S-TQAM and verified via simulation. The bit error performance of R-TQAM, I-TQAM and S-TQAM was compared. Results were presented which show that S-TQAM can have better performance than R-TQAM, and is slightly worse than I-TQAM. Thus, S-TQAM provides a good tradeoff between performance and complexity.

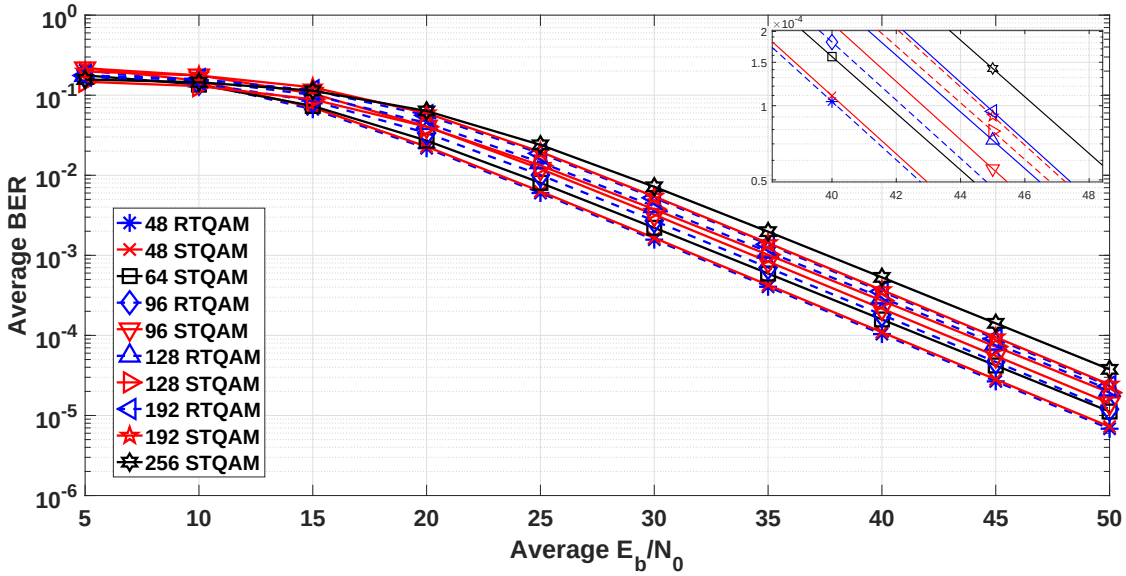

Figure 2.15: BER of R-TQAM and S-TQAM with $48 \leq M \leq 256$ over Rayleigh fading channels.

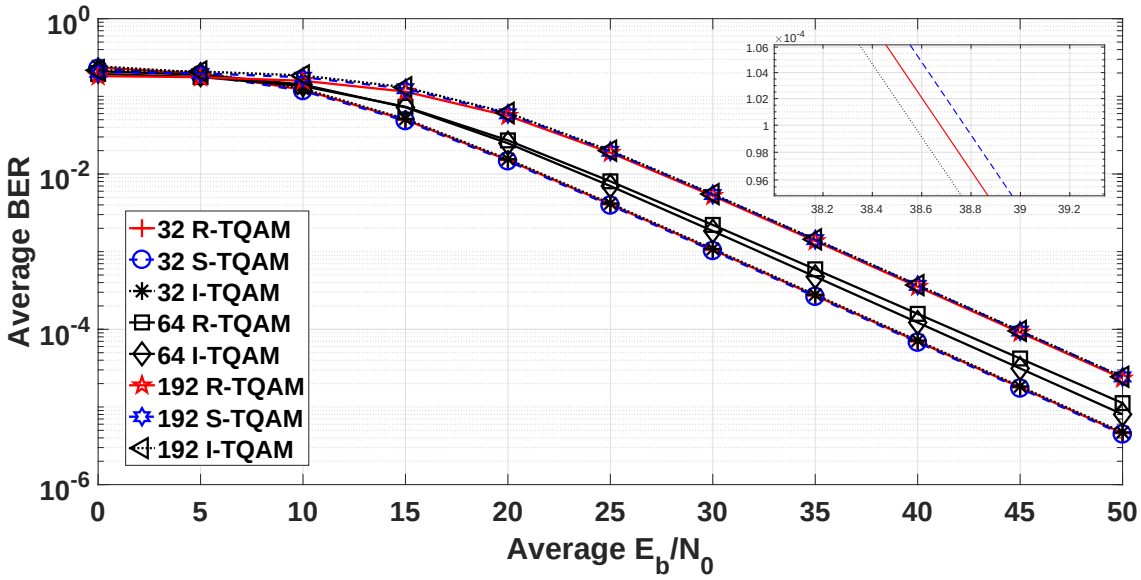

Figure 2.16: BER performance of 32, 64 and 192 TQAM over Rayleigh fading channels.

Chapter 3

Ternary Convolutional Codes

Wireless links are a critical component of many communication systems. Data services including web applications and multimedia are often transmitted over these links, and have different data rate, quality of service (QoS), and delay and rate variability requirements. The growing demand for these services motivates research on improving performance without increasing the complexity. Using ternary symbols is one approach to achieving this goal. The use of ternary systems can reduce the required hardware resources [45], and is considered a promising technology for the future [18]. A ternary symbol carries more information than a binary symbol as one trit equals $\log_2(3) = 1.58$ bits, and ternary phase shift keying (TPSK) modulation requires less bandwidth than binary phase shift keying (BPSK) [25]. In addition, the bit error rate (BER) with TPSK is lower than that with BPSK for the same signal to noise ratio (SNR) [25].

Convolutional codes are used in many practical communication systems. These codes convert the entire data stream into a single codeword. The encoded symbols depend not only on the current input symbols but also on past input symbols. A convolutional code is chosen for a particular application based on parameters such as the code rate R, constraint or memory length m, and free distance d_{free}. In this chapter, ternary convolutional codes with the highest free distance are presented for rates 1/2, 1/3 and 1/4. The performance of these TCCs is compared with that of BCCs from the perspective of memory length, free distance and complexity. Further, it is shown that TPSK is the most suitable modulation for TCCs.

If a TCC is used with binary data, the input bits must first be converted to ternary symbols. Converting binary data to ternary symbols was mentioned briefly in [19]. Converting 11 bits to 7 trits (11B7T) was preferred because of the high efficiency,

but others have suggested a simpler solution which converts 3 bits to 2 trits (3B2T) [20]. It will be shown in this chapter that the conversion employed affects both the efficiency and performance of the communication system.

This chapter is organized as follows. In Section 3.1, BT conversion is considered, and the construction of TCCs is presented in Section 3.2. Section 3.3 presents TCCs with the highest free distance. The advantages of TPSK over BPSK are discussed in Section 3.4. The performance of these codes is investigated in Section 3.5 and compared with the best binary codes. Finally, some conclusions are given in Section 3.6.

3.1 Binary to Ternary Conversion

BT conversion affects both the performance and efficiency of a communication system employing a TCC due to two factors. First, error propagation due to symbol errors at the output of the TCC can result from the ternary to binary conversion. For example, with 11B7T mapping, one trit error may result in 11 bit errors, while with 3B2T mapping, one trit error can produce at most 3 bit errors. The average number of bit errors due to a single trit error, e_{av}, has a significant effect the bit error rate. With mBnT conversion, a ternary string of length n trits has $n \times 2$ ternary string that are different by one trit. For example, with ternary strings of length 2 trits, 11 differs by one trit from the four strings 10, 12, 01, and 21. The number of bit errors due to a single trit error for the ith ternary pattern is

$$T_d(i) = \sum_{j=1}^{2n} T_d(i,j)\,, \tag{3.1}$$

where $T_d(i,j)$ is the number of bit errors due to a trit error between the ith ternary string and the jth ternary string. Therefore, the average number of bit errors with mBnT conversion is

$$e_{av} = \frac{\sum_{i=1}^{3^n} T_d(i)}{3^n \times 2n}\,. \tag{3.2}$$

For example, from Table 2.4, the five ternary strings in the previous example 11, 10, 12, 01, and 21 are mapped to 000, 001, 100, 110, and 011, respectively. Therefore, $T_d(1) = 1+1+2+2 = 6$ bits, and after calculating $T_d(i)$ for the remaining 8 ternary strings $e_{av} = \frac{56}{3^2 \times 4} = 1.555$ bits.

The second factor which affects performance is the conversion efficiency which is

the ratio of the number of input bits l_b in the conversion mapping to the number of output trits l_t expressed in bits [19]

$$\eta = \frac{l_b}{l_t \times \log_2 3}. \tag{3.3}$$

There is a tradeoff between the conversion efficiency and error propagation. For example, $l_b = 84$ and $l_t = 53$ provides a high conversion efficiency of 99.996%, but a poor performance as shown below.

Table 3.1 compares 11B7T conversion, the 3B2T conversion in [20], and the 3B2T conversion in Table 2.4. The comparison is in terms of η and e_{av}. Although the efficiency of 11B7T conversion is highest, both 3B2T conversions have significantly lower e_{av}. This indicates that 3B2T conversion is a better choice. The proposed conversion provides a smaller value of e_{av} than that in [20], and so is employed in the remainder of this letter.

Table 3.1: Binary to Ternary Conversion Comparison

Parameter	11B7T	3B2T [20]	3B2T
η (%)	99.15	94.65	94.65
e_{av}	4.376	1.666	1.555

3.2 Ternary Convolutional Codes

The block diagram of a TCC with TPSK is shown in Fig. 3.1. The serial to parallel block (SP) converts the input serial bits to three parallel bits (b_0, b_1, b_2). These three bits are converted to 2 trits (t_0, t_1) using 3B2T conversion. After conversion, the trits are encoded using a TCC and then each encoded trit is modulated using ternary PSK. The received signal is demodulated and then decoded using a ternary Viterbi decoder. Finally, the decoded trits are converted to bits via 3B2T conversion.

In this chapter, non-systematic, non-recursive convolutional codes are considered as they are the most commonly employed in communication applications [46]. A convolutional code is represented by three parameters (n, k, m) where k and n are the number of input and output data streams, respectively, and m is the encoder memory length. The code rate is $R = k/n$.

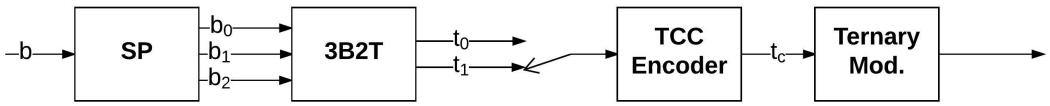

Figure 3.1: Block diagram of a ternary convolutional code with ternary modulation.

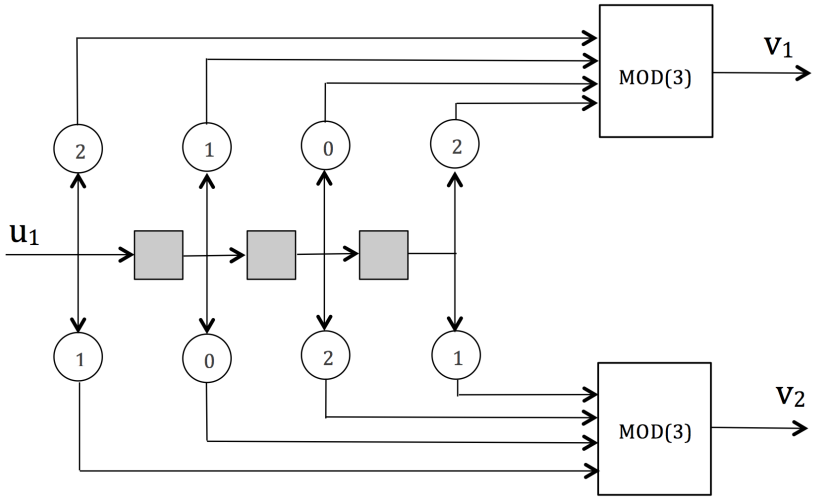

Figure 3.2: A rate 1/2 ternary convolutional encoder.

For a TCC, all encoding and decoding operations are done in the finite field of three elements, GF(3), i.e. modulo 3 arithmetic. A TCC encoder can be implemented using shift registers and modulo-3 adders and multipliers as shown in Fig. 3.2, where the squares are memory elements and the circled numbers are the ternary coefficients that the contents of the memory elements are multiplied by. As there is one input stream u_1 and two output streams v_1 and v_2, the code rate is 1/2. An (n, k, m) TCC can be represented by a $k \times n$ generator matrix $\mathbf{G}(D)$. $\mathbf{G}(D)$ has n generator polynomials $g_i(D)$ each of degree m which can be written as

$$g_i(D) = b_{i,m}D^m + b_{i,m-1}D^{m-1} + b_{i,m-2}D^{m-2} + \cdots + b_{i,0},$$

where $b_{i,j} \in \{0, 1, 2\}$. For example, the code in Fig. 3.2 has $\mathbf{G}(D) = [g_1(D), g_2(D)]$, where $g_1(D) = 2D^3 + D^1 + 2$ and $g_2(D) = D^3 + 2D^2 + 1$.

The complexity associated with a convolutional code is primarily in the decoder. The Viterbi algorithm (VA) [23] is widely employed as it is a maximum-likelihood decoder which has low implementation complexity. For the same values of m, k, and n, a ternary decoder is more complex than a binary decoder.

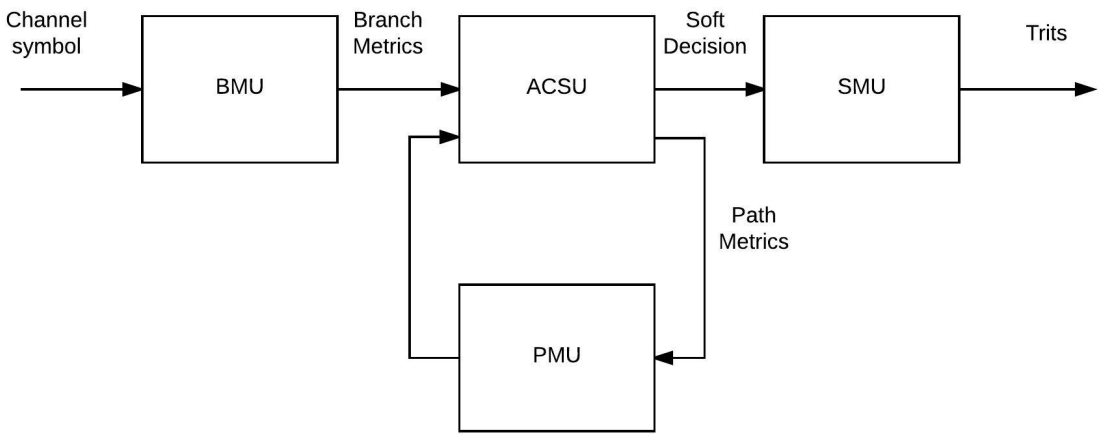

Figure 3.3: Block diagram of the Viterbi decoding algorithm.

A VA decoder has four main components, branch metrics unit (BMU), add-compare-select unit (ACSU), path metric unit (PMU), and select metric unit (SMU) as shown in Fig. 3.3. The SMU decides the trit value from the ACSU output. The BMU and ACSU require arithmetic operations, while the PMU requires only memory operations. The decoder complexity can therefore be divided into two groups, arithmetic operations and memory size.

A convolutional decoder can be represented by a semi-infinite trellis which (apart from a short transient at the beginning) is periodic, with the shortest period section called a trellis module. Fig. 3.4 shows trellis modules for binary and ternary convolutional codes. A binary trellis module consists of edges between the 2^m states, where each state connects to other states via 2^k edges. Therefore, the number of edges in a trellis module is $2^m \times 2^k$. For example, there are 16 edges in the trellis module of a BCC(2,1,3) as shown in Fig. 3.4(a). Each edge is labeled with a binary vector of length n, so the total number of symbols for a binary trellis module is $n \times 2^m \times 2^k$. Thus $n \times 2^{m+k}$ BMU and ACSU operations are required for each binary trellis module [48]. The decoding complexity is then

$$\frac{n \times 2^{m+k}}{k} = \frac{n}{k} \times 2^{m+k} \quad \text{per encoded bit.} \tag{3.4}$$

A ternary trellis module has 3^m states and each state has 3^k edges, so there are 27 edges in the trellis module of a TCC(2,1,2) as shown in Fig. 3.4(b). Therefore the

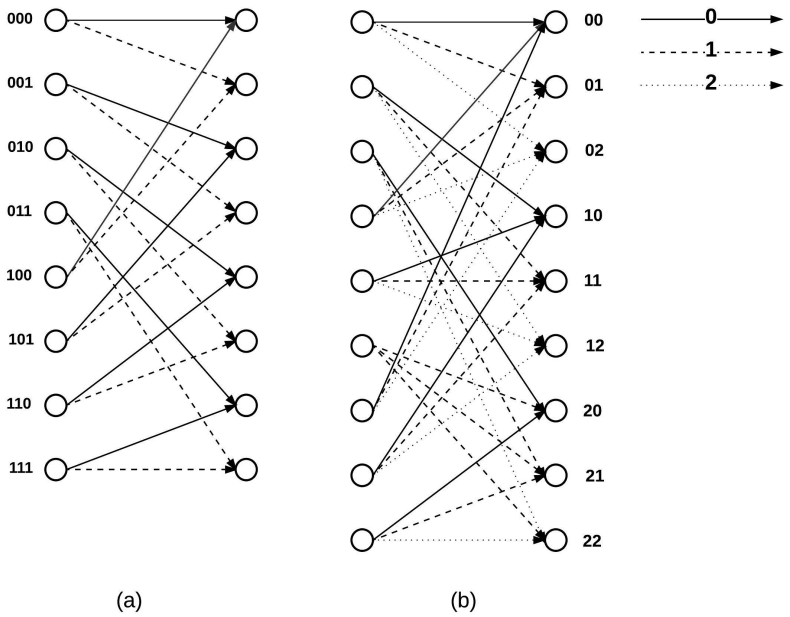

Figure 3.4: A trellis module for (a) binary and (b) ternary convolutional codes.

decoding complexity is

$$\frac{n}{k} \times 3^{m+k} \quad \text{per encoded trit.} \tag{3.5}$$

For comparison purposes, the complexity of a ternary operation is assumed to be similar to that of a binary operation [47]. A $(2, 1, 7)$ BCC is given in the IEEE 802.16 (WiMAX) standard [49]. From (3.4) and (3.5), a $(2, 1, 4)$ TCC has similar complexity.

The PMU has a traceback memory (TM) which keeps track of the survivor paths. The TM requires two memory banks, one to trace paths between states, and the second to write new survivor paths. For a BCC, each bank is L_b bits long and has 2^m states [50]. Therefore, the TM size for a BCC is

$$2 \times L_b \times 2^m \text{ binary memory cells.} \tag{3.6}$$

For a TCC, each bank is L_t trits long and has 3^m states, so the TM size is

$$2 \times L_t \times 3^m \text{ ternary memory cells.} \tag{3.7}$$

From (3.6) and (3.7), if the input data has length 99 bits, $L_b = 99$, and after converting bits to trits using 3B2T conversion, $L_t = 66$ trits. The TM size for a $(2, 1, 7)$ BCC is $25,344$ BMCs, while for a $(2, 1, 4)$ TCC it is $10,692$ TMCs. The size of a ternary

memory cell can be considered twice that of a binary memory cell [51], so the TM size for this TCC is $21,384$ BMCs. Thus the TM complexity of these codes is similar.

3.3 Code Search

The main parameter which affects the performance of a convolutional code is the free distance d_{free}, as this determines the error correction capability. The free distance is defined as [52]

$$d_{free} \triangleq \min_{\mathbf{u}'\mathbf{u}''}\{w(\mathbf{v}' + \mathbf{v}'') : \mathbf{u}' \neq \mathbf{u}''\}, \tag{3.8}$$

where $\mathbf{v}'$ and $\mathbf{v}''$ are the codewords corresponding to the input data sequences $\mathbf{u}'$ and $\mathbf{u}''$, respectively. d_{free} is the minimum Hamming weight of all codewords produced by finite length input sequences [52].

TCCs with maximum d_{free} were found by exhaustive search using all combinations of generator polynomials for $k = 1$ and $n = 2, 3, 4$. Many algorithms have been developed to find BCCs with maximum free distance, such as the approach in [53]. The algorithm employed here was designed to obtain one code with the maximum free distance. Weight calculations are done as each trit is input, and generator polynomials that produce low weight codewords are immediately discarded. This significantly reduces the time required to find the best codes. The number of candidate generator polynomials $g(D)$ was reduced by considering only polynomials of the form $g(D) = b_m D^m + b_{m-1}D^{m-1} + b_{m-2}D^{m-2} + \cdots + b_0$, where $b_m \in \{1, 2\}$, $b_0 \in \{1, 2\}$ and the remaining $b_i \in \{0, 1, 2\}$ as noted in [54, 55].

The algorithm has two steps, one to determine the minimum weight codewords for the trit inputs $\mathbf{u}$, and another to find the maximum d_{free} over all combinations of $\mathbf{G}(D)$. For each candidate set of generator polynomials $\mathbf{G}(D)$, all $3^{l_k} - 1$ nonzero ternary input sequences $\mathbf{u}$ of length l_k trits were considered, where $l_k = m + 1$ as in [53]. Denote the weight of the first nonzero codeword as d. For the remaining inputs, d is compared with the current weight. If this weight is larger than d, the encoding process is stopped and the next input is encoded. If the resulting weight is less than d, this becomes the new value of d. After all input trit sequences have been encoded, $d_{free} = d$. In the second part of the algorithm, d_{free} from the first candidate $\mathbf{G}(D)$ is set as the current maximum d_{free}. Then d_{free} from subsequent $\mathbf{G}(D)$ are compared with this value, and if it is larger, it becomes the new maximum d_{free}. Once all candidate $\mathbf{G}(D)$ have been considered, the maximum d_{free} of an (n, k, m) TCC has

Table 3.2: Maximum Free Distance TCCs for $R = \frac{1}{2}$

m	$g_1(D)$	$g_2(D)$	d_{free}	d^b_{free}
1	[1 1]	[1 2]	4	-
2	[1 1 2]	[2 1 1]	6	5
3	[2 2 1 1]	[1 2 1 1]	7	6
4	[1 1 2 0 1]	[1 2 1 1 1]	9	7
5	[2 2 1 1 0 1]	[1 2 2 1 0 1]	10	8
6	[1 2 2 1 2 0 1]	[1 1 2 0 1 1 1]	12	10
7	[1 0 1 1 0 2 0 2]	[1 0 1 1 1 1 1 2]	13	10
8	[1 1 2 2 2 2 0 2 1]	[1 0 1 2 1 1 2 0 2]	14	12
9	[1 2 2 1 0 2 1 0 0 1]	[2 2 1 1 0 0 1 1 2 2]	15	12

Table 3.3: Maximum Free Distance TCCs for $R = \frac{1}{3}$

m	$g_1(D)$	$g_2(D)$	$g_3(D)$	d_{free}	d^b_{free}
1	[1 2]	[1 1]	[1 1]	6	-
2	[1 1 1]	[1 1 2]	[1 2 1]	9	8
3	[1 0 1 1]	[1 1 1 1]	[1 2 1 2]	11	10
4	[1 0 1 0 1]	[1 1 2 2 2]	[1 1 2 2 1]	13	12
5	[1 0 1 0 0 1]	[1 2 2 2 1 1]	[2 1 1 1 2 1]	15	13
6	[1 2 1 2 2 1 2]	[1 0 1 0 1 2 2]	[1 2 1 2 2 1 2]	18	15
7	[2 2 1 1 0 1 0 1]	[2 1 2 2 1 1 2 1]	[1 1 0 2 2 0 1 2]	20	16

been found.

The search results for the best non-systematic non-recursive TCCs are shown in Table 3.4 for rates $R = 1/2$, $1/3$, and $1/4$, and different memory sizes. All TCC codes in Table 3.4 are non-catastrophic [52]. The values of d_{free} are also given in the table. As expected, the maximum d_{free} increases as the memory size m increases. In all cases, the maximum d_{free} for a TCC is greater than that for a BCC with the same parameters [53]. Further, the best free distances of the codes obtained for $n = 2$ and m up to 6 and $n = 3, 4$ and m up to 5 are the same as those given in [56], and the codes were determined to have the same performance. The remaining codes in Table 3.4 are new.

3.4 Ternary PSK

TPSK has an equilateral triangle shape as shown in Fig. 3.5(a). The distance from a TPSK symbol to the origin is A_3, where A_3 represents the signal amplitude. The

Table 3.4: Maximum Free Distance TCCs for $R = \frac{1}{4}$

m	$g_1(D)$	$g_2(D)$	$g_3(D)$	$g_4(D)$	d_{free}	d^b_{free}
1	[1 2]	[1 1]	[1 1]	[1 1]	8	-
2	[1 1 1]	[1 1 1]	[1 2 1]	[2 1 2]	12	10
3	[1 0 1 1]	[1 1 1 1]	[1 1 2 1]	[1 2 1 2]	15	13
4	[1 2 0 1 1]	[1 0 1 1 2]	[2 1 2 1 2]	[2 2 2 2 2]	18	16
5	[1 2 2 2 1 2]	[1 0 2 1 2 2]	[2 2 1 1 0 1]	[2 2 1 1 0 1]	21	18
6	[1 1 0 2 2 2 2]	[1 2 2 1 2 0 1]	[1 0 2 1 2 2 2]	[1 2 2 1 2 0 1]	24	20

distance between symbols is then

$$d_{3min} = \frac{\sqrt{3}}{2} A_3. \tag{3.9}$$

To compare TPSK and BPSK, the average energy per bit for TPSK should equal the average energy per bit for BPSK. If 3B2T conversion is used, each trit represents 1.5 bits. From Fig. 3.5 and (3.9), the average energy per bit for TPSK is

$$E_{TPSK} = \frac{1.5A_3^2 + 1.5A_3^2}{3 \times 1.5} = \frac{4}{4.5} d_{3min}^2. \tag{3.10}$$

If $E_{TPSK} = E_{BPSK}$, since $E_{BPSK} = \frac{2d_{2dim}^2}{2} = d_{2dim}^2$, then

$$\begin{aligned} d_{3min} &= \sqrt{\frac{4.5}{4}} d_{2min} \\ &= 1.06 d^2, \end{aligned} \tag{3.11}$$

where d_{2min} is the minimum distance between BPSK constellation points as shown in Fig. 3.5(b). This indicates that the minimum distance between TPSK constellation points is larger than with BPSK for the same average bit energy. TPSK has a power efficiency which is $20 \log_{10}(1.06) = 0.5$ dB larger than with BPSK.

3.5 Performance Results

The performance of TCCs with TPSK modulation is obtained for a system with binary inputs and binary outputs using Monte Carlo simulation. The input bits are converted to ternary symbols using the mapping in Table 2.4. With TPSK, the elements of GF(3), $0, 1, 2$, are mapped to $\{iA, -\frac{\sqrt{3}A}{2} - i\frac{A}{2}, \frac{\sqrt{3}A}{2} - i\frac{A}{2}\}$ respectively.

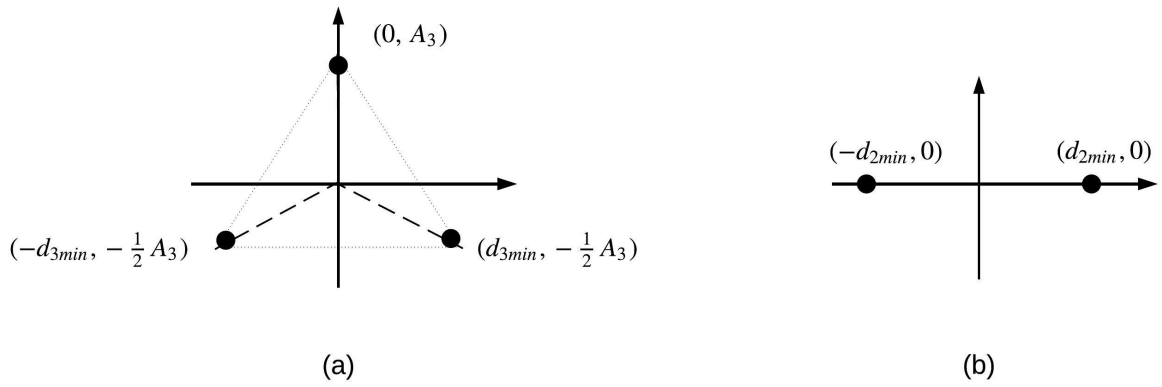

Figure 3.5: The constellation points of (a) TPSK and (b) BPSK.

For the same bit energy with BPSK, the bits are mapped to $\pm\sqrt{1.5}A_3$. Thus, the minimum distance between TPSK constellation points is greater than that of BPSK by a factor of $\frac{\sqrt{3\times1.5}}{2}$ for the same bit energy as shown in Fig. 3.7.

The soft ternary symbol information after demodulation is input to a soft decision (SD) VA decoder. It finds the maximum likelihood path through the trellis as noted in [25, 52]. For simulation purposes, the SD VA decoder employs double precision floating point arithmetic. With a TCC, the decoded ternary symbols are converted to binary data using Table 2.4. For comparison purposes, BCCs with maximum d_{free} from [53] are also considered with TPSK. In this case, the binary inputs are encoded and then converted to ternary symbols for TPSK modulation. The received ternary symbols are demodulated and then converted to binary before VA decoding. Both the BER and frame error rate (FER) are obtained for an additive white Gaussian noise (AWGN) channel. The signal to noise ratio is E_b/N_0 where E_b is the energy per bit and N_0 is the noise power spectral density (PSD).

Figure 3.7 presents the BER performance of TPSK with 11B7T conversion and 3B2T conversion, and uncoded BPSK and TPSK with no conversion. Without conversion, TPSK is 0.5 dB better than BPSK at BER = 10^{-5} [25]. As expected, the 3B2T conversion in [20] and 11B7T conversion results in a higher BER than the best 3B2T conversion given here. In particular, the 11B7T conversion performance is 1 dB worse at BER = 10^{-5}. This shows the impact of error propagation on the BER. Further, the 3B2T conversion presented here has approximately the same performance as TPSK without conversion. The performance of the proposed 3B2T conversion is better than with the conversion in [20] because e_{av} is lower.

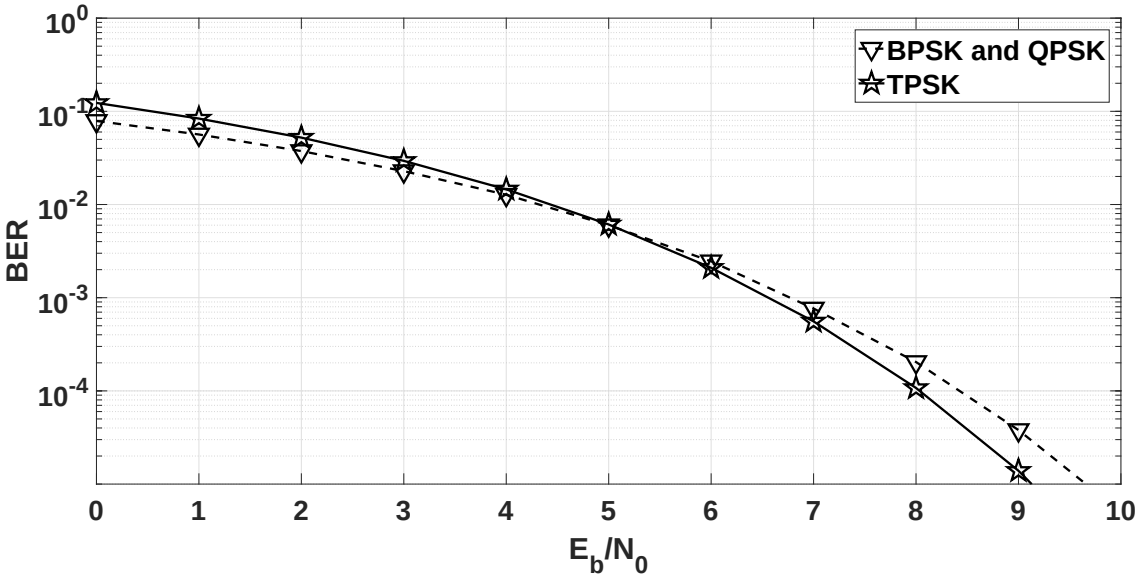

Figure 3.6: BER performance for BPSK and TPSK over an AWGN channel.

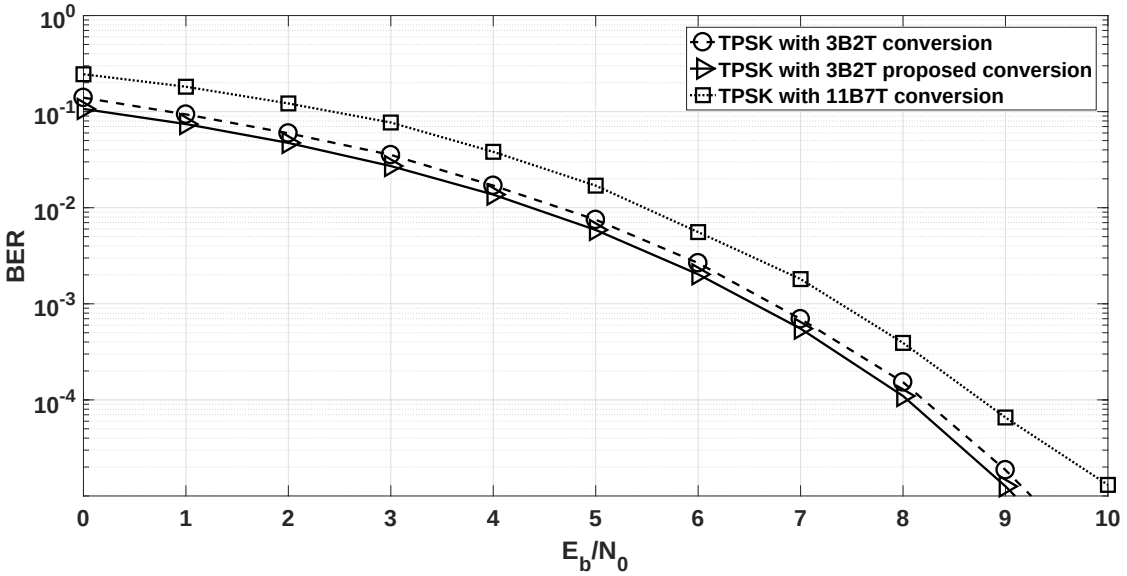

Figure 3.7: BER performance for TPSK with 3B2T, proposed 3B2T, and 11B7T conversion over an AWGN channel.

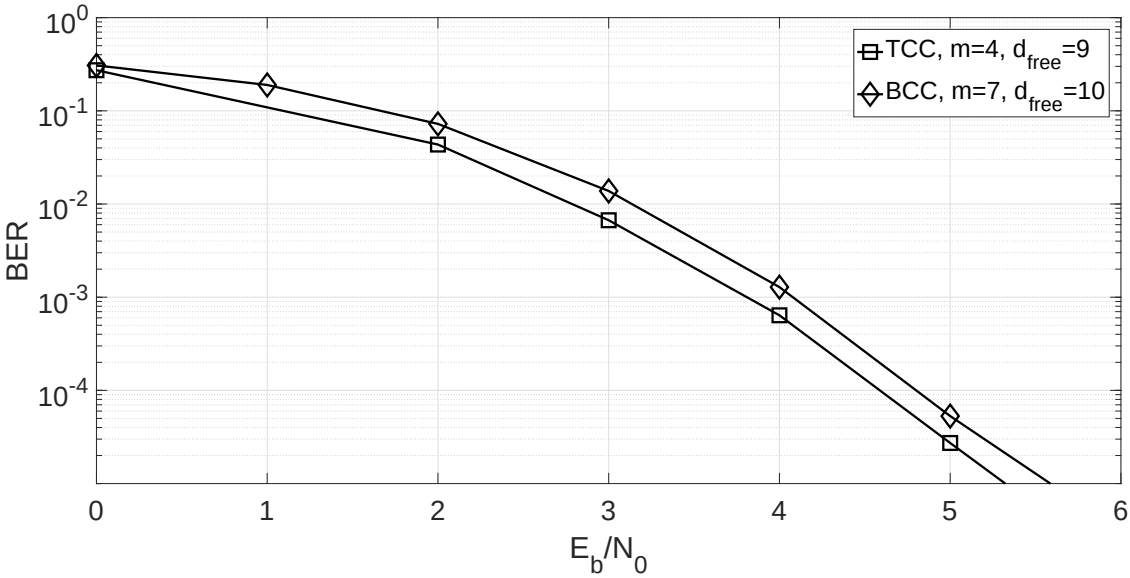

Figure 3.8: BER performance for (2,1,4)TCC with TPSK and (2,1,7)BCC with BPSK over an AWGN channel.

Figure 3.8 presents the BER performance of the $(2, 1, 4)$ TCC with TPSK and the $(2, 1, 7)$ BCC with BPSK. While these codes have similar complexity, the TCC has $d_{free} = 9$ while the BCC has $d_{free} = 10$. The BER with this TCC is slightly better than that of the BCC (0.3 dB at BER $= 10^{-5}$). This is partly due to the fact that the BER with TPSK modulation is better than that with BPSK, as noted above.

The performance of the $(2, 1, 3)$ BCC with BPSK and the $(2, 1, 2)$ TCCs with TPSK is given in Figure 3.9. The $(2, 1, 2)$ TCC has $3^2 = 9$ states while the $(2, 1, 3)$ BCC has $2^3 = 8$ states, and both codes have $d_{free} = 6$. The performance of this ternary code is better than that of the binary code by 0.5 dB at BER $= 10^{-5}$ because they have the same d_{free} but there is a gain due to TPSK modulation.

Figure 3.8 presents The $(2, 1, 3)$ TCC has $d_{free} = 6$ and the $(2, 1, 3)$ BCC has $d_{free} = 5$, and both codes have the same $m = 3$. The performance of the ternary code is better than that of the binary code by 0.9 dB at BER $= 10^{-5}$, partly because it has a larger d_{free}.

Figure 3.11 presents the FER of TCCs with TPSK and BCCs with TPSK and BPSK. The frame length is 99 bits, and after 3B2T conversion this becomes 66 trits. To compare the performance of the BCC with TPSK and the TCC with TPSK, hard decision (HD) VA decoders are employed with the Hamming distance. The results in the figure show that the performance of the $(2, 1, 2)$ TCC is better than that of the $(2, 1, 3)$ BCC by 1.9 dB at FER $= 10^{-5}$. This is because converting ternary symbols

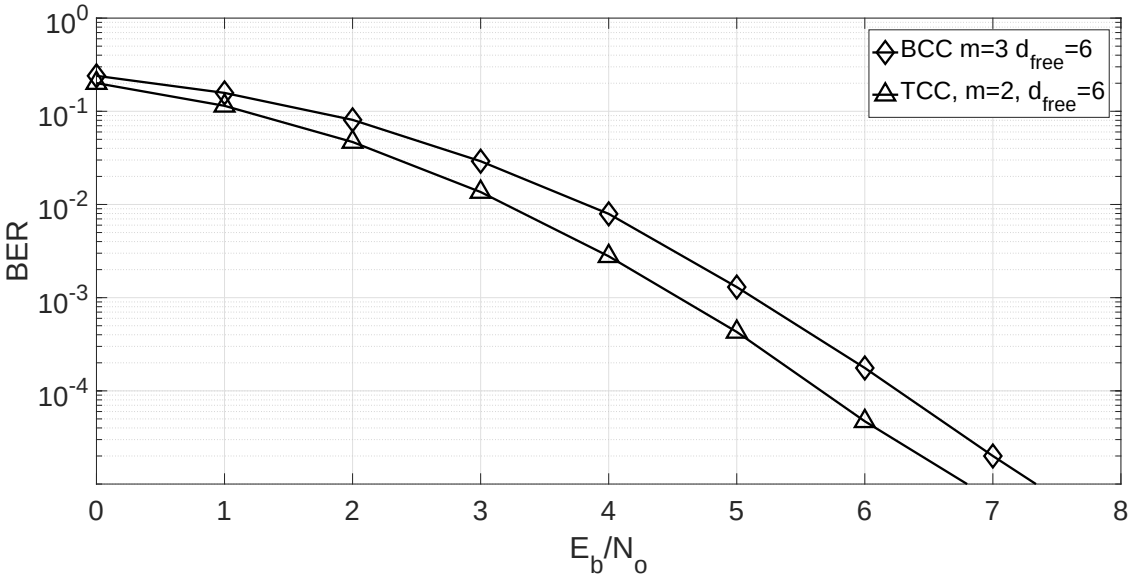

Figure 3.9: BER performance of (2,1,2) TCC with TPSK, and (2,1,3) BPSK with BCC over an AWGN channel.

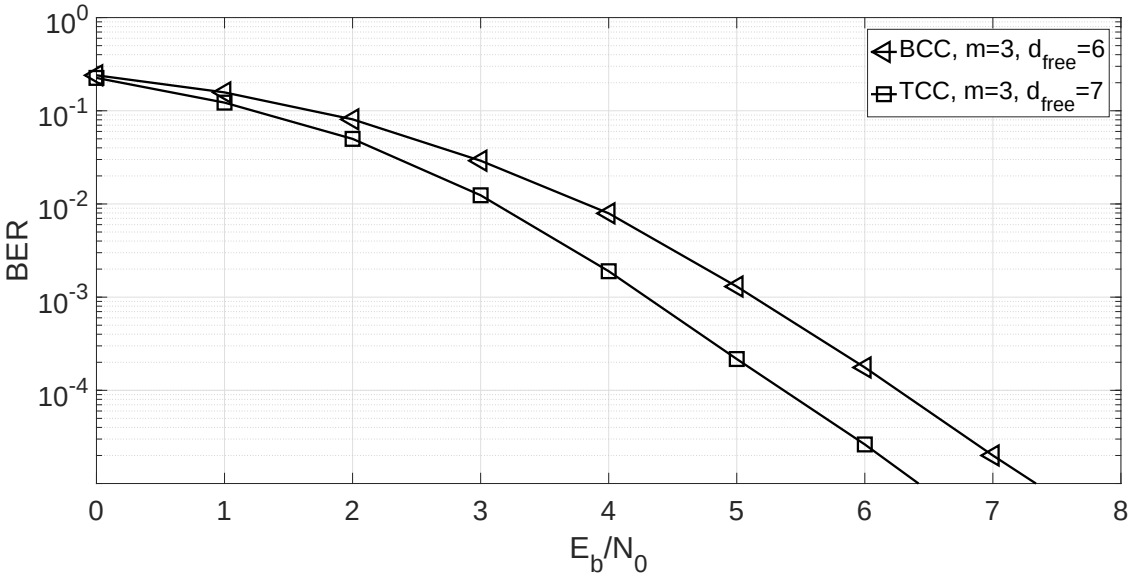

Figure 3.10: BER performance of (2,1,3) TCC with TPSK, and (2,1,3) BPSK with BCC over an AWGN channel.

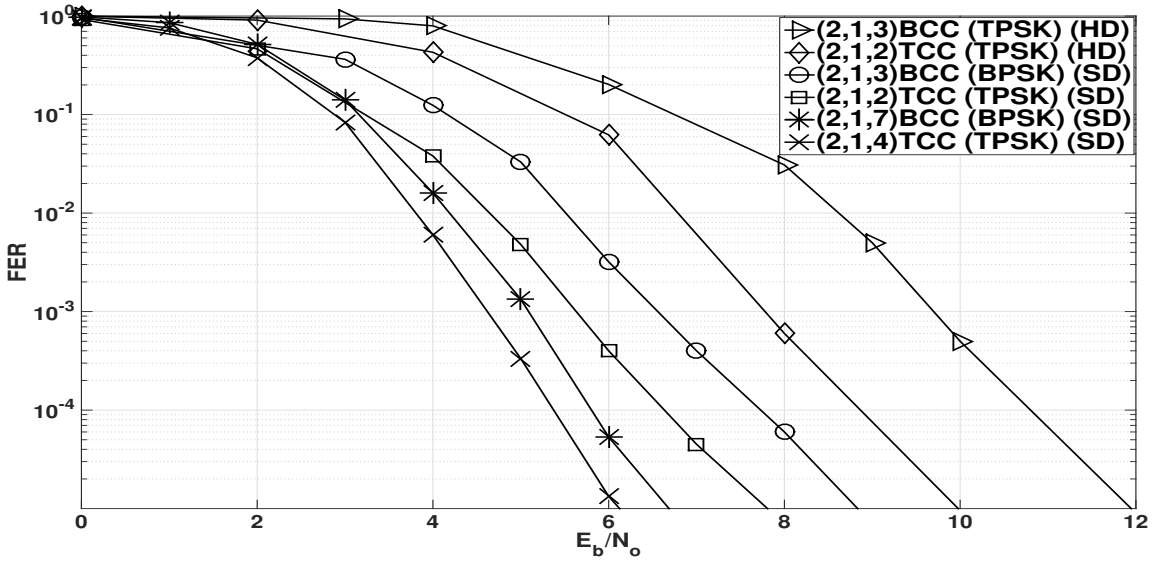

Figure 3.11: FER Performance of a TCC with TPSK, and a BCC with TPSK and BPSK.

to binary data before the decoder increases the number of errors, while with a TCC the conversion is done after the decoder so there is less error propagation. In addition, the FER of the $(2, 1, 2)$ TCC with SD decoding is 2 dB better than with HD decoding. With SD VA decoding and the same free distance $d_{free} = 6$, the performance of the (2,1,2) TCC with TPSK is better than that of the (2,1,3) BCC with BPSK by 1.1 dB at FER $= 10^{-5}$. Considering larger codes with similar complexity, the $(2, 1, 4)$ TCC with TPSK is 0.4 dB better than the $(2, 1, 7)$ BCC with BPSK at FER $= 10^{-5}$.

The bit error probability for power-of-three M-ary S-TQAM for $M = 9$, 27 and 81 is shown in Fig.3.12. The simulation result is verify the accuracy of (2.13) for AWGN channel. Fig.3.12 represents the comparison among power-of-two and non-power-of-two and power-of-three modulation orders. As expected 8, 24 and 27 S-TQAM have a higher performance than 9, 27 and 81 S-TQAM, respectively. At $P_b = 10^{-4}$, the 9, 27 and 81 S-TQAM are lower BER performance than 8, 24 and 27 S-TQAM by 0.3 dB, 0.3 dB and 0.7 dB, respectively.

3.6 Conclusion

In this chapter, ternary convolutional codes (TCCs) with code rates $R = 1/2$, $1/3$ and $1/4$ were obtained which have the maximum possible free distance d_{free}. The conversion from binary data to ternary symbols was considered, and the best three

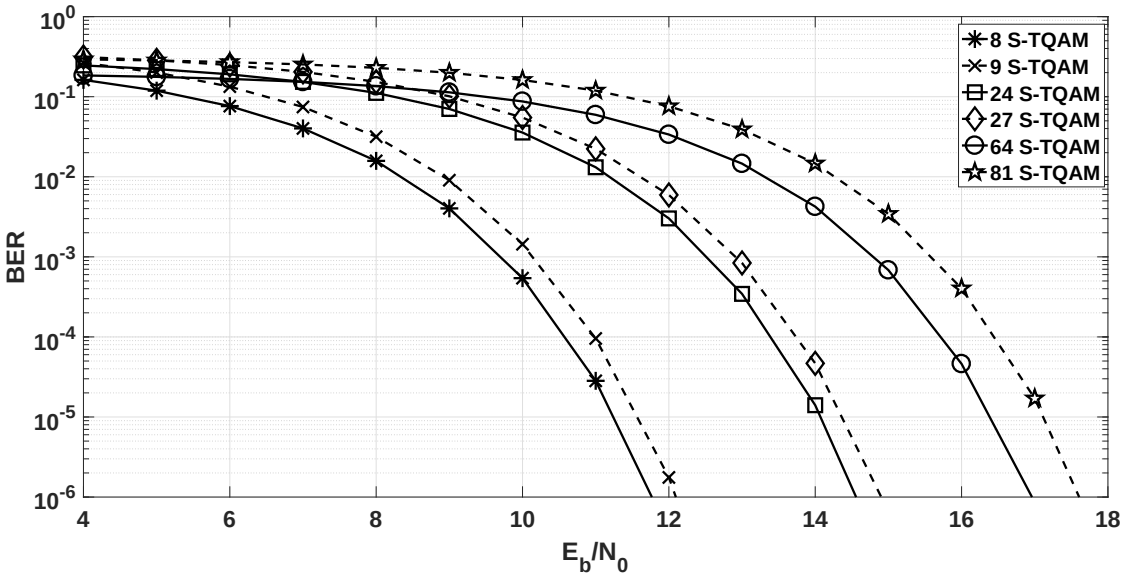

Figure 3.12: BER Performance for power-of-three, power-of-two and non-power-of-two S-TQAM over AWGN channels.

bits to two trits (3B2T) conversion was determined. It was shown that a BCC is not compatible with TPSK modulation because of the error propagation with ternary to binary symbol conversion before decoding. The best TCCs and BCCs were compared in terms of memory length, free distance, and complexity. It was found that TCCs with TPSK provide better BER and FER performance over AWGN channels than BCCs with BPSK and TPSK.

Chapter 4

Ternary Trellis Coded Modulation

4.1 Introduction

Ungerboeck proposed a technique called trellis coded modulation (TCM) which can efficiently provide high data rates over bandwidth limited channels [26]. TCM is employed in communication systems such as IEEE 802.16, CATV, HDTV and DSL [58], as well as optical communications [59] and cooperative communications [60]. To provide the redundancy necessary for coding, the signal constellation is expanded rather than increasing the bandwidth. TCM combines a trellis code with modulation so at the receiver decoding and demodulation are combined [26]. The performance with TCM depends on the minimum distance between constellation symbol sequences, which is called the free Euclidean distance. For the same transmit power, the free Euclidean distance with TCM can be larger than the minimum Euclidean distance between symbols of the uncoded (smaller) constellation, which results in a lower bit error rate (BER). Therefore, the goal is to maximize the free Euclidean distance.

The signal constellation plays an important role in the power efficiency and BER performance of a communication system. The power efficiency depends on the distances between the points in the signal constellation and the origin. Square quadrature amplitude modulation (SQAM) was proposed in [5] and is commonly employed because of its simple structure [61]. Subsequently, several signal constellations such as triangular, pentagonal and hexagonal [6] were examined which have better power efficiency than SQAM. However, these constellations have higher detection complexity. The highest power efficiency constellations without a point at the origin were presented in [33]. However, the irregularity of these constellations makes detection

very complex [33]. In [7], triangular QAM (TQAM) was introduced which has signal points from a triangular lattice. TQAM has a power efficiency which is close to optimum and higher than SQAM, but SQAM has a lower detection complexity. TQAM provides a good tradeoff between BER and detection complexity [7], and so is considered here for TCM.

Ungerboeck introduced a mapping for TCM that maximizes the minimum distance between symbol sequences [62]. This mapping labels the constellation symbols using set partitioning. Set partitioning initially divides the constellation symbols into two subsets. In subsequent levels, each subset is divided into two new subsets. The last level is reached when each subset has two symbols. This is called binary set partitioning (BSP) and is based on two rules [63]. First, all subsets have an equal number of constellation points. Second, coded symbols originating from the same state or merging into the same state in the trellis are assigned in the same subsets. With SQAM or phase shift keying (PSK), BSP increases the minimum Euclidean distance within the subsets in each partitioning level [64]. However, this property of BSP does not hold with TQAM because of the triangular structure of TQAM which results in symbols having more nearest neighbors on average than with SQAM. To solve this problem, ternary set partitioning (TSP) is introduced here. This solution results in an increase in the Euclidean distance within the subsets each partitioning level. Thus, in this work TSP is employed with TQAM constellations.

TCM with TQAM uses TSP for the mapping, so the constellation symbols are labeled with trits, i.e. $\{0, 1, 2\}$. Therefore, ternary arithmetic and ternary logic must be employed. Ternary systems have been shown to be faster than binary systems [65, 45]. Further, ternary systems can be implemented in hardware more efficiently than for any other integer base [45], and can provide higher data storage densities [45]. Binary TCM (BTCM) employs a binary convolutional code [26], but TCM with TQAM operates on a ternary alphabet so a ternary convolutional code should be employed. Ternary convolutional codes (TCCs) have been shown to provide better BER performance than binary convolutional codes (BCCs), for the same blocklength and complexity. Here, TCM with a TCC is called ternary trellis coded modulation (TTCM).

Although ternary systems have several advantages over binary systems, commercial communication systems operate with binary data. Therefore, the performance of TTCM must be evaluated considering binary inputs and binary outputs. This requires that binary data be converted to ternary data (trits) before encoding. Then

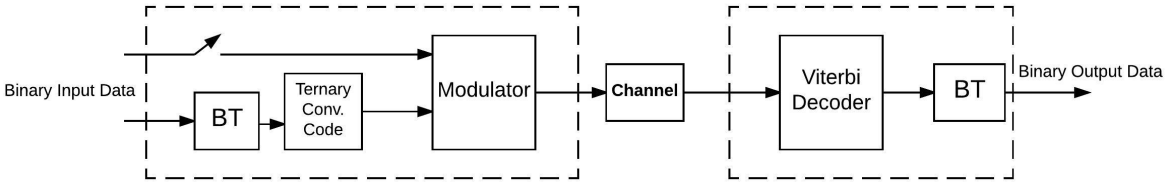

Figure 4.1: Block diagram of a ternary trellis coded modulation (TTCM) system.

after TTCM decoding, the output trits must be converted to bits. Binary to ternary (BT) conversion was considered in [20, 16]. With BT conversion, one trit error at the output may cause more than one bit error. Thus, the conversion should be designed to minimize these bit errors.

The block diagram of a TTCM system is shown in Fig. 4.1. First, binary input data is converted to ternary data and then encoded by the TCC. The encoded symbols along with uncoded binary or/and ternary data are mapped to symbols in the signal constellation. These symbols are then transmitted over the channel. In this dissertation, additive white Gaussian noise (AWGN) and Rayleigh fading channels are considered. At the receiver, the received signals are demodulated and decoded using a soft decision ternary Viterbi decoder [46]. Finally, the resulting trits are converted to bits.

The rest of the chapter is organized as follows. In Section 4.2, signal constellations are examined, and the advantages of triangular constellations are discussed. Section 4.3 introduces BTCM with SQAM and considers BTCM with TQAM. Section 4.4 presents TSP for TQAM and analysis the TTCM. Further, the construction of TQAM constellations which are compatible with TSP (denoted C-TQAM), is presented and the corresponding BT conversion is investigated. Performance and simulation results are given in Section 4.5 to illustrate the advantages of TTCM over BTCM.

4.2 Signal Constellations

The structure and shape of the signal constellation have a significant impact on the modulation power efficiency which can be expressed as [66]

$$\eta_P = \frac{d_{min}}{E_b}, \tag{4.1}$$

where E_b is the average bit energy and d_{min} is the minimum Euclidean distance between constellation symbols. A better power efficiency means a lower E_b and/or larger d_{min}. Signal constellations with points close to the origin will have a low E_b, but a small distance between symbols. Thus, maximizing the power efficiency of a signal constellation is a tradeoff between minimizing E_b and maximizing d_{min}. A larger d_{min} results in a lower BER, so the constellation should have a large d_{min}. Consider the 16 PSK and 16 SQAM constellations shown in Figs. 4.2(a) and 4.2(b), respectively. With 16 PSK, $d_{min} = 2\sqrt{E_S}\sin(\frac{\pi}{16})$, while for 16 SQAM, $d_{min} = 2\sqrt{\frac{E_S}{10}}$, where $E_S = E_b \log_2 M$ [66]. For the same value of E_S, the distance between 16 SQAM symbols is 1.62 times larger than 16 PSK symbols. This implies that for the same BER, 16 SQAM requires a signal to noise ratio (SNR) $20\log_{10}(1.62) = 4.19$ dB less than 16 PSK [66].

It has been shown that TQAM, which has constellation points from a triangular lattice, provides a larger d_{min} than SQAM, which has points from a square lattice [7, 67]. Thus for the same average symbol energy and number of constellation points (called the modulation order M), TQAM has better BER performance than SQAM [7]. Fig. 4.2 shows the constellations of 16 TQAM, 16 SQAM and 16 PSK. For TQAM, the points on the edge of the constellation have at least two nearest neighbors (NNs), while the middle points have six NNs. Further, these points do not lie on lines parallel to the axes. Therefore for a given M, TQAM has a higher detection complexity than SQAM because it has a more complex structure and a larger average number of NNs [41]. For example, the average number of nearest neighbors for 16 SQAM is $NN = 3$, but for 16 TQAM it is $NN = 4.125$. The ML detection of TQAM was considered in [7, 30], and shown to be higher than that of SQAM for all M.

Regular TQAM (R-TQAM) and irregular TQAM (I-TQAM) were introduced in [7, 30] and the constellations for $M = 16$ are shown in Figs. 4.2(c) and 4.2(d), respectively. R-TQAM has a symmetric constellation about the origin, while the I-TQAM constellation is more irregular. The power efficiency of I-TQAM is higher than that of R-TQAM, but it has a higher detection complexity [30]. For 16 R-TQAM, $d_{min} = 2\sqrt{\frac{E_S}{9}}$, while for 16 I-TQAM, $d_{min} = 2\sqrt{\frac{E_S}{8.75}}$, which is 1.054 and 1.069 times that of 16 SQAM for the same E_S, respectively [7, 30]. Therefore for the same BER, 16 R-TQAM and 16 I-TQAM require an SNR $20\log_{10}(1.054) = 0.46$ dB and $20\log_{10}(1.069) = 0.58$ dB less than 16 SQAM, respectively. Further, 16 R-TQAM has $NN = 4.123$ and 16 I-TQAM has $NN = 4.3125$, so the detection ocmplexity of I-TQAM is higher. Table 4.1 gives the values of d_{min} for SQAM and TQAM with

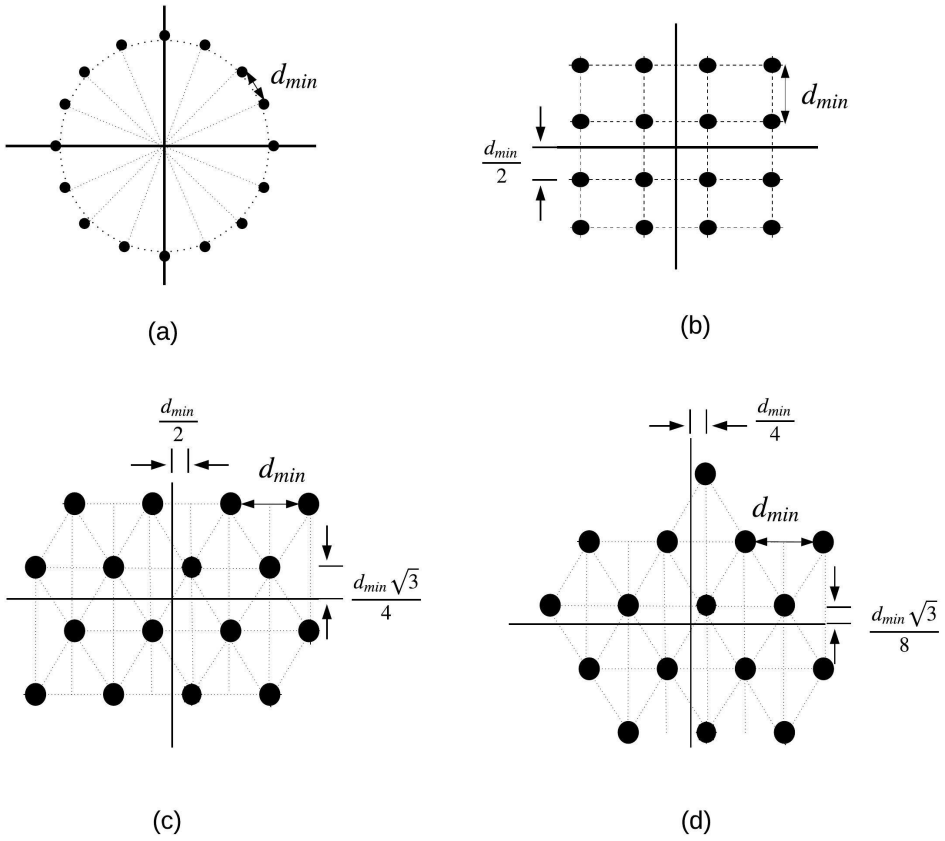

Figure 4.2: The (a) 16 PSK, (b) 16 SQAM, (c) 16 R-TQAM, and (d) 16 I-TQAM signal constellations.

$4 \leq M \leq 265$. For the same E_S, SQAM has the smallest d_{min} and I-TQAM has the largest d_{min} for all values of M.

The second parameter that affects the signal constellation is the number of bit differences between adjacent symbols. A smaller number of differences results in better BER performance. With a Gray mapping, SQAM constellations have one bit difference between adjacent symbols. A Gray mapping is not possible with TQAM constellations because of the number of nearest neighbors. The Gray penalty G_P is the average number of bit differences between a symbol and its nearest neighbors, so $G_P = 1$ for a Gray mapping. G_P for R-TQAM and I-TQAM for $M = 16$ and 64 was given in [7, 30]. G_P is greater than 1 for both R-TQAM and I-TQAM, but it is larger with I-TQAM. However, TQAM has better BER performance than SQAM [7, 30]. Given the results in this section, TCM with TQAM is considered in this dissertation.

Table 4.1: d_{min} for SQAM, R-TQAM, and I-TQAM

	d_{min}		
M	SQAM	R-TQAM	I-TQAM
8	$2\sqrt{\frac{E_S}{6}}$	$2\sqrt{\frac{E_S}{5}}$	$2\sqrt{\frac{E_S}{4.5}}$
16	$2\sqrt{\frac{E_S}{10}}$	$2\sqrt{\frac{E_S}{9}}$	$2\sqrt{\frac{E_S}{8.75}}$
32	$2\sqrt{\frac{E_S}{20}}$	$2\sqrt{\frac{E_S}{17.75}}$	$2\sqrt{\frac{E_S}{16.625}}$
64	$2\sqrt{\frac{E_S}{42}}$	$2\sqrt{\frac{E_S}{37}}$	$2\sqrt{\frac{E_S}{35.25}}$
128	$2\sqrt{\frac{E_S}{82}}$	$2\sqrt{\frac{E_S}{72}}$	$2\sqrt{\frac{E_S}{70.54}}$
256	$2\sqrt{\frac{E_S}{170}}$	$2\sqrt{\frac{E_S}{149}}$	$2\sqrt{\frac{E_S}{141.01}}$

4.3 Binary Trellis Coded Modulation

Ungerboeck introduced binary TCM (BTCM), which combines a binary convolutional code (BCC) with M-ary SQAM or M-ary PSK [26]. The advantage of BTCM arises from the fact that the coding and modulation are combined. The performance of BTCM is determined by the asymptomatic coding gain (ACG) which is a function of the free Euclidean distance d_{Efree}. The free Euclidean distance is the shortest distance between symbol sequences so that

$$d_{Efree}^2 = \sum_{i=0}^{N-1} d_i^2, \tag{4.2}$$

and N is the length of the symbol sequence that diverges from a state in the trellis and then joins that state as shown in Fig. 4.3, and d_i is the distance between the symbol sequences at trellis stage i.

The asymptotic coding gain (ACG) of TCM is defined as [26]

$$\gamma = 10 \log_{10} \left(\frac{d_{Efree}^2 / E_S}{d_{min}^2 / E_S'} \right), \tag{4.3}$$

where E_S and E_S' are the average symbol energy for coded and uncoded symbols, and d_{min} is the minimum Euclidean distance for the uncoded signal constellation. As E_S and E_S' are fixed, the goal with TCM is to maximize d_{Efree}.

The value of d_{Efree} depends on the mapping of constellation symbols and the code employed. Ungerboeck mapped the constellation symbols using a technique

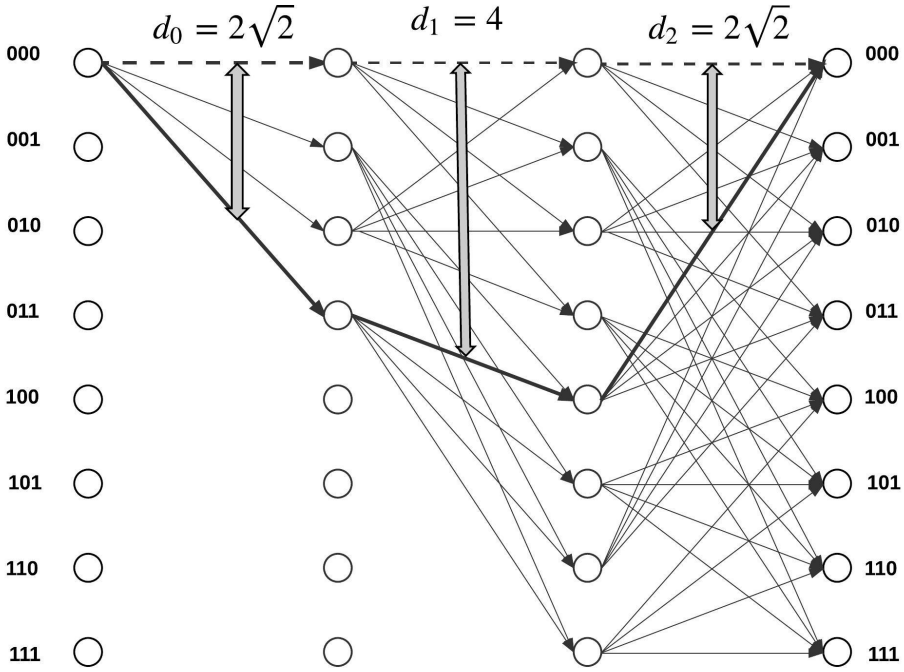

Figure 4.3: The binary trellis diagram for 16 S-BTCM.

called set partitioning. Here, this is denoted as binary set partitioning (BSP). BSP divides the constellation symbols into two equal subsets, and the symbols in each subset are assigned the same binary label. The partitioning continues until there are only two symbols in the each subset. The number of partition levels is L, where 2^{L+1} is the number of constellation symbols. For example, 16 SQAM has three BSP levels as shown in Fig. 4.4. The minimum distance between constellation symbols in the subsets is denoted by $d^{(l)}$, where l is the partition level. Note that $d^{(l)}$ increases as the level increases, which indicates that BSP is compatible with SQAM, i.e. in Fig. 4.4 $d^{(1)} = 2\sqrt{2}$, $d^{(2)} = 4$ and $d^{(3)} = 4\sqrt{2}$.

A BCC is used in BTCM to increase d_{Efree} by increasing the distance between sequences of constellation symbols. This code is represented by three parameters (n, k, m) where k and n are the number of input and output data streams respectively, and m is the encoder memory length. The code rate of a BCC is $R = \frac{k}{n}$. A systematic feedback BCC is used in BTCM with $n = k+1$ [26, 63]. Thus, a BCC(3, 2, 3) code is used with 16 S-BTCM as shown in Fig. 4.5, where $\oplus$ denotes modulo 2 addition. The generator sequences for this code are $G = [(0100), (0010), (1001)]$, where a 1 indicates a connection among the inputs, modulo 2 adders and/or memory elements, and a

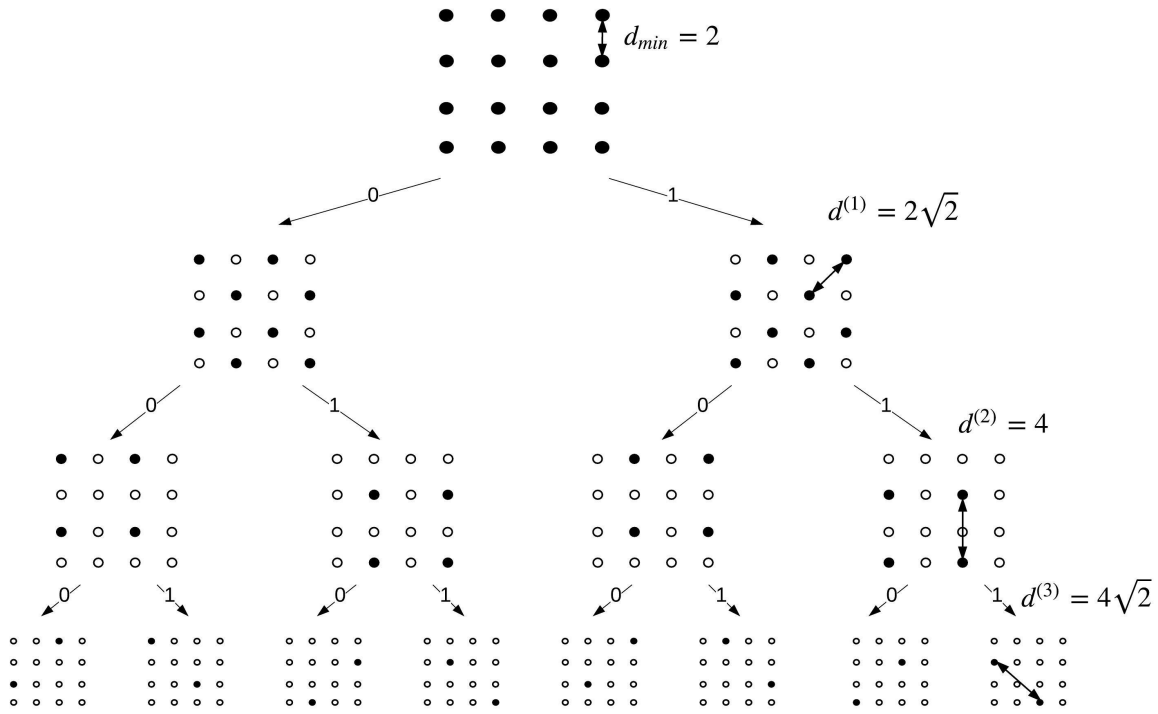

Figure 4.4: Binary set partitioning for 16 SQAM.

0 indicates no connections. For example, the first sequence indicates a connection between the first input and the first modulo 2 adder, while the second sequence indicates a connection between the second input and the second modulo 2 adder. Each time step, 3 coded bits are combined with an uncoded bit and mapped to a 16 SQAM symbol. This is the best BCC for BTCM with 16 SQAM (16 S-BTCM) as it provides the maximum d_{Efree} [26]. The trellis for this coding is shown in Fig. 4.3 and has

$$\frac{d^2_{Efree}}{E_S} = \frac{(2\sqrt{2})^2}{10} + \frac{(2)^2}{10} + \frac{(2\sqrt{2})^2}{10} = 2. \tag{4.4}$$

The corresponding ACG over uncoded 8 PSK [26] is

$$\gamma = 10 \log_{10} \left(\frac{20/10}{0.586/1} \right) = 5.33 \, \text{dB}. \tag{4.5}$$

Now BTCM is considered with TQAM (T-BTCM), so that BSP is used for mapping the constellation symbols. Many symbols in a TQAM constellation have six neighbors, so it is not possible to have $d^{(1)} > d_{min}$. However in subsequent levels, $d(l)$ can be increased as the number of NNs is reduced. For example, Fig. 4.6 shows BSP

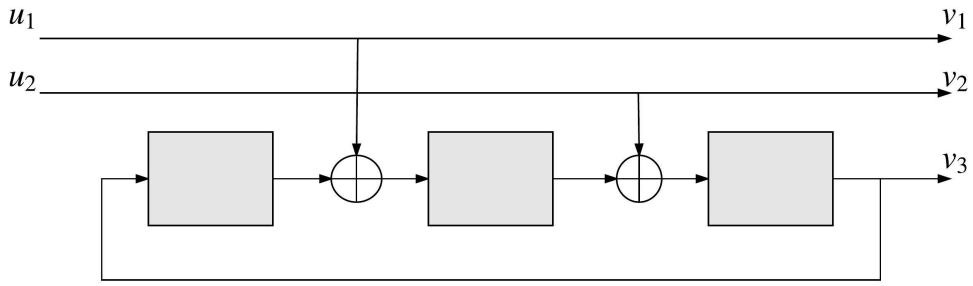

Figure 4.5: A systematic binary feedback convolutional code with $R = \frac{2}{3}$ and $m = 3$.

for 16 TQAM, and in the first level $d^{(1)} = d_{min} = 2$. Thus, BSP is not compatible with TQAM. In subsequent levels, the distances between constellation symbols in a subset increases to $d^{(2)} = 2\sqrt{3}$ and $d^{(3)} = 2\sqrt{7}$. The BCC that provides the largest d_{Efree} for 16 T-BTCM was obtained using a search as in [26]. For 16 T-BTCM, this code gives

$$\begin{aligned} \frac{d^2_{Efree}}{E_S} &= \frac{1}{E_S}({d^{(1)}}^2 + {d^{(0)}}^2 + {d^{(1)}}^2), \\ &= \frac{2^2}{9} + \frac{2^2}{9} + \frac{2^2}{9} = 1.33, \end{aligned} \tag{4.6}$$

and the corresponding ACG over uncoded 8 PSK is

$$\gamma = 10 \log_{10} \left(\frac{12/9}{0.586/1} \right) = 3.57 \, \text{dB}. \tag{4.7}$$

.

From the previous results, the ACG of 16 T-BTCM is 1.76 dB less than the ACG of 16 S-BTCM, which confirms that BSP is not compatible with TQAM. Therefore, a suitable set partitioning for TQAM is introduced in the next section.

4.4 Ternary Trellis Coded Modulation

4.4.1 Ternary Set Partitioning

Set partitioning with TQAM should divide the constellation into more than two groups, so here three groups are considered which is called ternary set partitioning (TSP). As in [63], the number of constellation symbols in each subset should be equal, so the modulation order cannot be a power-of-two. Therefore, TSP can be employed

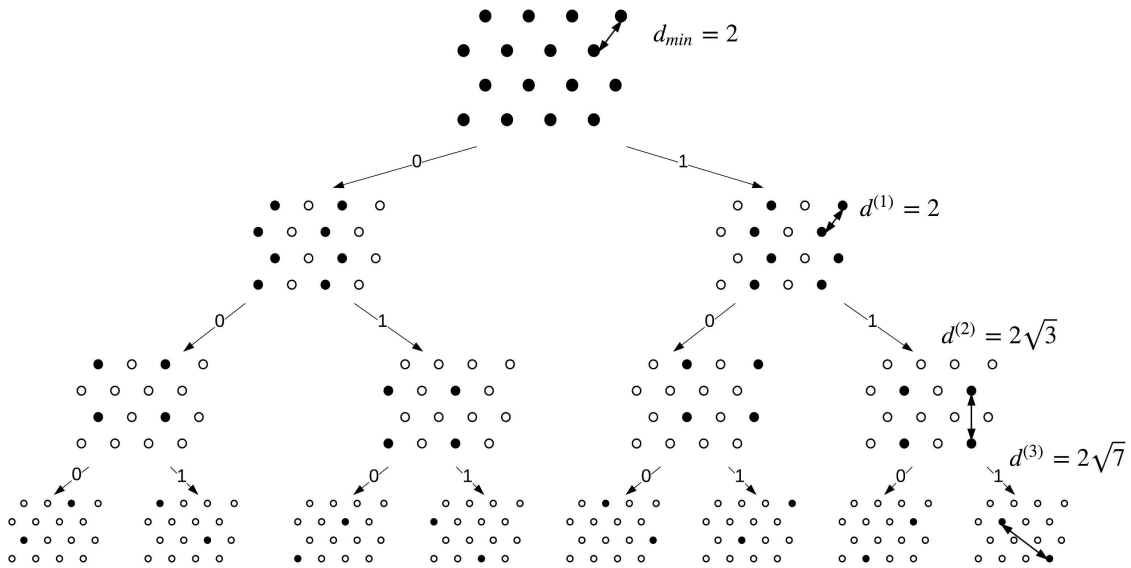

Figure 4.6: Binary set partitioning (BSP) for 16 R-TQAM.

if $M = 2^j \times 3^{t+1}$, where t is the number of coded and uncoded trits and j is the number of uncoded bits. For $j > 0$, TSP continues until the number of constellation symbols in each subset is 2 symbols, while for $j = 0$, the subsets in the last TSP level have 3 symbols. The number of set partitioning levels is $j + t$. For example, for $M = 18 = 2 \times 3^2$, the number of levels is 2, and each symbol corresponds to two trits and one bit. In addition, the subsets in the last level have 2 symbols. For $M = 27 = 3^3$, the number TSP levels is 2, so the subsets in the last level have 3 symbols.

A ternary convolutional code is required when TSP is employed, as shown in Fig. 4.7. Here there are two possible cases, with or without uncoded bits and/or trits. For example, TCC(2, 1, 2) is employed with 27 TQAM so there are two coded trits and an uncoded trit. Conversely, 36 TQAM employs TCC(2, 1, 2) with two coded trits and two uncoded bits, and both TSP and BSP are used. BSP is used last because the uncoded bits have less protection, and the largest distance between constellation symbols is in the last level of partitioning [63]. In the next section, the performance of ternary trellis coded modulation (TTCM) with TSP is analyzed.

4.4.2 TTCM with 18 TQAM

A block diagram of the proposed ternary trellis coded modulation system is shown in Fig. 4.1. The TTCM encoder consists of a BT converter, TCC encoder, and

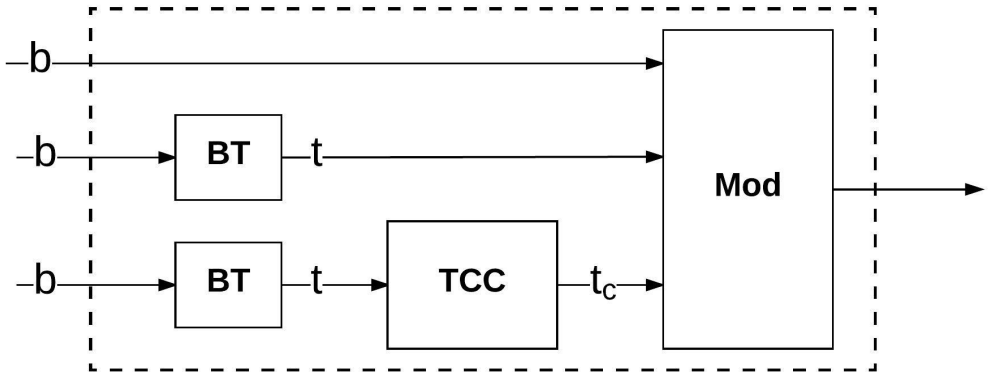

Figure 4.7: Block diagram for a TCM encoder which employs a TCC with uncoded bits and trits.

modulator, while the decoder has a soft decision Viterbi decoder and BT converter. TTCM is embedded in a binary communication system where the input and output are binary data. First the binary data is converted to trits using BT conversion. These trits are then encoded by the TCC. The coded trits with uncoded bits or/and trits are mapped to a constellation symbol, and this symbol is labeled using TSP (and BSP if there are uncoded bits).

The binary to ternary (BT) conversion employed is important because it affects the BER performance. At the decoder output, one trit error causes one or more bit errors because of this conversion. The goal is to minimize the average number of bit errors due to a trit error, denoted e_{av}. Three bit to two trit conversion (3B2T) was shown to provide the smallest value of e_{av}. Therefore, 3B2T conversion is used here. For $M = 2^j \times 3^{t+1}$, each constellation symbol represents j bits and t trits. However, as the input to the system is binary, the number of bits per symbol with 3B2T conversion is

$$I = t \times \frac{3}{2} + j. \tag{4.8}$$

For example, with $M = 2^2 \times 3^2$, $I = 1 \times (1.5) + 2 = 3.5$ bits/symbol, and with $M = 2^0 \times 3^3 = 27$, $I = 2 \times (1.5) + 0 = 3$ bits/symbol.

To evaluate the performance of TTCM and compare it with that of BTCM, both 18 TQAM and 16 SQAM are considered in this section. The 18 TTCM block diagram is shown in Fig. 4.8. First, 3 bits are converted to 2 trits using 3B2T conversion, and the trits are input to the TCC. A ternary convolutional code TCC(2, 1, 2) is employed and the best code obtained using the search method in [26] is shown

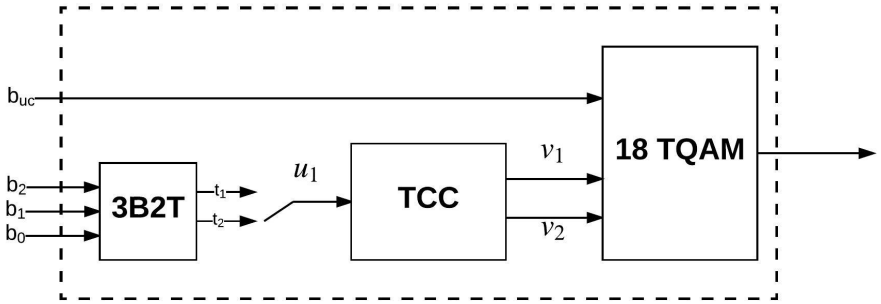

Figure 4.8: TTCM with 18 TQAM and a ternary convolutional code (TCC) using 3B2T conversion.

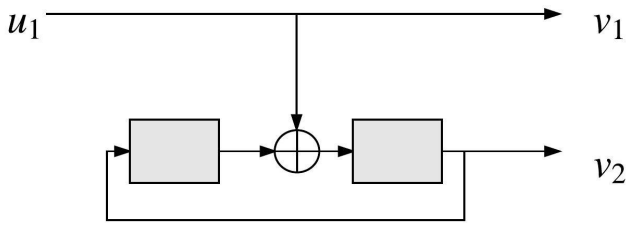

Figure 4.9: The best TCC for TTCM with 18 TQAM.

in Fig. 4.9. In this case, $\oplus$ denotes a modulo 3 adder. This code has generator sequences $G = [(010), (101)]$. The two encoded trits are combined with an uncoded bit and mapped to an 18 TTCM symbol. Therefore, there are $I = 2.5$ bits/symbol. In this section, regular, irregular and hexagonal 18 TQAM are considered, and the constellations are shown in Fig. 4.10. The structure of the constellation affects d_{Efree}, so the performance of TTCM will differ for these constellations.

Fig. 4.12 shows the ternary set partitioning for 18 R-TQAM. Note that $d^{(l)}$ increases with each level. For this constellation, if $d_{min} = 2$ then $E_S = 13.92$. The trellis diagram for the TCC in Fig. 4.9 is given in Fig. 4.11. This shows that four transitions are required to diverge and then merge with the same state, so that for TTCM with 18 R-TQAM (18 R-TTCM)

$$\frac{d^2_{Efree}}{E_S} = \frac{(2\sqrt{3})^2 + 2^2 + (2\sqrt{3})^2 + 2^2}{13.92} = 2.29. \tag{4.9}$$

For comparison purposes, the ACG of 18 TTCM over uncoded 8 PSK is employed. However, each 18 TTCM symbol represents only $I = 2.5$ uncoded bits whereas un-

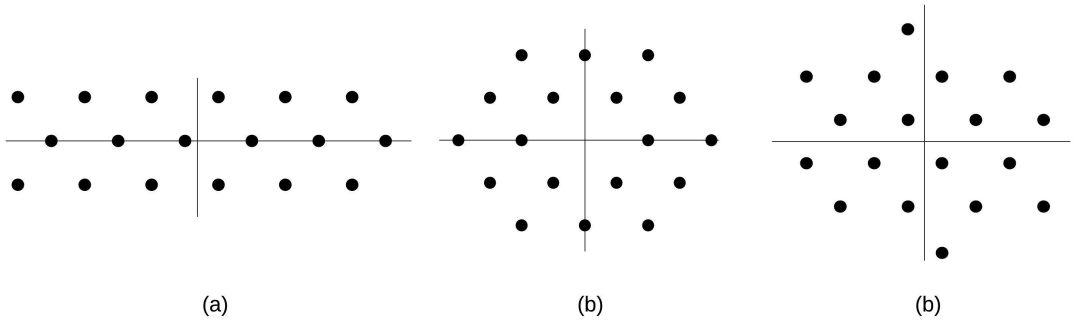

Figure 4.10: The constellations for (a) 18 R-TQAM, (b) 18 I-TQAM, and (c) 18 H-TQAM.

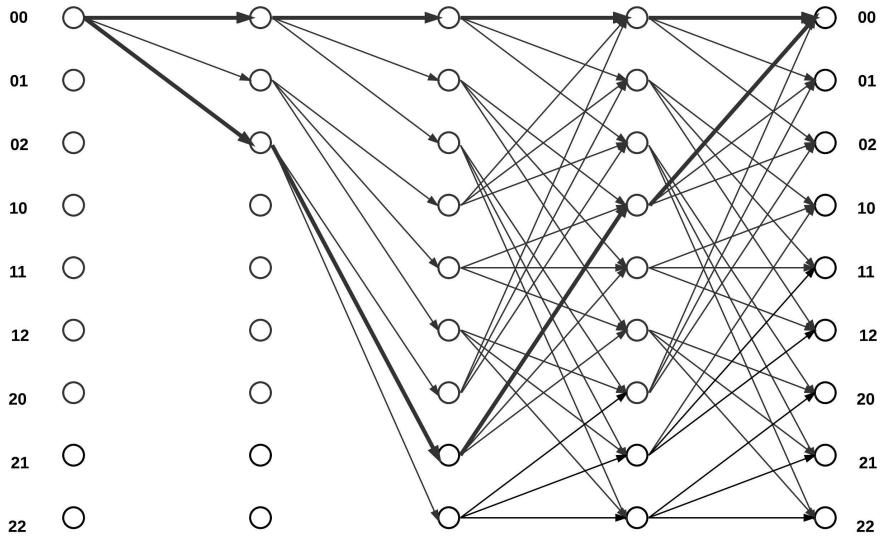

Figure 4.11: Trellis diagram for TCC(2,1,2).

coded 8 PSK represents 3 bits, which represents a loss of

$$10\log_{10}\left(\frac{3}{2.5}\right) = 0.792\,\text{dB}. \tag{4.10}$$

Thus, the ACG of 18 R-TTCM over uncoded 8 PSK is

$$\gamma = 10\log_{10}\left(\frac{2.29}{0.586}\right) - 0.792 = 5.13\,\text{dB}. \tag{4.11}$$

H-TQAM has constellation points from a triangular lattice in a hexagonal shape as shown in Fig. 4.10(b). Fig. (4.13) shows the TSP for 18 H-TQAM. The average symbol energy of 18 H-TQAM is $E_S = 10.67$ for $d_{min} = 2$, which is lower than with

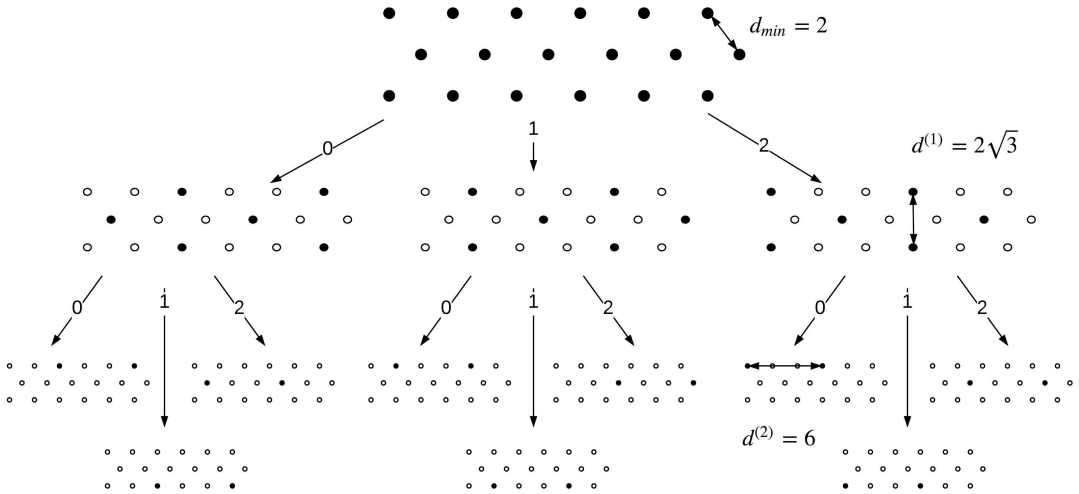

Figure 4.12: Ternary set partitioning for 18 R-TQAM.

R-TQAM. TTCM with 18 H-TQAM (18 H-TTCM) gives

$$\frac{d^2_{Efree}}{E_S} = \frac{(2\sqrt{3})^2 + 2^2 + (2\sqrt{3})^2 + 2^2}{10.67} = 3.00, \tag{4.12}$$

and the corresponding ACG over 8 PSK is

$$\gamma = 10 \log_{10}\left(\frac{3}{0.586}\right) - 0.792 = 6.30\,\text{dB}. \tag{4.13}$$

This is 1.17 dB better than R-TTCM because of the lower value of E_S.

The 18 I-TQAM constellation shown in Fig. 4.10(c) has $E_S = 10.17$, which is lower than with R-TQAM and H-TQAM. Fig. 4.14 shows the TSP for 18 I-TQAM, and illustrates that 18 I-TQAM is not compatible with TSP as $d_{min} = d^{(1)}$. TTCM with 18 I-TQAM (18 I-TTCM) gives

$$\frac{d^2_{Efree}}{E_S} = \frac{2^2 + 2^2 + 2^2 + 2^2}{10.17} = 1.57, \tag{4.14}$$

and the corresponding ACG over 8 PSK is

$$\gamma = 10 \log_{10}\left(\frac{1.57}{0.586}\right) - 0.792 = 3.50\,\text{dB}. \tag{4.15}$$

I-TQAM provides the lowest ACG for the three 18 TQAM constellations, and is also 1.04 dB lower than 16 S-BTCM because of the incompatibility with TSP. To make 18

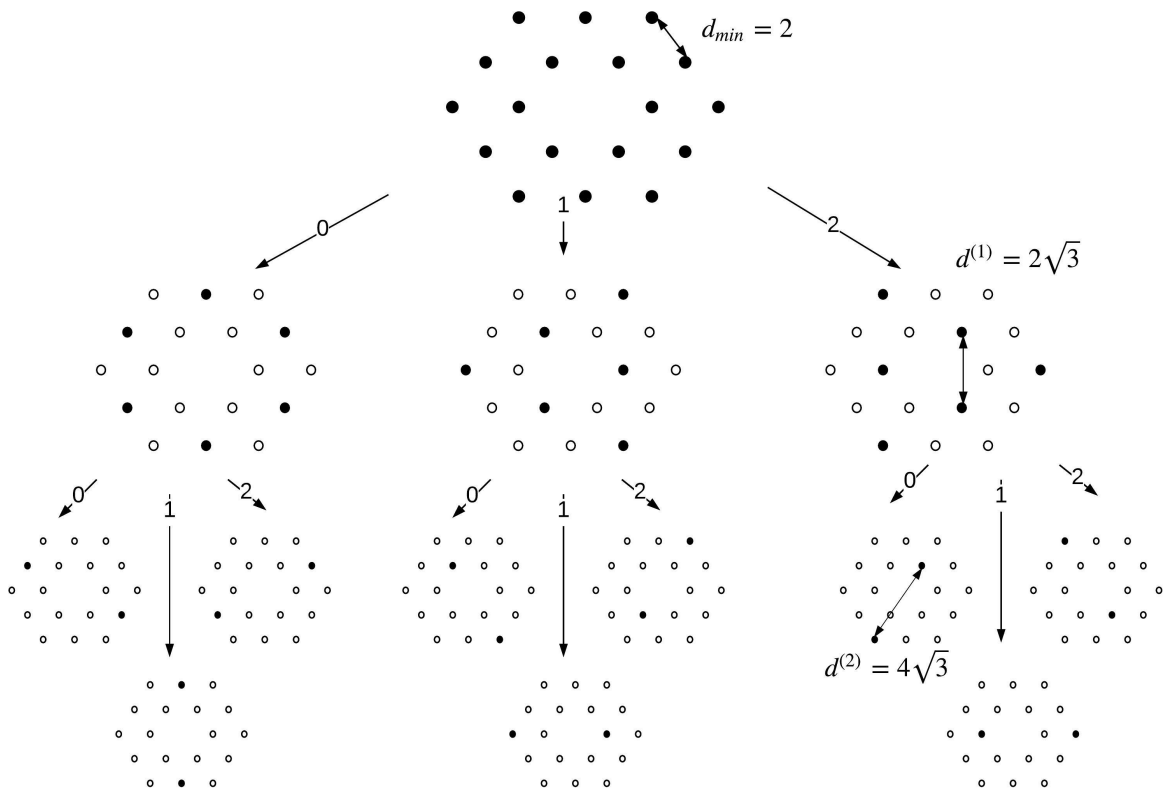

Figure 4.13: Ternary set partitioning for 18 H-TQAM.

I-TQAM compatible with TSP, some of the constellation points must be relocated. Although E_S for this new constellation will be larger, the TTCM ACG will be lower. Fig. 4.15 shows the relocation of two 18 I-TQAM constellation points. This new constellation is compatible with TSP, and so is called compatible 18 TQAM, (18 C-TQAM). For $d_{min} = 2$, $E_S = 10.33$, which is lower than with R-TQAM and H-TQAM, but higher than with 18 I-TQAM. Fig. 4.16 shows the TSP for 18 C-TQAM. TTCM with 18 C-TQAM (18 C-TTCM) gives

$$\frac{d^2_{Efree}}{E_S} = \frac{(2\sqrt{3})^2 + 2^2 + (2\sqrt{3})^2 + 2^2}{10.33} = 3.09, \tag{4.16}$$

and the corresponding ACG over 8 PSK is

$$\gamma = 10 \log_{10} \left(\frac{3.09}{0.586} \right) - 0.792 = 6.43 \, \text{dB}. \tag{4.17}$$

As expected, C-TTCM provides the best ACG because E_S for C-TQAM is lower than with R-TQAM and H-TQAM and it is compatible with TSP.

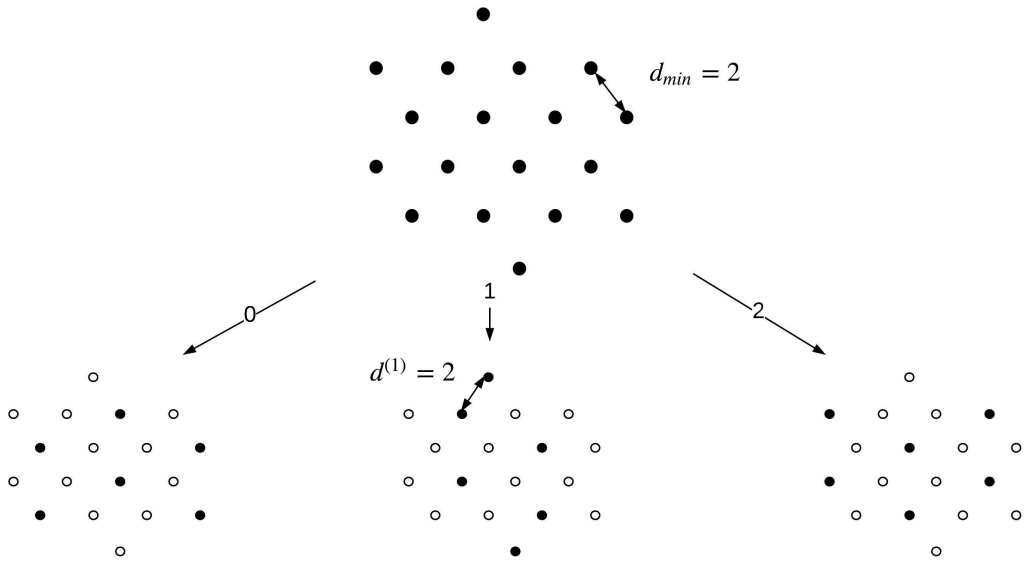

Figure 4.14: Ternary set partitioning for 18 I-TQAM.

Table 4.2: Comparison between 18 TTCM and 16 S-BTCM

	E_S	$\frac{d^2_{Efree}}{E_S}$	ACG over 8 PSK
18 R-TTCM	13.92	2.29	5.13
18 H-TTCM	10.67	3.00	6.30
18 I-TTCM	10.17	1.57	3.50
18 C-TTCM	10.33	3.09	6.43
16 S-BTCM	10.00	2.00	5.33

Table 4.2 gives the values of E_S, d^2_{Efree}/E_S, and ACG for regular, irregular, hexagonal and compatible 18 TTCM, and 16 S-BTCM. As mentioned above, for comparison purposes the ACG of TTCM should be reduced by 0.79 dB. From the table, 18 H-TTCM and C-TTCM have a better ACG than 16 S-BTCM by $6.30 - 5.33 = 0.97$ dB and $6.43 - 5.33 = 1.10$ dB, respectively. Thus, C-TTCM provides the highest ACG. The construction of M-ary C-TTCM is considered in the next section.

4.4.3 M-ary C-TTCM

The I-TQAM constellations presented in [30] provide the lowest values of E_S, but are not compatible with TSP. The I-TQAM constellations for small M can easily be modified to obtain compatible constellations, but for large M this can be difficult. Therefore, a construction technique for compatible TQAM (C-TQAM) is introduced here and is given in the following steps.

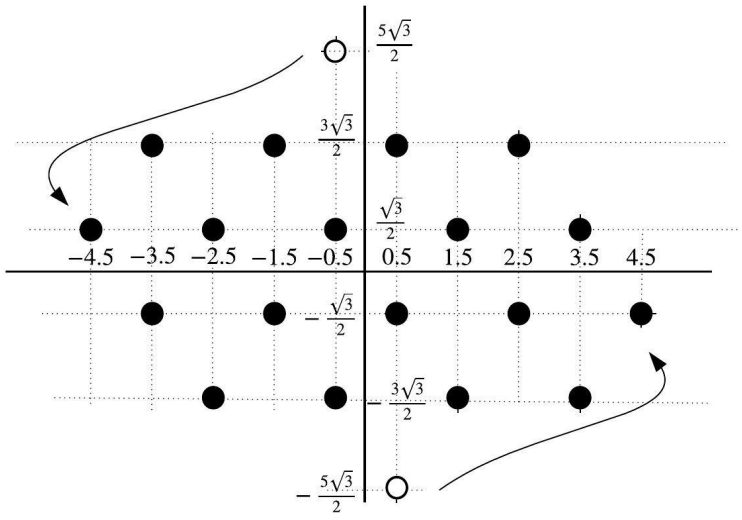

Figure 4.15: Modifying 18 I-TQAM to be compatible with TSP, denoted 18 C-TQAM.

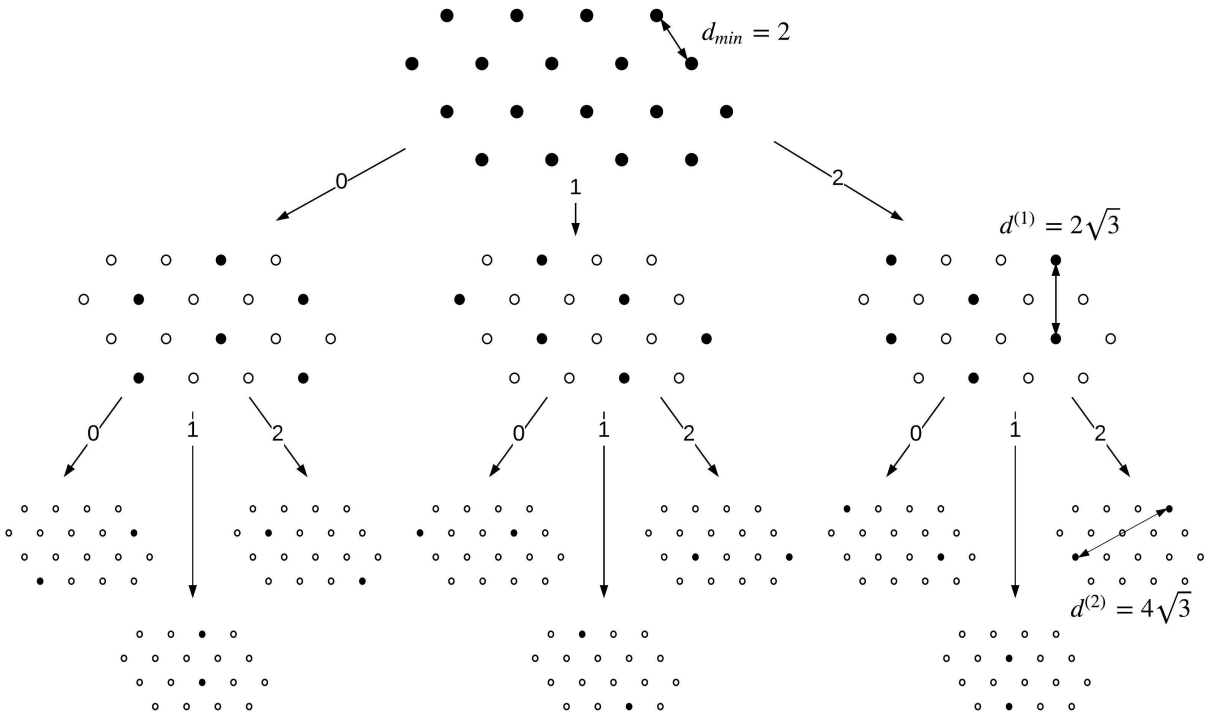

Figure 4.16: Ternary set partitioning for 18 C-TQAM.

1. Construct a rectangle of points from a triangular lattice with the origin at the center. The rectangle dimensions are the two integers closest to $\sqrt{2M}$, with the largest equal to the number of rows and the smallest equal to the number of columns. In particular, the number of rows is $\lceil\sqrt{2M}\rceil$ and the number of columns is $\lfloor\sqrt{2M}\rfloor$.

2. Divide the points into three groups as follows.

   (a) The first group is selected by choosing the first of every three points in the odd numbered rows, and the second of every three points in the even numbered rows.

   (b) The second group is selected by choosing the second of every three points in the odd numbered rows, and the third of every three points in the even numbered rows.

   (c) The third group is selected by choosing the third of every three points in the odd numbered rows, and the first of every three points in the even numbered rows.

3. The $\frac{M}{3}$ constellation points in each group closest the origin are selected, and the remaining points are deleted.

4. The selected points constitute the M-ary C-TQAM constellation that is compatible with TSP and has the lowest value of E_S.

For example, Fig. 4.17 shows the 27 C-TQAM constellation. In the construction, a rectangle of $2 \times 27 = 54$ points is used, so the number of rows is 8 and the number of points in each row is 7. The colors in the figure represent the three groups. The $\frac{27}{3} = 9$ points in each group closest to the origin are selected (shown within the dashed line), and the remaining points are deleted. This construction ensures that $d^{(1)} > d_{min}$. The resulting constellations for $M = 27$, 36, 54 and 108 are shown in Fig. 4.18.

The TCC code rate is related to the TQAM modulation order M. Tables 4.3 and 4.4 presents the parameters for C-TTCM with $R = \frac{1}{2}$ and $R = \frac{2}{3}$, respectively. The average symbol energy was calculated using the constellations shown in Fig. 4.18 with $d_{min} = 2$. The best TCCs were found using the search method in [26]. The corresponding values of d_{Efree} are given in the tables.

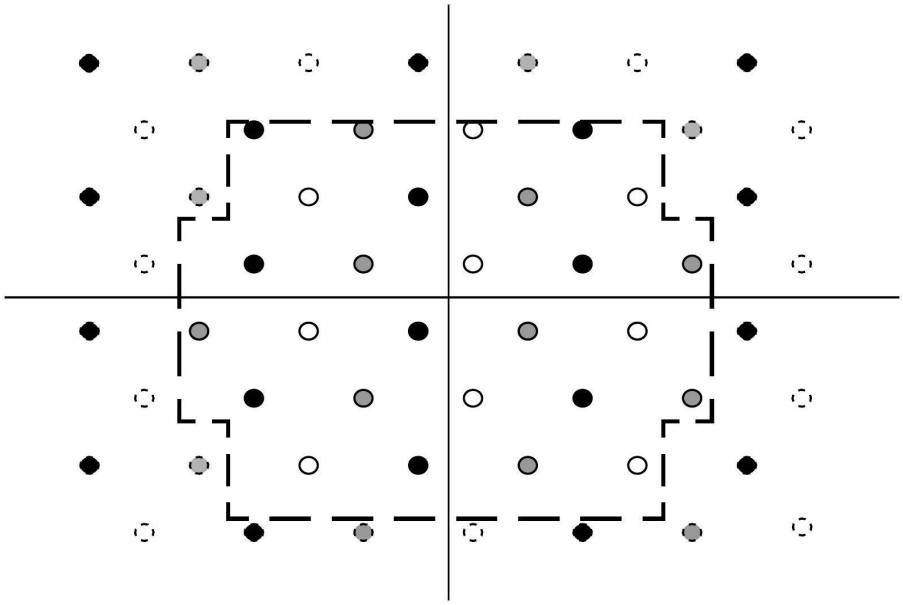

Figure 4.17: The 27 C-TQAM constellation which is compatible with TSP.

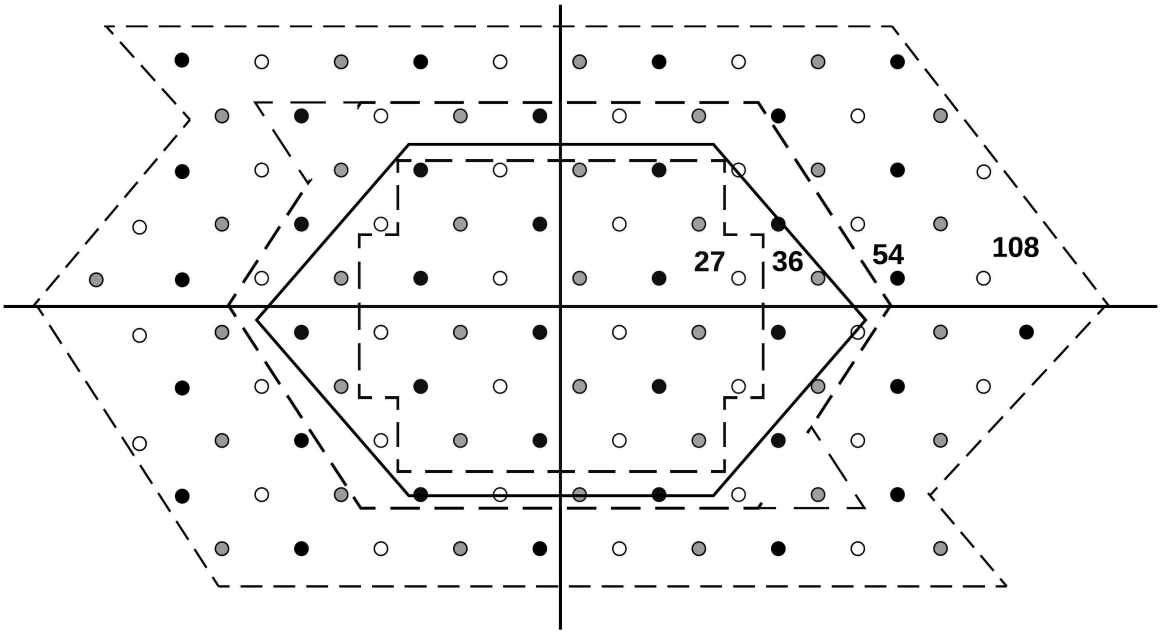

Figure 4.18: The C-TQAM constellations for $M = 27$, 36, 54 and 108.

Table 4.3: Parameters for M-ary C-TTCM with TCC(2, 1, m)

R	M	m	E_S	$\frac{d^2_{Efree}}{E_S}$	G	I
$\frac{1}{2}$	9	1	4.92	1.62	$[(01), (11)]$	1.5
		2		2.02	$[(010), (101)]$	
	18	2	10.67	3.16	$[(010), (101)]$	2.5
		3		3.81	$[(0120), (2021)]$	
	27	2	15.00	3.20	$[(010), (101)]$	3
		3		3.92	$[(0110), (2101)]$	
		4		4.25	$[(01000), (11002)]$	
	36	2	20.33	3.52	$[(010), (101)]$	3.5
		3		4.33	$[(0110), (1011)]$	
		4		4.52	$[(01000), (12011)]$	

Table 4.4: Parameters for M-ary C-TTCM with TCC(3, 2, m)

R	M	m	E_S	$\frac{d^2_{Efree}}{E_S}$	G	I
$\frac{2}{3}$	27	2	15.00	2.75	$[(010), (001), (101)]$	3
		3		3.33	$[(0100), (0010), (1201)]$	
		4		3.62	$[(01000), (01100), (12101)]$	
	54	2	28.47	3.25	$[(010), (001), (101)]$	4
		3		3.55	$[(0100), (0010), (2102)]$	
		4		4.02	$[(01000), (02100), (12201)]$	
	81	3	49.90	3.67	$[(0100), (0010), (1201)]$	4.5
		4		4.22	$[(01000), (02100), (12201)]$	
	108	3	62.77	4.22	$[(0100), (0010), (1201)]$	5
		4		4.84	$[(01000), (02100), (12201)]$	

4.4.4 Binary to Ternary Conversion in TTCM

3B2T conversion maps every string of 3 bits to a unique string of 2 trits. The goal is to have a low value of e_{av} considering d_{Efree} rather than d_{min} as in Table 2.4. A TTCM decoding error occurs when a wrong trellis path is chosen. Therefore, e_{av} can be reduced by minimizing the number of trit differences between branches leaving a state.

TCC(2, 1, 2) is considered here to illustrate the steps in creating the 3B2T conversion that provides the lowest e_{av}. The trellis diagram of TCC(2, 1, 2) is shown in Fig. 4.11. For 18 C-TTCM, the lines between states represent two parallel branches, so each state has six output branches. The outputs of the first state are (000, 001, 100, 101, 200, 201), where the first two digits are encoded trits and the last is an

uncoded bit. The focus here is on trit errors, so the uncoded bit is ignored, in which case there are only three branches leaving a state given by (00, 10, 20). These ternary strings are mapped to binary strings so that the average bit difference is lowest. For example, mapping to (000, 001, 101) results in an average bit difference of 1.33 bits.

The difference between the three ternary blocks is one trit, so choosing an incorrect branch results in one trit error, or from the given mapping 1.33 bit errors on average. The same occurs for the fourth and seventh states in this example. Following a similar procedure for the second, fifth, and eighth states, (01, 11, 21) is mapped to (111, 011, 010). The average difference between these ternary stings is one trit, and the average bit difference is 1.33 bits. For the third, sixth, and ninth states, (02, 12, 22) is mapped to the remaining binary strings giving (110, 100, 100), where the last binary string is repeated. A different between these ternary strings of one trit results in an average difference between the mapped binary strings of 0.67 bit. Thus, the average number of bit errors due to a trit error for this 3B2T conversion in TTCM is

$$e_{av} = \frac{6(1.33) + 3(0.67)}{9} = 1.11 \text{ bits/trit error.} \tag{4.18}$$

This 3B2T conversion is shown in Table 4.5. Based on an exhaustive search, it has the lowest average number of bit errors for BT conversion with 18 C-TTCM using TCC(2, 1, 2).

The 3B2T conversion given above is used for coded trits. For uncoded trits, the 3B2T conversion in Table 2.4 is optimal and has $e_{av} = 1.55$. For example, 27 C-TTCM with TCC(2, 1, 2) has two coded trits and one uncoded trit. Therefore, the first two trits are mapped using Table 4.5, while the uncoded trit is mapped using Table 2.4.

Therefore, for the three trits $e_{av} = \frac{1.55+2(1.11)}{3} = 1.26$ bits/trit error.

4.5 Performance Results

In this section, the probability of bit error for 16 S-BTCM and 18 TTCM is evaluated over additive white Gaussian noise (AWGN) and Rayleigh fading channels. Monte Carlo simulation is employed with 10^8 bits for each value of E_b/N_0 where E_b is the energy per bit given by $E_b = E_s/I$ and N_0 is the noise power spectral density. $I = 3$ for 16 S-BTCM while $I = 2.5$ for 18 TTCM. For a fair comparison, the values of E_b for 16 S-BTCM and 18 TTCM should be the same. This is done by reducing d_{min}

Table 4.5: Optimal Three Bit to Two Trit Conversion

Binary Block Input	Ternary Block	Binary Block Output
0 0 0	0 0	0 0 0
0 0 1	1 0	0 0 1
1 0 1	2 0	1 0 1
1 1 1	0 1	1 1 1
0 1 1	1 1	0 1 1
0 1 0	2 1	0 1 0
1 1 0	0 2	1 1 0
1 0 0	1 2	1 0 0
x x x	2 2	1 0 0

of 16 S-BTCM and 18 TTCM by $\sqrt{\frac{I}{E_S}}$ [66]. Therefore from Tables 4.2 and 4.3, d_{min} becomes 1.095, 0.848, 0.968, and 0.991 for 16 SQAM, 18 R-TQAM, 18 H-TQAM, and 18 C-TQAM, respectively.

The bit error probability over an AWGN channel for 16 S-BTCM and 16 T-BTCM, and uncoded 16 SQAM and 16 TQAM, is shown in Fig. 4.19. The BER performance of uncoded 16 TQAM is better than uncoded 16 SQAM by 0.43 dB. However, 16 S-BTCM is better than 16 T-BTCM by 1.42 dB at BER = 10^5, which shows that BSP is not compatible with TQAM.

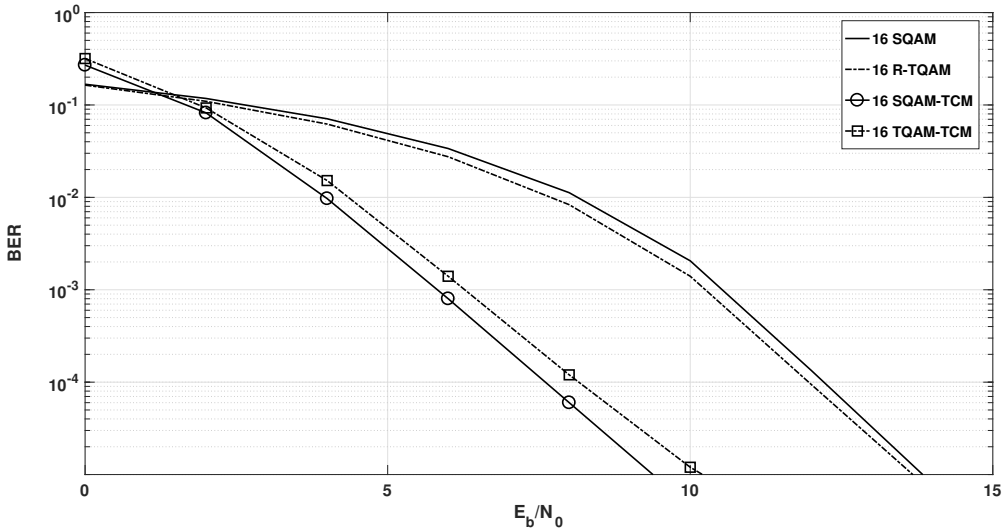

Figure 4.19: Bit error rates for 16 S-BTCM and 16 T-BTCM over an AWGN channel.

Fig. 4.20 presents the BER for 18 TTCM and 16 S-BTCM. 18 C-TTCM is better than 16 S-BTCM by 1.72 dB at BER = 10^{-5}, while 18 H-TTCM is better than 16

B-STCM by 1.64 dB. The performance of 18 R-TTCM is better than that of 16 S-BTCM by 0.51 dB. Therefore, for the same average bit energy, 18 TTCM provides better BER performance than 16 S-BTCM.

Fig. 4.21 presents the BER performance of 18 TTCM and 16 S-BTCM over a frequency-flat Rayleigh fading channel. The average SNR is $\bar{E}_b/N_0$ bit where $\bar{E}_b = \bar{E}_S/I$ and $\bar{E}_S = E\{E_S\}$. These results show that 18 C-TTCM and 18 H-TTCM are better than 16 S-BTCM by 1.45 dB and 1.10 dB, respectively, at BER = 10^{-5}. Thus, BER performance of 18 TTCM is closer to that 16 S-BTCM in Rayleigh fading channels compared to AWGN channels.

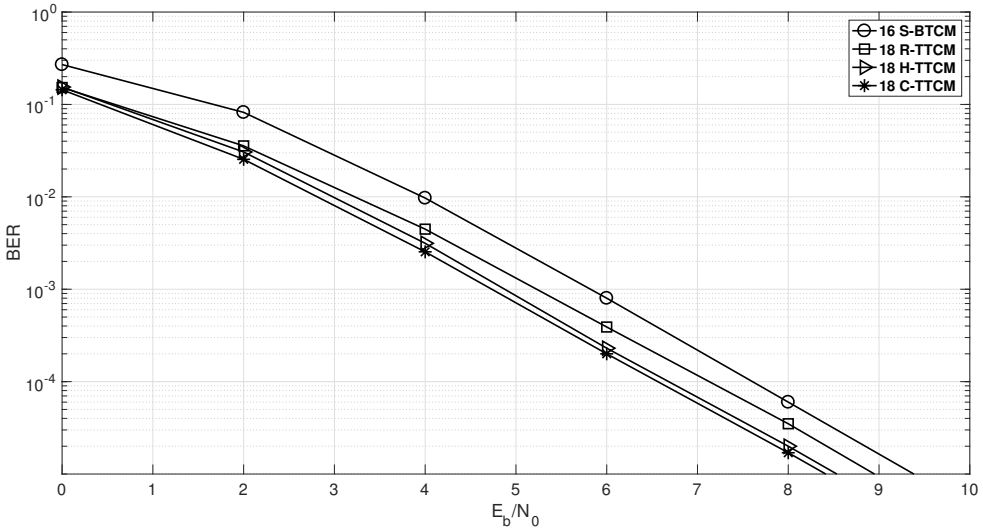

Figure 4.20: Bit error rates for TTCM with 18 R-TQAM, 18 C-TQAM, and 18 H-TQAM, and 16 S-BTCM over an AWGN channel.

4.6 Conclusion

A new form of coded modulation was introduced called ternary trellis coded modulation (TTCM). This employs triangular quadrature modulation (TQAM) which provides better performance than square QAM. It was shown that binary set partitioning (BSP) is not compatible with TQAM, so ternary set partitioning (TSP) was introduced. The advantage of TTCM over binary TCM (BTCM) with SQAM was illustrated. A new class of TQAM constellations called compatible TQAM (C-TQAM) was introduced that is compatible with TSP and has a low average symbol energy. As communication systems have binary inputs and outputs, a new binary to ternary

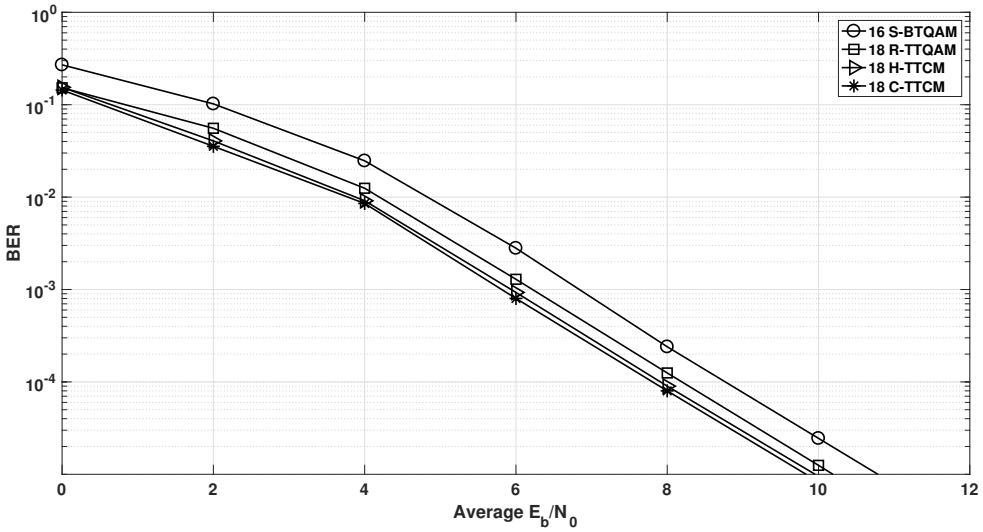

Figure 4.21: Bit error rates for TTCM with 18 R-TQAM, 18 C-TQAM, and 18 H-TQAM, and 16 S-BTCM over a Rayleigh fading channel.

(BT) conversion technique was proposed for TTCM. For the same average bit energy, results were presented which show that the bit error rate (BER) with 18 C-TTCM, 18 R-TTCM and 18 H-TTCM is better than that with 16 S-BTCM in both AWGN and Rayleigh fading channels. Further, TTCM with C-TQAM provides the best performance compared with the TQAM constellations in the literature, namely regular TQAM (R-TQAM), irregular TQAM (I-TQAM), and hexagonal TQAM (H-TQAM).

Chapter 5

Conclusions and Future Work

5.1 Conclusions

A new type of ternary quadrature amplitude modulation (T-QAM) was introduced called semi-regular TQAM (S-TQAM). In addition, a new mapping methodology for TQAM was presented. This methodology is suitable for both power-of-two and non-power-of-two TQAM, and provides a lower Gray penalty than previous mappings presented in the literature. For most modulation orders M, S-TQAM was shown to have a higher power gain and lower average energy per symbol than R-TQAM with a similar detection complexity. The probability of symbol error and bit error were derived for S-TQAM and verified via simulation. The bit error performance of R-TQAM, I-TQAM and S-TQAM was compared. Results were presented which show that S-TQAM can have better performance than R-TQAM, and is slightly worse than I-TQAM. Thus, S-TQAM provides a good tradeoff between performance and complexity.

Ternary convolutional codes (TCCs) with code rates $R = 1/2$, $1/3$ and $1/4$ were obtained which have the maximum possible free distance d_{free}. The conversion from binary data to ternary symbols was considered, and the best three bits to two trits (3B2T) conversion was determined. It was shown that a BCC is not compatible with TPSK modulation because of the error propagation with ternary to binary symbol conversion before decoding. The best TCCs and BCCs were compared in terms of memory length, free distance, and complexity. It was found that TCCs with TPSK provide better BER and FER performance over AWGN channels than BCCs with BPSK and TPSK.

A new form of coded modulation was introduced called ternary trellis coded modulation (TTCM). This employs triangular quadrature modulation (TQAM) which provides better performance than square QAM. It was shown that binary set partitioning (BSP) is not compatible with TQAM, so ternary set partitioning (TSP) was introduced. The advantage of TTCM over binary TCM (BTCM) with SQAM was illustrated. A new class of TQAM constellations called compatible TQAM (C-TQAM) was introduced that is compatible with TSP and has a low average symbol energy. As communication systems have binary inputs and outputs, a new binary to ternary (BT) conversion techniques was proposed for TTCM. For the same average bit energy and average data rate, results were presented which show that the bit error performance of 18 C-TTCM and 18 H-TTCM is better than 16 S-BTCM.

5.2 Future Work

Multi-level coded-modulation (MLCM) can be considered in future work. MLCM is based on partitioning the modulation symbols into subsets and applying appropriate coding at different partitions. MLCM protect each bit of the signal points by a binary code at the partitioning level. At the receiver side, each code is decoded individually starting from the lowest level and taking into account decisions of prior decoding stages. This method is called multistage decoding. In contrast to TCM, the multilevel code could be any code, such as a block code or convolutional code. Future work can consider ternary convolutional codes. Binary and ternary codes could be applied in MLCM. The information from a binary decoder to a ternary decoder or the opposite can be examined. Triangular QAM can be used with binary MLCM without any compatibility issues, therefore MLCM with TQAM is an interesting topic for future research.

Iterative decoding is widely used in communication systems. The most commonly employed codes are turbo codes and low-density parity-check (LDPC) codes. Turbo codes were introduced in 1993 [57], while LDPC codes were devised by Gallager in 1963 and rediscovered in 1997 [68, 69]. Turbo codes and LDPC codes are used in modern communication systems because they provided near capacity performance. However, for large block lengths turbo codes have a higher decoding complexity than LDPC codes, while LDPC codes have a higher encoder complexity. Therefore, the challenge is to reduce the complexity for the same coding gain. In 1998 turbo-like codes were introduced [70]. Turbo-like codes are a subclass of turbo codes with a

simple form [70], and are serial concatenated codes. The simplest turbo-like code is a repeat-accumulate (RA) code, which has linear encoding complexity [70]. Non-binary RA codes were studied in [71]. Future work can consider ternary RA codes and examine their performance. The complexity can be compared with that of binary RA codes for the same performance.

Bibliography

[1] A. J. Goldsmith, *Wireless Communications*, Cambridge, UK: Cambridge University Press, 2005.

[2] J. Jeganathan, A. Ghrayeb, and L. Szczecinski, "Spatial modulation: Optimal detection and performance analysis," *IEEE Commun. Lett.*, vol. 12, no. 8, pp. 545–547, Aug. 2008.

[3] E. Yoon, "Maximum likelihood detection with a closed-form solution for the square QAM constellation," *IEEE Commun. Lett.*, vol. 21, no. 4, pp. 829–832, Apr. 2017.

[4] J. G. Proakis and M. Salehi, *Digital Communications*. New York, NY, USA: McGraw-Hill, 2008.

[5] C. Campopiano and B. Glazer, "A coherent digital amplitude and phase modulation scheme," *IRE Trans. Commun. Systems*, vol. 10, no. 1, pp. 90–95, Mar. 1962.

[6] M. Simon and J. Smith, "Hexagonal multiple phase-and-amplitude-shift-keyed signal sets," *IEEE Trans. Commun.*, vol. 21, no. 10, pp. 1108–1115, Oct. 1973.

[7] S. Park, "Triangular quadrature amplitude modulation," *IEEE Commun. Lett.*, vol. 11, no. 4, pp. 292–294, Apr. 2007.

[8] J. G. Proakis and M. Salehi, *Communication Systems Engineering*, 2nd ed.,Upper Saddle River, NJ, USA: Prentice-Hall, 1994.

[9] S. Noda, Y. Saito, and T. Yoshida, "Configuration and error ratio performance of M-QAM whose number of signal points is not a power of 2," *Elec. Comm. Jpn.*, vol. 90, no. 2, pp. 46–57, Feb. 2007.

[10] A. T. Le and K. Araki, "A group of modulation schemes for adaptive modulation," in *Proc. IEEE Singapore Int. Conf. on Commun. Syst.*, Guangzhou, China, pp. 864–869, Nov. 2008.

[11] D. Zrilic, A. Mavretic, and M. Freedman, "Arithmetic ternary operations on delta-modulated signals and their application in the realization of digital filters," *IEEE Trans. Acoustics, Speech, and Signal Process.*, vol. 33, no. 3, pp. 760–764, Jun. 1985.

[12] B. Srinivasu and K. Sridharan, "A Synthesis methodology for ternary logic circuits in emerging device technologies," *IEEE Trans. Circuits and Syst. I, Reg. Papers*, vol. 64, no. 8, pp. 2146–2159, Aug. 2017.

[13] S. Sahoo, A. Gangishetty, R. Sahoo, and M. Muglikar, "High performance ternary adder using CNTFET," *IEEE Trans. Nanotechnology*, vol. 16, no. 3, pp. 368–374, May 2017.

[14] Z. Ullah, M. K. Jaiswal, and R. C. Cheung, "Z-TCAM: An SRAM-based architecture for TCAM," *IEEE Trans. Very Large Scale Integr. (VLSI) Syst.*, vol. 23, no. 2, pp. 402–406, Feb. 2015.

[15] S. Lin, Y. Kim, R. Sahoo, and F. Lombardi, "Design of a ternary memory cell using CNTFETs," *IEEE Trans. Nanotechnology*, vol. 11, no. 5, pp. 1019–1025, Sep. 2012.

[16] T. Koike and S. Yoshida, "Space-time trellis-coded ternary PSK for mobile communications," *Electron. Lett.*, vol. 40, no. 16, pp. 1011–1012, Aug. 2004.

[17] O. Porokhov and P. Radev, "3B2T-RBS an efficient transmission method for digital fibre-optic communications," *Electron. Lett.*, vol. 22, no. 21, pp. 1125–1126, Aug. 1986.

[18] D. E. Knuth, *The Art of Computer Programming.* vol. 2, 3rd ed., Boston, MA, USA: Addison-Wesley, 1998.

[19] M. Tanahashi and H. Ochiai, "A multilevel coded modulation approach for hexagonal signal constellation," *IEEE Trans. Wireless Commun.*, vol. 8, no. 10, pp. 4993–4997, Oct. 2009.

[20] N. Ekanayake and T. T. Tjhung, "On ternary phase-shift keyed signaling," *IEEE Trans. Inform. Theory*, vol. 28, no. 4, pp. 658–660, Jan. 1982.

[21] P. Elias, "Coding for noisy channels," *IRE Int. Conv. Rec.*, vol. 43, no. 3, pp. 37–46, 1955.

[22] S. B. Wicker, *Error Control Systems for Digital Communication and Storage*, 1st ed., Englewood Cliffs, USA: Prentice-Hall, 1995.

[23] A. J. Viterbi, "Error bounds for convolutional codes and an asymptotically optimum decoding algorithm," *IEEE Trans. Inform. Theory*, vol. 13, no. 2, pp. 260–269, Apr. 1967.

[24] G. D. Forney, "The Viterbi algorithm," *Proc. IEEE*, vol. 61, no. 3, pp. 268–278, Mar. 1973.

[25] M. Nakamura and H. Torii, "Ternary phase shift keying and its performance," in Proc. *Int. Symp. on Wireless Pers. Multimedia Commun.*, pp. 1284–1288, Honolulu, HI, USA, Oct. 2002

[26] G. Ungerboeck, "Channel coding with multilevel/phase signals," *IEEE Trans. Inform. Theory,* vol. 28, no. 1, pp. 55–67, Jul. 1982.

[27] J. He, Z. Wang and H. Liu, "IEEE transactions on very large scale integration (VLSI) systems," *IEEE Trans. Very Large Scale Integr. (VLSI) Syst.*, vol. 18, no. 5, pp. 808–817, May 2010.

[28] S. Chatterjee, W. A. Fernando, and M. K. Wasantha, "Adaptive modulation based MC-CDMA systems for 4G wireless consumer applications," *IEEE Trans. Consumer Elect.*, vol. 49, no. 4, pp. 995–1003, Nov. 2003.

[29] A. J. Goldsmith and S. G. Chua, "Adaptive coded modulation for fading channels," *IEEE Trans. Commun.*, vol. 46, no. 5, pp. 595–602, May 1998.

[30] S.-J. Park and M.-K. Byeon, "Irregularly distributed triangular quadrature amplitude modulation," in *Proc. IEEE Int. Symp. on Pers., Indoor and Mobile Radio Commun.*, Cannes, France, pp. 1–5, Sep. 2008.

[31] R. Amutha, "Performance analysis of 64-ary triangular quadrature amplitude modulation," *J. Discr. Mathematical Sci. Crypt.*, vol. 14, no. 4, pp. 317–332, Jun. 2011.

[32] L. Hanzo, W. W. Webb, and T. Keller, *Single-and Multi-Carrier Quadrature Amplitude Modulation: Principles and Applications for Personal Communications: WLANs and Broadcasting*, Chichester, UK: IEEE Press-Wiley, 2000.

[33] G. Foschini, R. Gitlin, and S. Weinstein, "Optimization of two-dimensional signal constellations in the presence of Gaussian noise," *IEEE Trans. Commun.*, vol. 22, no. 1, pp. 28–38, Jan. 1974.

[34] S.-J. Park, M.-K. Byeon, and J. Jeon, "Odd bit mapping of triangular quadrature amplitude modulation," in *Proc. IEEE Int. Symp. on Pers., Indoor and Mobile Radio Commun.*, Tokyo, Japan, pp. 2419–2423, Sep. 2009.

[35] F. Gray, Pulse Code Communication, US Patent 2,632,058, Mar. 1953.

[36] J. Cavers, "Variable-rate transmission for Rayleigh fading channels," *IEEE Trans. Commun.*, vol. 20, no. 1, pp. 15–22, Feb. 1972.

[37] R. E. Goot and E. Dolev, "Variable rate data transmission by size of constellation and symbol duration adaptation," *Elect. Lett.*, vol. 50, no. 3, pp. 230–232, Feb. 2014.

[38] S. J. Park, "Bit mapping of triangular quadrature amplitude modulation," in *Proc. IEEE Int. Symp. on Pers., Indoor and Mobile Radio Commun.*, Athens, Greece, pp. 1–3, Sep. 2007.

[39] M. J. Ariyoshi and I. Sasase, "Trellis coded modulation using partially overlapped signal sets of non-equiprobable signalling," *IEICE Trans. Commun.*, vol. E-79B, no. 9, pp. 1242–1247, Sep. 1996.

[40] S. J. Park and M. Byeon, "Error performances of 64-ary triangular quadrature amplitude modulation in AWGN channel," in *Proc. IEEE Vehic. Techn. Conf.*, Dublin, Ireland, pp. 1752–1755, Apr. 2007.

[41] B. Hassibi and H. Vikalo, "On the sphere-decoding algorithm I. Expected complexity," *IEEE Trans. Signal Process.*, vol. 53, no. 8, pp. 2806–2818, Jul. 2005.

[42] S. J. Park, "Performance analysis of triangular quadrature amplitude modulation in AWGN channel," *IEEE Commun. Lett.*, vol. 16, no. 6, pp. 765–768, Jun. 2012.

[43] F.-H. Qureshi, Q.-U. Khan, and S.-A. Sheikh, "SEP performance of triangular QAM with SC and GSC spatial diversity over Rayleigh channels," *in Proc. IEEE Comput. and Inform. Sci.*, Okayama, Japan, pp. 1-6, Jun. 2016.

[44] L. Rugini, "Symbol error probability of hexagonal QAM," *IEEE Commun. Lett.*, vol. 20, no. 8, pp. 1523–1526, Aug. 2016.

[45] B. Hayes, "Third base," *Amer. Scientist*, vol. 89, no. 6, pp. 490–494, 2001.

[46] A. J. Viterbi and J. K. Omura, *Principles of Digital Communication and Coding*, New York, NY, USA: McGraw-Hill, 1979.

[47] B. Parhami, "Truncated ternary multipliers," *IET Comput. Digital Tech.*, vol. 9, no. 2, pp. 101–105, Mar. 2015.

[48] R. McEliece and W. Lin, "The trellis complexity of convolutional codes," *IEEE Trans. Inform. Theory*, vol. 42, no. 6, pp. 1855–1864, Nov. 1996.

[49] C. Xu, "Soft decoding algorithm for RS-CC concatenated codes in WiMAX system," in Proc. *IEEE Veh. Tech. Conf.*, Dublin, Ireland, Apr. 2007, pp. 740–742.

[50] O. Collins and F. Pollara, "Memory management in traceback Viterbi decoders," *Telecommun. and Data Acquisition Progress Rep.*, vol. 42-99, pp. 98–104, Nov. 1989.

[51] S. C. Krishnan, R. Panigrahy, and S. Parthasarathy, "Error-correcting codes for ternary content addressable memories," *IEEE Trans. Comput.*, vol. 58, no. 2, pp. 275–279, Jan. 2009.

[52] S. Lin and D. J. Costello, *Error Control Coding*, 2nd ed., Upper Saddle River, NJ, USA: Prentice-Hall, 2004.

[53] M. L. Cedervall and R. Johannesson, "A fast algorithm for computing distance spectrum of convolutional codes," *IEEE Trans. Inform. Theory*, vol. 35, no. 6, pp. 1146–1159, Nov. 1989.

[54] F. Pollara and D. Divsalar, "Cascaded convolutional codes" *JPL TDA Prog. Rep.*, vol. 42-110, pp. 202–207, Aug. 1992.

[55] D. Bitzer, A. Dholakia, H. Koorapaty, and M. Vouk, "On locally invertible rate-1/n convolutional encoders," *IEEE Trans. Inform. Theory*, vol. 44, no. 1, pp. 420–422, Jan. 1998.

[56] R. Urbanke, "On multiple-access communication," Ph.D. dissertation, Washington Univ., St. Louis, MO, Aug. 1995.

[57] C. Berrou, A. Glavieux, and P. Thitimajshima, "Near Shannon limit error-correcting coding: Turbo codes," *in Proc. IEEE Int. Conf. on Commun.*, Geneva, Switzerland, pp. 1064-1070, May 1993.

[58] Y. Kokuryo and N. Tsukamoto, "Pragmatic trellis coding applied to rectangular QAM," *IEEE Trans. Consumer Elect.*, vol. 51, no. 2, pp. 365–370, Jul. 2005.

[59] S. Alreesh, C. Schmidt-Langhorst, R. Emmerich, P. Wilke Berenguer, C. Schubert and J. K. Fischer, "Four-dimensional trellis coded modulation for flexible optical communications," *J. Lightw. Technol.*, vol. 35, no. 2, pp. 152–158, Jan. 2017.

[60] H. Sun, S. X. Ng, C. Dong, and L. Hanzo. "Decode-and-forward cooperation-aided triple-layer turbo-trellis-coded hierarchical modulation," *IEEE Trans. Commun.*, vol. 63, no. 4, pp. 1136–1148, Jul. 2015.

[61] C. Cahn, "Combined digital phase and amplitude modulation communication system," *IRE Trans. Commun. Syst.*, vol. 8, no. 3, pp. 150–155, Sep. 1960.

[62] L.-F. Wei, "Trellis-coded modulation with multidimensional constellations," *IEEE Trans. Inform. Theory*, vol. 33, no. 4, pp. 483–501, Jul. 1987.

[63] S. Pietrobon, R. Deng, and A. Lafanechere, "Trellis-coded multidimensional phase modulation," *IEEE Trans. Inform. Theory*, vol. 36, no. 1, pp. 63–89, Jan. 1990.

[64] R. Wesel, X. Liu, J. Cioffi, and C. Komninakis, "Constellation labeling for linear encoders," *IEEE Trans. Inform. Theory*, vol. 28, no. 1, pp. 43–55, Jan. 1982.

[65] T. N. Rajashekhara and I.-S. E. Chen, "A fast adder design using signed-digit numbers and ternary logic," in *Proc. IEEE Southern Tier Tech. Conf.*, Binghamton, NY, pp. 187–194, Apr. 1990.

[66] U. Madhow, *Fundamentals of Digital Communication*. Cambridge, UK: Cambridge University Press, 2008.

[67] J. Lee, D. Yoon, and K. Cho, "Error performance analysis of M-ary θ-QAM," *IEEE Trans. Vehic. Tech.*, vol. 61, no. 3, pp. 1423–1427, Mar. 2012.

[68] R. Gallager, "Low-density parity-check codes," *IRE Trans. Inform. Theory*, vol. IT-B, pp. 21–28, Jan. 1962.

[69] D. MacKay and R. Neal,, "Near Shannon limit performance of low density parity check codes," *Elect. Lett.*, vol. 33, pp. 457–458, Mar. 1997.

[70] D. Divsalar, H. Jin, and R. McEliece, "Coding theorems for" turbo-like" codes," *Proc. Ann. Allerton Conf. on Commun. Control and Comput.*, Urbana, Champaign, IL, USA: vol. 36, pp. 201–210, Sep. 1998.

[71] J. Yuan, L. Yang, T. Yang, and J. An, "Design of non-binary irregular repeat-accumulate codes for reliable physical-layer network coding," *Int. Conf. on Telecommun.*, Prague, Czech Republic: pp. 265–271, Jul. 2015.